c59 Quantitative *In Vivo* NMR

R. de Beer

University of Technology Delft, Department of Applied Physics
P.O. Box 5046, 2600 GA Delft, The Netherlands
e-mail: beer@si.tn.tudelft.nl

August 3, 1994

Contents

1 Introduction **4**

1.1 MRS and the importance of quantitative data analysis 4

1.2 Mathematical description of the NMR signal 7

1.2.1 The NMR FID experiment 7

1.2.2 NMR time domain *versus* frequency domain 8

1.2.3 The Fourier Transform and the convolution theorem 12

1.2.4 The discrete Fourier Transform (DFT) 12

1.2.5 The *in vivo* NMR lineshape 14

1.2.6 The NMR spin echo experiment 15

2 Time Domain Quantification **16**

2.1 Quantitative data analysis and the choice of the analysis domain 16

2.2 Quantitative data analysis by means of fitting of model functions 17

2.3 Noniterative *versus* iterative fitting methods 17

2.4 Noniterative fitting methods 18

2.4.1 Introduction 18

2.4.2 The data matrix 18

2.4.3 Singular Value Decomposition (SVD) and rank analysis of the data matrix 19

2.4.4 SVD-based signal enhancement 20

2.4.5 Linear Prediction (LP) and SVD 22

2.4.6 Example 1: Application of LPSVD to an *in vivo* ^{31}P NMR FID signal 24

2.4.7 The SVD-based State Space method 26

2.4.8 Calculation of the SVD via the normal equations approach 28

2.4.9 Rapid SVD of a Hankel data matrix using the Lanczos algorithm . 28

2.4.10 Example 2: Application of HSVD to an *in vivo* ^{31}P NMR FID signal 30

2.5 Iterative fitting methods 32

2.5.1 The Maximum Likelihood (ML) method 32

2.5.2 The Cramer-Rao (CR) lower bounds 33

2.5.3 The Monte Carlo study 34

2.5.4 Quantitative data-analysis methods and the threshold signal-to-noise-ratio 35

2.5.5 The VARiable PROjection (VARPRO) method 37

2.5.6 Example 3: Application of HSVD and VARPRO to ^{23}Na signals of the heart of a rat 38

2.5.7 An iterative Least Squares Gauss-Newton implementation for the exponential decay model 40

2.5.8 Imposing linear relations on model parameters (Prior Knowledge) in the Gauss-Newton program . . . 43
2.5.9 Example 4: Application of the Gauss-Newton program to an *in vivo* ^{31}P NMR FID of calf muscle . . . 45
2.6 Quantification of two-dimensional (2-D) *in vivo* NMR time-domain signals 47
2.6.1 Introduction . . . 47
2.6.2 Examples of 2-D NMR time-domain model functions . . . 49
2.6.3 The 2-D version of the SVD-based State Space method . . . 51
2.6.4 Example 5: Application of 2-D HSVD to a 2-D *in vivo* ^{1}H FID of the brain of a rat . . . 51
2.6.5 Example 6: Application of a 2-D version of the Gauss-Newton program to an *in vivo* ^{31}P longitudinal relaxation experiment of a human brain . . . 52

3 Magnetic Resonance Imaging (MRI) and Spectroscopic Imaging (MRSI) 55
3.1 Introduction . . . 55
3.2 Basic principle of MRI . . . 55
3.3 Basic principle of MRSI . . . 57
3.4 Example 7: Application of time-domain fitting techniques to *in vivo* ^{1}H MRSI signals . . . 59
3.5 An alternative way of writing the MRSI equation . . . 61

4 Miscellaneous 64
4.1 DFT as linear Least Squares fit in the time domain . . . 64
4.2 Zero-residue modelling by the SVD-based State Space method . . . 65
4.3 Example 8: Zero-residue modelling of a noiseless simulated signal . . . 66
4.4 Frequency-selective quantitative data analysis in the time domain . . . 67

5 Examples 71
5.1 Example 9: An EU multicentre quantification trial of *in vivo* NMR test signals . . . 71
5.2 Example 10: Quantification of a water suppressed 600 MHz single pulse signal of human blood plasma . . . 76

Bibliography 80

Foreword

These lecture notes describe the lectures "c59 Quantitative *in vivo* NMR", as given in the second half of 1994. The lectures are concerned with the signal processing and quantitative data-analysis work of the section Spin Imaging (SI) (leader Prof. Dr. A.F. Mehlkopf) of the research group "Spectroscopie en Stralingstechnologie" (SST) of the Department of Applied Physics, University of Technology Delft.

With the word "quantitative" we mean, that the relevant physical parameters of NMR time-domain signals are determined, i.e. the frequencies, decay constants, amplitudes and phases. The quantitative data analysis is realized by fitting model functions to the data by means of Least Squares fitting methods. These fitting methods may be noniterative as well as iterative. Important aspects of the methods are the precision, with which the parameters can be determined and the amount of prior knowledge about the *in vivo* NMR signals, that can be incorporated into the quantification algorithms.

With the words "*in vivo* NMR" we indicate, that the NMR experiments are carried out on *living* objects. The living objects may be animals but also human volunteers and patients. An important aspect of *in vivo* NMR is, that a so-called volume of interest is to be selected, i.e. some form of localization is to be performed. Another aspect of *in vivo* NMR, particularly if the NMR experiments are carried out in clinical circumstances, is that the measurement time is limited. That is to say, in general the signal-to-noise-ratio (SNR) of the *in vivo* NMR signals will be low. Given this low SNR, it is the task of the signal processing and quantitative data-analysis methods to determine the parameters of interest as precise as possible.

The following persons have contributed to the work, decribed in these lecture notes:

H. Barkhuijsen, R. de Beer, A. van den Boogaart, W.M.M.J. Bovee, J.H.C. Creygton, J.W. Deumens, J.E. van Dijk, A.C. Drogendijk, R. van Duuren, C. Huegen, A. Knijn, J. van Leeuwen, H.F.M. Lohman, G.J. Marseille, A.F. Mehlkopf, R.P.J. Merks, F. Michels, K. Nederveen, D. van Ormondt, W.W.F. Pijnappel, A.M. Salomons, M. Schramp, S. Slegt, B.P.O. van Tongeren, J.W.C. van der Veen, C. van der Voort, F.T.A.W. Wajer, K.M. Wiacek, J. Zonneveld, W.R. van der Zwan

R. de Beer
1994

Chapter 1

Introduction

1.1 MRS and the importance of quantitative data analysis

At present, Nuclear Magnetic Resonance (NMR) on *living* objects (animals, human volunteers, patients) is widely accepted. As one of the outcomes, the speciality Magnetic Resonance *Imaging* (MRI) is already used in clinical practice for a number of years [1]. Another area of the *in vivo* NMR, the Magnetic Resonance *Spectroscopy* (MRS) [2], is also subject to important developments, which has raised high hopes for MRS becoming a medical diagnostic tool. In the mean time it has been established that the success of MRS as a medical tool among other things depends on the way in which the NMR data can be analysed by the computer. In that context especially the *quantitative* data analysis

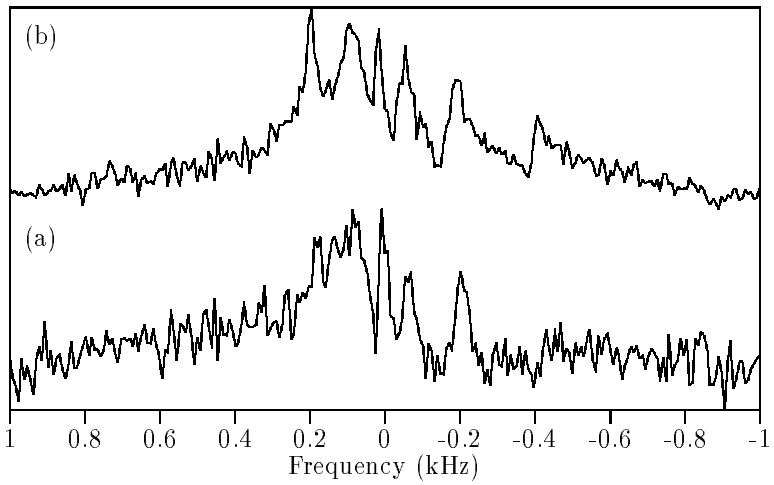

Figure 1.1: *In vivo* ^{31}P *NMR spectra of the human brain. (a) Healthy volunteer. (b) Patient with a tumor. Notice the much larger peak at 0.2 kHz.*

is important. With quantitative data analysis we mean that the measured NMR time-domain signals are interpreted in terms of relevant physical parameters, such as frequencies, decay constants and amplitudes. These parameters, in turn, can be translated into relevant biochemical or medical parameters such as ratios of metabolite concentrations and the pH value of the tissue, concerned.

When estimating the quantitative parameters, a correct interpretation of the NMR *decay function* plays an important role. The physiscs of the underlying NMR experiment can provide decisive information about that aspect. Also an accurate estimation of the NMR *amplitudes* is important. The latter plays an essential role when applying MRS in medical diagnostics (see Figure 1.1).

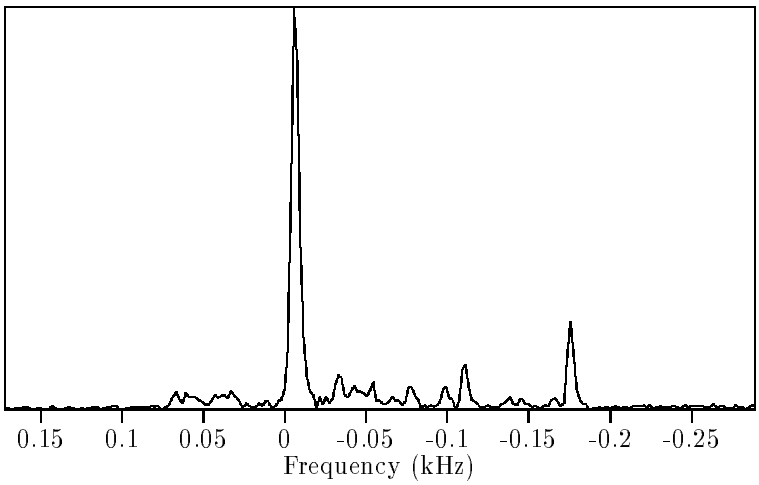

Figure 1.2: *In vivo* ^{1}H *NMR spectrum of a human brain. The large peak at 0 kHz is due to the water protons.*

In clinical circumstances time consuming measurements usually are not allowed. As a consequence *in vivo* NMR spectra are often characterized by a low signal-to-noise-ratio (SNR) (see Figure 1.1). Another characteristic feature of *in vivo* NMR signals is that the spectra may be disturbed by unwanted artificial effects, caused by the localization

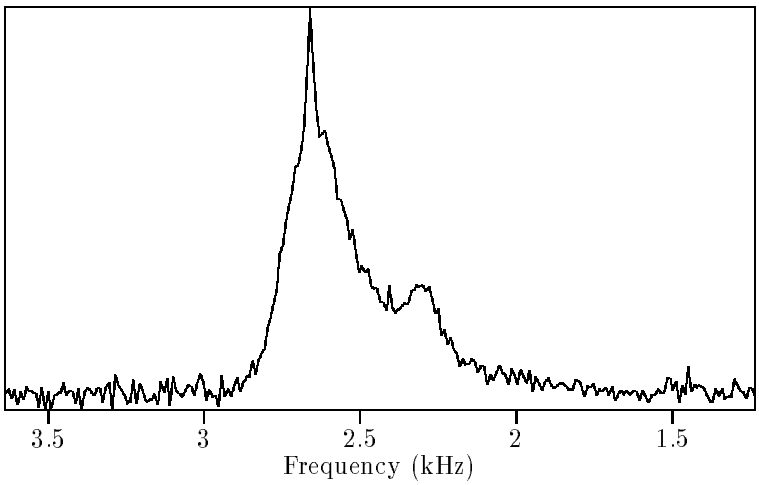

Figure 1.3: *In vivo* ^{23}Na *NMR spectrum of the heart of a rat. The small peak is due to intra- and the large peak due to extracellular* ^{23}Na. *The separation between the two peaks is introduced by a shift reagent.*

method, applied. A third typical aspect of *in vivo* NMR spectroscopy is that the spectra strongly differ, when measuring on the various nuclei. We mention the following characteristic properties:

- In ^{31}P spectra there are heavily overlapping NMR lines and a dominant broad background signal (see Figures 1.1, 1.5 and 1.6).
- In ^{1}H spectra there is a dominant H_2O signal and unresolved multiplet structure (see Figure 1.2).
- When measuring on the ^{23}Na nucleus, often shift reagents are applied to separate the intra- and extracellular ^{23}Na. Also multiple quantum excitation is used for that purpose. Furthermore, unresolved quadrupole interaction is a typical aspect of ^{23}Na spectroscopy (see Figure 1.3).
- Concerning the ^{13}C nucleus it can be said that its *in vivo* spectrum often contains much detailed information and therefore ^{13}C spectroscopy appears to be promishing for medical diagnostics (see Figure 1.4).

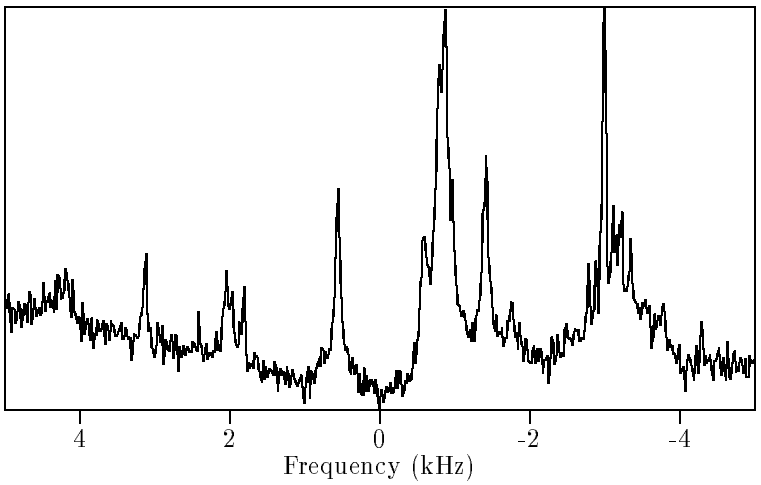

Figure 1.4: *In vivo* ^{13}C *NMR spectrum of perfused rat liver.*

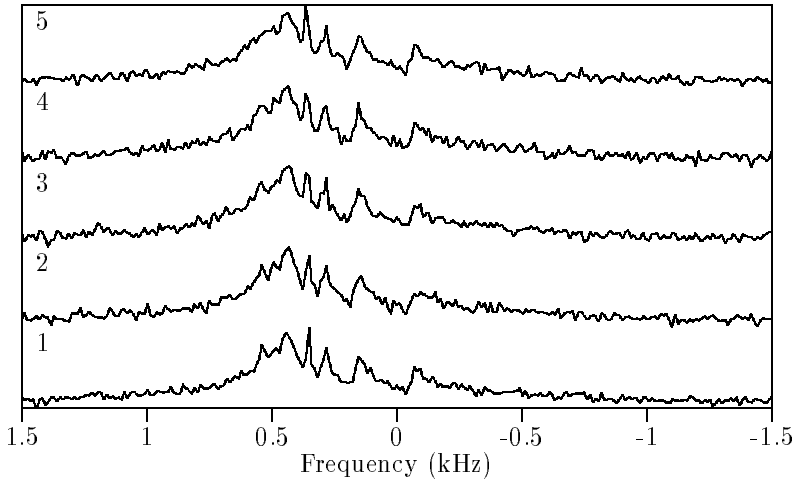

Figure 1.5: *In vivo* ^{31}P *NMR spectra of a human brain. The spectra were taken from the same volunteer. The differences in the spectra are caused by noise.*

In the mean time it has been established in a number of quantitative studies [3] that variations in the parameters of *in vivo* NMR spectra for a large portion are caused by human interactions. Even in computerized quantifications significant variations still can occur. In the latter case they may be caused by the disturbing influence of noise (see Figure 1.5 and [4]). In order to improve the quantitative data analysis, an important step is to introduce *prior knowledge* about the *in vivo* NMR signals in the computer algorithms [5] [6]. By using prior knowledge it was found to be possible in certain cases to reduce the variations in the quantitative parameters by an order of magnitude (see Figure 1.6).

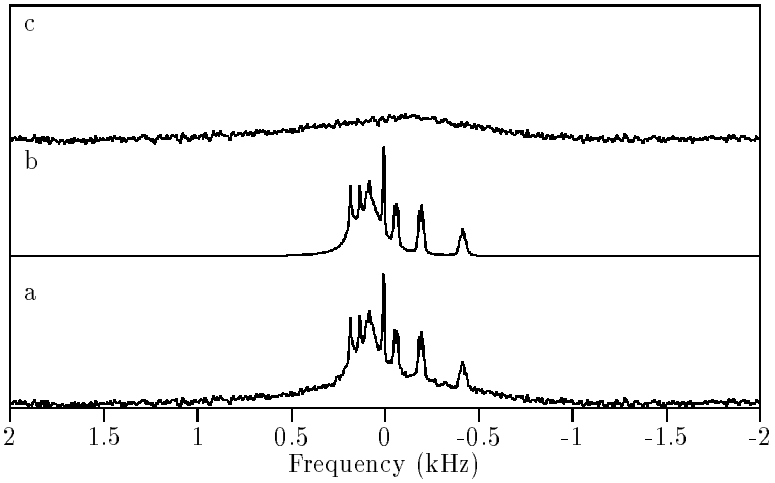

Figure 1.6: *(a) Proton decoupled in vivo* ^{31}P *NMR spectrum of a human brain. (b) Spectrum of a fitted model function, obtained via nonlinear least squares fitting and prior knowledge on ATP. As many as 15 NMR peaks could be quantified. (c) Spectrum of the residue signal.*

Conclusion:

Quantification in MRS has specific aspects due to the typical features of *in vivo* NMR signals. It plays an essential role in developing MRS as a clinical tool.

1.2 Mathematical description of the NMR signal

1.2.1 The NMR FID experiment

The motion of a nuclear magnetization vector $\vec{M}$ in a *constant* magnetic field $\vec{B}_0$ and an *oscillating* magnetic field (r.f. field) $\vec{B}_1$ perpendicular to $\vec{B}_0$ and rotating around it with an angular velocity ω, is described by the equations of Bloch [7]

$$\frac{\mathrm{d}\vec{M}}{\mathrm{d}t} = \gamma\vec{M} \times [(B_0 + \frac{\omega}{\gamma})\,\vec{u}_z + B_1\vec{u}_x] - \frac{M_z - M_0}{T_1}\,\vec{u}_z - \frac{M_x\vec{u}_x + M_y\vec{u}_y}{T_2}, \qquad (1.1)$$

where

t	is the sampling time,	
γ	is the gyromagnetic ratio,	
$\vec{u}_x, \vec{u}_y, \vec{u}_z$	are the unit vectors along the rotating frame,	(1.2)
M_0	is the equilibrium magnetization at $t = 0$,	
T_1	is the longitudinal relaxation time and	
T_2	is the transverse relaxation time.	

If the r.f. field $\vec{B}_1$ is present in a time, much shorter than T_1 or T_2, one speaks of a pulse. During the pulse the magnetization makes a precession around $\vec{B}_1$ in the rotating frame. The pulse is called a 90^0 pulse if this precession is over 90^0. Once the pulse is switched off, the magnetization starts to precess around the z-axis with an angular velocity $\Delta\omega = (\omega - \omega_0)$, where ω_0 is the *resonance* angular velocity, defined by

$$\omega_0 = -\gamma B_0. \tag{1.3}$$

The precessing magnetization induces a time-domain signal in the detection system of the NMR scanner, which after down transformation of the frequency can be described by

$$s(t) = a \exp(-\frac{t}{T_2}) \exp[i(2\pi\Delta\nu t + \phi)], \tag{1.4}$$

where the amplitude a is proportional to the number of nuclei, concerned, $\Delta\omega = 2\pi\Delta\nu$ and $i^2 = -1$. One speaks of a Free Induction Decay (FID). With the words *number of nuclei, concerned* we mean the number nuclei of the same kind, i.e. belonging to the same molecule.

Conclusion:

In the ideal case the NMR FID of a certain nucleus can be described by an *exponentially* decaying *complex-valued* sinusoid, the amplitude of which is proportional to the number of nuclei of that kind, the decay constant is equal to the reciprocal of the transverse relaxation time of that nucleus, the frequency is equal to the difference between the frequency of the NMR spectrometer and the resonance frequency of that nucleus and the overall (zero-order) phase is determined by the spectrometer setting.

1.2.2 NMR time domain *versus* frequency domain

It is well known that the resonance frequency is different for a *bare* nucleus and for a nucleus embedded in *bulk* matter. This frequency difference can be included into the resonance condition as

$$\omega_0 = -\gamma B_0(1 - \sigma), \tag{1.5}$$

where σ is the so-called chemical shift. The chemical shift can be different for different molecules or different parts of a molecule. As a result, the time-domain signal of an NMR FID experiment in general can be described by

$$s(t) = \sum_{k=1}^{K} a_k \exp(-\alpha_k t) \exp[i(2\pi\Delta\nu_k t + \phi_k)], \tag{1.6}$$

where K is the number of harmonic components, i.e. the number of NMR peaks in the related frequency domain and the symbol $\alpha_k = \frac{1}{T_{2k}}$ denotes the decay constant of the k'th component.

When speaking about *quantitative* data analysis we in fact mean the estimation of four parameters for each harmonic component: the amplitude, the decay constant, the frequency and the phase. In the NMR world it is common use to perform the data analysis not directly on the time-domain (measurement-domain) data but on the related Fourier Transform (FT) data. This FT is defined as [8]

$$S(\nu') = \int_{-\infty}^{\infty} s(t) \exp(-i2\pi\nu' t) \mathrm{d}t. \tag{1.7}$$

We now consider the FT of a single harmonic component. For the sake of simplicity we drop the subscript k and the symbol Δ (of $\Delta\nu$). Moreover we assume momentarily, that the phase ϕ of the harmonic component is equal to zero. If we take into account that $s(t) = 0$ for $t < 0$, then the FT can be written as

$$\begin{aligned} S(\nu') &= \int_0^{\infty} a \exp\{[-\alpha + i2\pi(\nu - \nu')]t\} \mathrm{d}t = \left| \frac{a \exp\{[-\alpha + i2\pi(\nu - \nu')]t\}}{-\alpha + i2\pi(\nu - \nu')} \right|_0^{\infty} = \\ &= -\frac{a}{-\alpha + i2\pi(\nu - \nu')} = R(\nu') + iI(\nu'), \end{aligned} \tag{1.8}$$

where $R(\nu')$ and $I(\nu')$ are the real and imaginary part, respectively, of the *complex Lorentz line*

$$R(\nu') = \frac{a}{\alpha} \frac{1}{1 + [\frac{2\pi(\nu - \nu')}{\alpha}]^2} \quad \text{and} \quad I(\nu') = \frac{a}{\alpha} \frac{\frac{2\pi(\nu - \nu')}{\alpha}}{1 + [\frac{2\pi(\nu - \nu')}{\alpha}]^2}. \tag{1.9}$$

In Figure 1.7 the real and imaginary part of an exponentially decaying, complex-valued, sinusoid are displayed, together with the real and imaginary part of the related Lorentz line in the frequency domain. Typical for the Lorentz line are the long tails, especially of the imaginary part. Since neighbouring lines may overlap with these long tails, in practice one works with the real part of the Lorentz line. When looking at Equation 1.9, the following can be concluded:

- The maximum value (the height) of $R(\nu')$ is $\frac{a}{\alpha}$ (at $\nu = \nu'$). This maximum value thus also depends on the decay constant α.
- The width at half height (i.e. the line width) is $\frac{\alpha}{\pi}$.
- The area under $R(\nu')$ is

$$\int_{-\infty}^{\infty} R(\nu') \mathrm{d}\nu' = \frac{a}{\alpha} \int_{-\infty}^{\infty} \frac{\mathrm{d}\nu'}{1 + [\frac{2\pi(\nu - \nu')}{\alpha}]^2} = \frac{a}{2\pi} \int_{-\infty}^{\infty} \frac{\mathrm{d}x}{1 + x^2} = \frac{a}{2}, \tag{1.10}$$

  thus only proportional to the amplitude a. In these lecture notes we will use the name *line intensity* to indicate the amplitude in the time domain as well as the peak area in the frequency domain.

In practice an NMR FID will never be acquired from $t = 0$ to ∞, but for instance from $t = t_1$ to $t = t_2$. One speaks of a *truncated* signal. Moreover, in general the overall phase of a FID will not be equal to zero. Both effects have significant consequences for the FT of the FID

$$\begin{aligned} S(\nu') &= \int_{t_1}^{t_2} a \exp(i\phi)\ \exp\{[-\alpha + i2\pi(\nu - \nu')]t\}\ \mathrm{d}t = \\ &= a \exp(i\phi)\ \left| \frac{\exp\{[-\alpha + i2\pi(\nu - \nu')]t\}}{-\alpha + i2\pi(\nu - \nu')} \right|_{t_1}^{t_2} = \\ &= a \exp(i\phi)\ \frac{\exp\{[-\alpha + i2\pi(\nu - \nu')]t_2\} - \exp\{[-\alpha + i2\pi(\nu - \nu')]t_1\}}{-\alpha + i2\pi(\nu - \nu')} \quad .(1.11) \end{aligned}$$

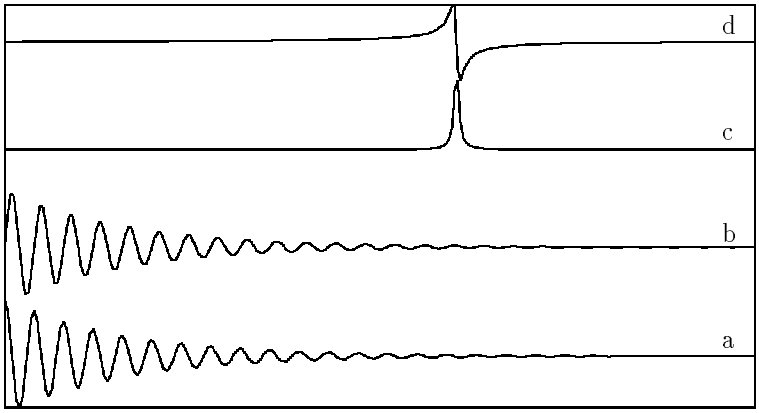

Figure 1.7: *(a) Real and (b) imaginary part of an exponentially decaying, complex-valued, sinusoid. (c) Real and (d) imaginary part of the related Lorentz line in the frequency domain.*

We now consider three cases:

(1) $\phi \neq 0$, $t_1 = 0$ and $t_2 = \infty$.

This yields for the FT

$$S(\nu') = \exp(i\phi)\ [R(\nu') + iI(\nu')]. \tag{1.12}$$

The effect of $\phi \neq 0$ is that the frequency domain is composed of a linear combination of the real and imaginary part of the complex Lorentz line (see Figure 1.8). One can undo this linear combination by multiplying Expression 1.12 by $\exp(-i\phi)$. This correction is called the *zero-order phase correction* (i.e. not dependent on the frequency).

(2) $\phi = 0$, $t_1 \neq 0$ and $t_2 = \infty$.

This yields for the FT

$$S(\nu') = -a\frac{\exp\{[-\alpha + i2\pi(\nu - \nu')]t_1\}}{-\alpha + i2\pi(\nu - \nu')}. \tag{1.13}$$

For the real part of Expression 1.13 one can write

$$R'(\nu') = \exp(-\alpha t_1)\ \{\cos[2\pi(\nu - \nu')t_1]\ R(\nu') - \sin[2\pi(\nu - \nu')t_1]\ I(\nu')\}. \tag{1.14}$$

Notice that (see also Figure 1.8):

- There is an oscillating behaviour with period $\frac{1}{t_1}$.
- At $\nu' = \nu$ the FT behaves as a complex Lorentz line.
- The maximum height at $\nu' = \nu$ is decreased to $\frac{a}{\alpha}\ \exp(-\alpha t_1)$.

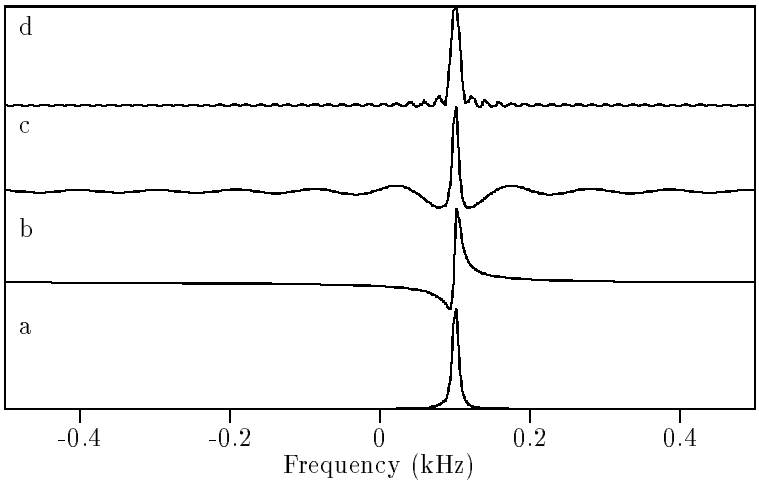

Figure 1.8: *Effects of a zero-order phase and time-domain signal truncation. (a) Original Lorentz line (real part), originating from 256 time-domain data points. (b) With a zero-order phase of* 60^0. *(c) After truncation of the first 10 data points. (d) After truncation of the last 200 data points.*

(3) $\phi = 0$, $t_1 = 0$ and $t_2 \neq \infty$.

This yields for the FT

$$S(\nu') = a\frac{\exp\{[-\alpha + i2\pi(\nu - \nu')]t_2\} - 1}{-\alpha + i2\pi(\nu - \nu')}. \tag{1.15}$$

For the real part of Expression 1.15 one can write

$$R'(\nu') = \{1 - \exp(-\alpha t_2)\ \cos[2\pi(\nu - \nu')t_2]\}\ R(\nu') + \exp(-\alpha t_2)\ \sin[2\pi(\nu - \nu')t_2]\ I(\nu'). \tag{1.16}$$

Notice that (see also Figure 1.8):

- There is an oscillating behaviour with period $\frac{1}{t_2}$. The amplitude of this oscillation is small since usually $\alpha t_2 \gg 1$.
- At $\nu' = \nu$ the FT behaves as a complex Lorentz line.
- The maximum height at $\nu' = \nu$ is decreased to $\frac{a}{\alpha}\,[1 - \exp(-\alpha t_2)]$.

Conclusions:

(a) In the ideal case the FT of a FID harmonic component is a complex Lorentz line.
(b) If the zero-order phase $\phi \neq 0$ the FT becomes a linear combination of the real and imaginary part of the complex Lorentz line.
(c) Truncation of the FID at the beginning or end yields an oscillating behaviour of the FT. The period of the oscillation is determined by the shape of the truncation (step) function, concerned.

1.2.3 The Fourier Transform and the convolution theorem

The effect of time-domain truncation on the related FT can be described alternatively by using the convolution theorem [8]. This theorem says that the FT of a *product* of two time-domain functions $f(t)$ and $g(t)$ is equal to $F(\nu') * G(\nu')$, where the symbol $*$ denotes the so-called convolution integral, defined by

$$F(\nu') * G(\nu') = \int_{-\infty}^{\infty} F(\tau)G(\nu' - \tau)\mathrm{d}\tau. \tag{1.17}$$

A truncated signal now can be considered as being the product of the original signal and a step function of the proper length and position. Application of the convolution theorem on this product then yields the same FT as shown in Equation 1.11.

Conclusion:

If a real-world NMR time-domain signal has been truncated, the correct FT of that signal can only be determined if ones succeeds in properly *deconvoluting* the frequency domain. If one fails in performing this deconvolution, this could be an argument for quantifying the data directly in the *measurement* domain (i.e. the time domain).

1.2.4 The discrete Fourier Transform (DFT)

In practice an NMR FID is not acquired continuously but discretely at sampling times $t_n = n\Delta t + t_{beg}$, with $n = 0, 1, \ldots, N-1$. Consequently the desired transformation to the frequency domain has to be realized by a discrete Fourier Transform (DFT), defined as [8]

$$\hat{S}_k = \Delta t \sum_{n=0}^{N-1} a \exp(i\phi)\ \exp[(-\alpha + i2\pi\nu)(n\Delta t + t_{beg})]\ \exp(\frac{-i2\pi nk}{N}), \tag{1.18}$$

where the $k = 0, 1, \ldots, N-1$ denotes the frequency-domain points and the caret indicates, that the DFT of a *model function* is taken (i.e. without having the disturbances of

noise). It should be noted that the quantity $\nu_{Nyq} = \frac{1}{2\Delta t}$ is called the Nyquist frequency. Apparently the DFT of the time-domain data points is a periodic function with a period of $2\nu_{Nyq}$.

When using the property

$$\sum_{n=0}^{N-1} z^n = \frac{1 - z^N}{1 - z}, \tag{1.19}$$

where z is a complex number, it follows that

$$\hat{S}_k = a\Delta t \ \exp[-\alpha t_{beg} + i(2\pi\nu t_{beg} + \phi)] \ \frac{1 - \exp\{[-\alpha + i2\pi(\nu - \frac{k}{N\Delta t})]N\Delta t\}}{1 - \exp\{[-\alpha + i2\pi(\nu - \frac{k}{N\Delta t})]\Delta t\}}. \tag{1.20}$$

For the sake of simplicity we assume that $\phi = 0$, that Δt is very small and that $\alpha N\Delta t \gg 1$. Equation 1.20 then can be written as

$$\hat{S}_k = -a\frac{\exp[(-\alpha + i2\pi\nu)t_{beg}]}{-\alpha + i2\pi(\nu - \frac{k}{N\Delta t})}. \tag{1.21}$$

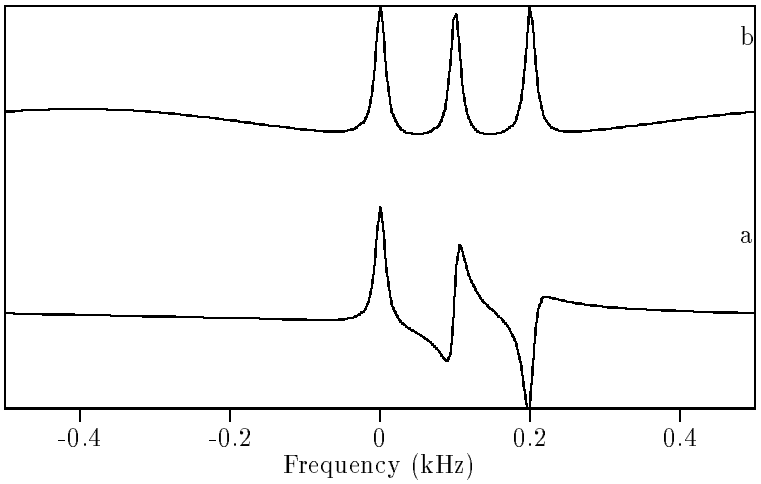

Figure 1.9: *Graphical presentation of the first-order phase correction. (a) DFT of a time-domain signal, truncated at the beginning. The zero-order phase $\phi = 0$. The first two data points were truncated. (b) DFT of the same signal, after applying first-order phase correction. Only the real parts of the DFT's are shown.*

We see that, apart from its discrete character, Equation 1.21 almost has the same shape as Equation 1.13. The difference in the numerator is caused by the fact that the continuous FT starts its integration at $t = t_{beg} = t_1$ whereas the DFT starts its summation at $n = 0$. As a result, the numerator of the DFT does not depend on k (i.e. has not an oscillating behaviour) but contains only a constant, complex-valued, factor. That is to say, there is a phase effect, that now depends on the first power of the frequency. This effect can be corrected for by multiplying Expression 1.21 by $\exp(-i2\pi\frac{kt_{beg}}{N\Delta t})$, which is called the *first-order phase correction.* After this correction one obtains an expression that is similar to Expression 1.13 (i.e. now also with an oscillating behaviour; see Figure 1.9).

1.2.5 The *in vivo* NMR lineshape

It was shown in subsection 1.2.2 that the FT of an NMR FID yields a complex-valued Lorentz line. This lineshape is directly related to the *exponential* decay of the FID, which according to the equations of Bloch is determined by the transverse relaxation of the nucleus, concerned (see Equations 1.1 and 1.6). In real-world *in vivo* NMR experiments there may be other causes for the decay of the FID's such as inhomogeneity of the constant magnetic field $\vec{B}_0$ due to instrumental effects or to the susceptibility of the living object. One or the other is the cause that a mathematical description of the decay of the NMR FID's by a single exponential actually is too simple. However, it should be noted, when setting the instrumental conditions of an *in vivo* NMR experiment, that it always is attempted to correct for the magnetic field inhomogeneity in such a way, that the additional decay also has a exponential character.

For the sake of completeness we consider in this subsection a few other time-domain decay functions. After applying Fourier Transformation these decay functions lead to other lineshapes. We mention:

- The Gaussian decay:
$$\exp(-\alpha t^2). \tag{1.22}$$
- The Voigt decay:
$$\exp(-\alpha t)\ \exp(-\beta t^2). \tag{1.23}$$
- The triangle decay:
$$\frac{1 - i2\pi\ \delta\nu\ t - \exp(-i2\pi\ \delta\nu\ t}{(2\pi\ \delta\nu\ t)^2}, \tag{1.24}$$
where $\delta\nu$ is equal to the width of the triangle in the frequency domain at zero height.

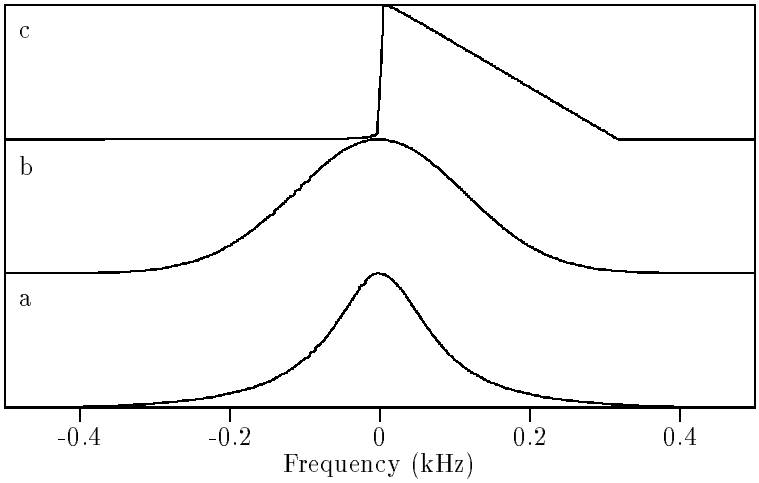

Figure 1.10: *Graphical presentation of three lineshapes. (a) Lorentz. (b) Gauss. (c) Triangle.*

In Figure 1.10 the related frequency domains of the exponential, the Gauss and the triangle decay are displayed. Notice the long tail of the Lorentz line. Notice also that the triangle decay function is capable of describing an *asymmetrical* lineshape.

1.2.6 The NMR spin echo experiment

Sofar we have described the NMR FID experiment. We have seen that the essence of that experiment is the usage of a single 90^0 r.f. pulse. However, an alternative way of measuring an NMR signal is the spin echo method. In that case a second r.f. pulse is given after a certain delay time τ, now with a related precession angle of 180^0. The effect of the second pulse is that at time $t = 2\tau$ a so-called nuclear spin echo can be detected [7]. This spin echo has an increasing character for $t < 2\tau$ and a decreasing character for $t > 2\tau$ (see Figure 1.11). In general the increasing or decreasing behaviour need not to be according to an exponential function, but for the sake of simplicity we will assume so in these lecture notes. In that case the lineshape function for the spin echo becomes

$$\exp[\alpha_1(t-2\tau)] \text{ for } t < 2\tau \text{ and } \exp[-\alpha_2(t-2\tau)] \text{ for } t > 2\tau, \tag{1.25}$$

where $\alpha_1 > 0$, $\alpha_2 > 0$ and in general $\alpha_1 \neq \alpha_2$.

In principle the NMR spin echo time-domain signal contains the same information concerning frequencies and line intensities as the NMR FID signal. However, an important reason for using the spin echo pulse sequence is that the delay time between the r.f. pulses offers the opportunity of manipulating the nuclear magnetization, for instance for creating spatial localization.

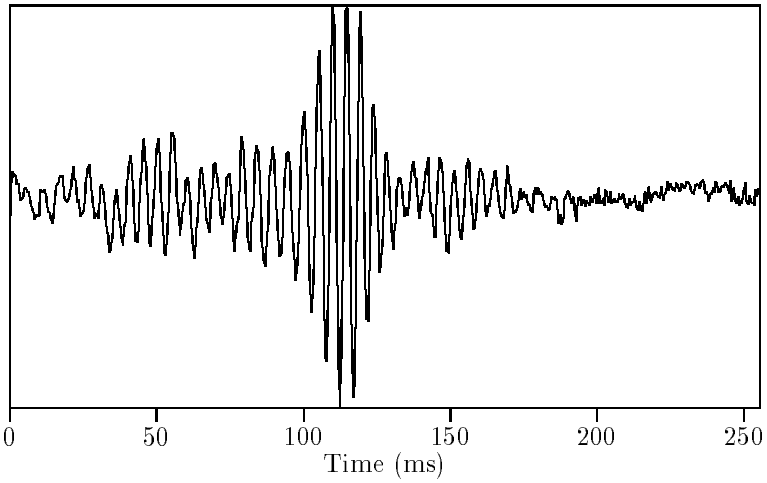

Figure 1.11: *Real part of a complex-valued* ^{1}H *spin echo time-domain signal of a human brain.*

Chapter 2

Time Domain Quantification

2.1 Quantitative data analysis and the choice of the analysis domain

In the previous chapter a mathematical description was given of the NMR FID signal, in the measurement (time) domain as well as in the transformation (frequency) domain. Also a short description of the NMR spin echo signal was given. Both types of NMR signals have in common that they can contain the same information concerning frequencies and line intensities. When quantifying the latter parameters one can use the time-domain as well as the frequency-domain data. Concerning the line intensities this means that one has to determine either the time-domain amplitudes or the frequency-domain peak areas.

Regarding the choice of the domain for performing the quantitative data analysis we note the following:

- Working in the frequency domain offers an easy opportunity of reducing the data analysis to a limited frequency region of the NMR spectrum. However, under certain conditions frequency-selective quantitative data analysis in the time domain is also feasible [9].
- The FT of truncated time-domain data needs to be deconvoluted, before or during the quantitative data analysis [10].
- When quantifying in the time domain, one can employ the specific mathematical properties of the exponential decay [11], assuming that this decay function correctly describes the decay of the *in vivo* NMR signals, concerned.
- If the decay of the NMR time-domain signal is other than exponential, the related FT may be a complicated mathematical function. For instance, the Voigt decay, shown in Equation 1.23, leads to a very complicated FT [12] which consequently is difficult and time consuming to quantify.

When choosing the analysis domain, we give priority to the latter two items. This means that in these lecture notes we will limit ourselves to dealing with quantitative data analysis methods *in the time domain*.

2.2 Quantitative data analysis by means of fitting of model functions

In these lecture notes the quantitative data analysis in fact boiles down to fitting the correct mathematical function (the model function) to the NMR time-domain data. This in general will leed to applying a Least-Squares (LS) procedure [13]. We will limit ourselves thereby to quantifying NMR FID signals. If we assume that Equation 1.6 correctly describes the *in vivo* NMR FID signals, then in case of K harmonic components (K peaks) one has to estimate $4K$ unknown parameters. Among these parameters the decay constants and frequencies appear *nonlinearly* in the model function whereas the amplitudes and phases can be combined to complex-valued *linear* parameters via the equation $c_k = a_k \exp(i\phi_k)$. As a consequence of the appearance of nonlinear parameters, in general the LS methods will be *iterative*. However, when applying the specific mathematical properties of the exponential decay model, in certain quantification methods it is possible to estimate the nonlinear parameters in a linear way, i.e. *noniteratively*.

2.3 Noniterative *versus* iterative fitting methods

Specific properties of noniterative and iterative fitting methods are:

Noniterative

- The model parameters are calculated in one single step.
- There is no need for supplying starting values for the nonlinear parameters.
- Human decisions concerning the quantification methods can be minimized.
- The model function is limited to the exponential decay model.
- Application of prior knowledge on the model function is only possible on a limited scale.

Iterative

- The model parameters are to be estimated via a number of iteration steps.
- In the first iteration step there should be starting values for the nonlinear parameters.
- There are no limitations concerning the mathematical shape of the model functions.
- One can employ prior knowledge on model parameters in an easy fashion.
- If one applies a so-called Maximum Likelihood method [13], there are no systematic errors in the values of the parameters and the statistical errors can be approximated by theoretical lower bounds.
- In general the computer algorithms will be time consuming.

2.4 Noniterative fitting methods

2.4.1 Introduction

If one wants to perform the quantitative data analysis in a noniterative fashion, one has to replace the original, nonlinear, model function by an alternative function containing only linear parameters. A necessary condition then is, of course, that one can transform the new, linear, parameters into the original ones. In these lecture notes we will show two examples of this approach. They both have in common that they are based on the so-called Singular Value Decomposition (SVD) [14] of a two-dimensional (2-D) matrix, composed of the data points of the NMR time-domain signal. In the next sections the concepts *data matrix* and *SVD of the data matrix* will be introduced.

2.4.2 The data matrix

Starting from Equation 1.6 we can write in case of a discretely sampled NMR FID signal

$$s_n = \sum_{k=1}^{K} c_k \zeta_k^{n+\delta} + \epsilon_n = \hat{s}_n + \epsilon_n, \tag{2.1}$$

where

$n = 0, \ldots, N-1$	denotes the sampling times $n\Delta t$,
$c_k = a_k \exp(i\phi_k)$	is the k'th complex-valued amplitude,
$\zeta_k = \exp[(-\alpha_k + i2\pi\nu_k)\Delta t]$	is the k'th so-called signal pole,
Δt	is the sampling step,
δ	denotes a delay time $t_{beg} = \delta\Delta t$,
$\hat{s}_n$	is the model function contribution and
ϵ_n	is the noise contribution.

(2.2)

Given the time-domain data points s_n, we can define a so-called *data matrix* according to

$$S = \begin{pmatrix} s_0 & s_1 & s_2 & \cdots & s_{M-1} \\ s_1 & s_2 & s_3 & \cdots & s_M \\ \vdots & \vdots & \vdots & \cdots & \vdots \\ s_{L-1} & s_L & s_{L+1} & \cdots & s_{N-1} \end{pmatrix}, \tag{2.3}$$

where L and M should be chosen greater than K (the number of NMR components), subject to the constraint $L + M = N + 1$. Notice that the data matrix possesses so-called Hankel structure, i.e. all elements on the anti diagonals are equal.

We now first consider a *noiseless* NMR FID signal, containing only one single complex-valued, exponentially decaying, sinusoid. In that case $s_n = \hat{s}_n$ and the data matrix has the following simple form

$$S_1 = c_1 \zeta_1^{\delta} \begin{pmatrix} \zeta_1^0 & \zeta_1^1 & \zeta_1^2 & \cdots & \zeta_1^{M-1} \\ \zeta_1^1 & \zeta_1^2 & \zeta_1^3 & \cdots & \zeta_1^M \\ \vdots & \vdots & \vdots & \cdots & \vdots \\ \zeta_1^{L-1} & \zeta_1^L & \zeta_1^{L+1} & \cdots & \zeta_1^{N-1} \end{pmatrix}, \tag{2.4}$$

where the subscript 1 denotes that the signal contains one component (i.e. $K = 1$). Notice that the matrix S_1 has only one linearly independent row (or column), or in other words that the so-called *rank* of the matrix is equal to one.

The next step is to consider a noiseless time-domain signal with K exponentially decaying sinusoids. In that case the data matrix is equal to

$$S = S_1 + S_2 + \ldots + S_K. \tag{2.5}$$

Adding the K matrices S_k yields a matrix S, having K linearly independent rows (or columns), i.e. having a rank equal to K.

If noise has been added to the NMR FID signal, the linear dependence of the rows (or columns) is destroyed, resulting in a data matrix with full rank, i.e. equal to $\min(L, M)$. However, as long as the SNR of the signal is not too low, one can still define a rank being approximately equal to K. This means that a rank analysis of the data matrix gives insight into the number of NMR components, present in the NMR FID. One way of performing this rank analysis is to perform SVD (see next subsection).

Conclusions:

(a) The rank of a Hankel data matrix of a noiseless time-domain signal, comprising K exponentially decaying, complex-valued, sinusoids is equal to K.
(b) If noise is present, in general the rank becomes full.
(c) If the SNR is not too low, the rank still can be approximated by K.
(d) A rank analysis of the data matrix gives insight into the number of harmonic components.

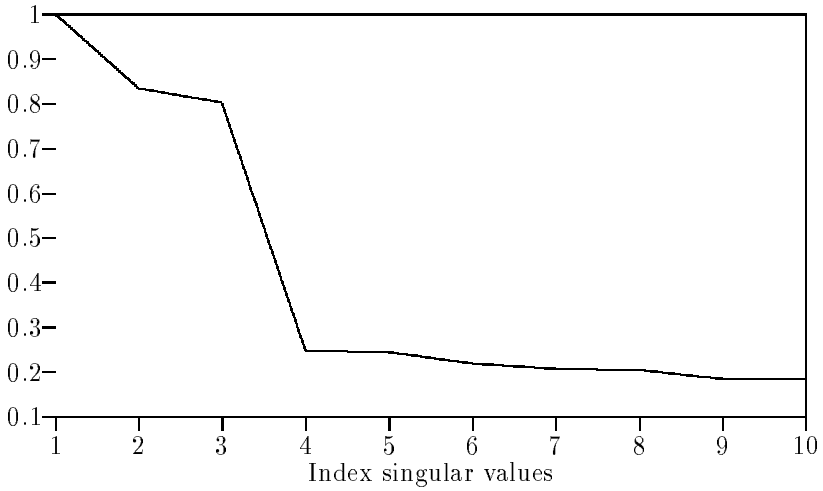

Figure 2.1: *Plot of the singular values of a simulated time-domain signal, containing three exponentially decaying sinusoids and computer-simulated noise. The SNR = 10.*

2.4.3 Singular Value Decomposition (SVD) and rank analysis of the data matrix

Any rectangular data matrix can be brought into diagonal form with the aid of Singular Value Decomposition (SVD) [14], which means the following matrix factorization

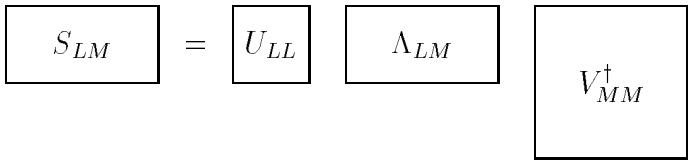

$$S_{LM} = U_{LL}\Lambda_{LM}V^{\dagger}_{MM}, \tag{2.6}$$

where U_{LL} and V_{MM} are the singular matrices and Λ_{LM} is a diagonal matrix whose entries are called the singular values. Furthermore, the † denotes hermitian conjugation.

It can be shown that the singular values are always ≥ 0. Once the SVD has been carried out according to Equation 2.6, one can immediately determine the rank of the data matrix S_{LM}. This can be seen as follows. Since the singular matrices U and V are unitary matrices (i.e. they have full rank) the rank of the product $U_{LL}\Lambda_{LM}V^{\dagger}_{MM}$ is determined by the rank of Λ_{LM}. The latter, in turn, is equal to the number of singular values differing from zero. From the theory of the previous subsection it follows that this number is equal to K in case of a noiseless, exponentially decaying, time-domain signal.

When noise has been added to the time-domain data, all singular values are > 0. However, if the SNR is not too low, one can always see a discontinuity (a jump) in the graphical presentation of the singular values, assuming that they are plotted in descending order. In Figure 2.1 an example of such a plot is given for the case of a simulated time-domain signal, containing three exponentially decaying sinusoids and computer-simulated noise. Notice that for a SNR = 10 there is a very clear distinction between the signal and noise related singular values.

2.4.4 SVD-based signal enhancement

The SVD can be employed to enhance the SNR of the *in vivo* NMR FID time-domain signals. A reason for doing such an enhancement can be that after that a noiseless signal is obtained that may yield the same quantification results for all quantification methods, available.

To realize the signal enhancement, Equation 2.6 should be *cleaned*, that is setting the noise related singular values equal to zero. As a consequence of this cleaning the matrices U, Λ and V should be stripped from the rows and columns, that have ceased to contribute to the SVD. The whole process results into a truncated SVD

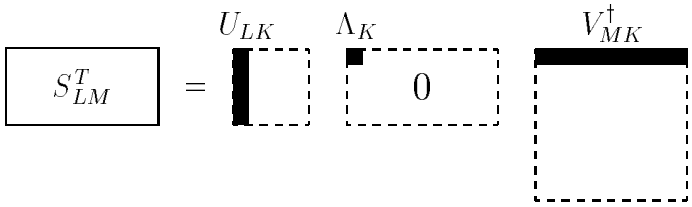

$$S^{T}_{LM} = U_{LK}\Lambda_{K}V^{\dagger}_{MK}, \tag{2.7}$$

where the inked boxes indicate the parts of the matrices that still are to be taken into account in the truncated SVD. The new, cleaned, matrix S^T_{LM} has the property that its rank is exactly equal to K while the sum $\sum |s_{lm} - s^T_{lm}|^2$ is minimal. However, due to the influence of the noise on the signal related singular values and vectors, the new data matrix S^T_{LM} has ceased to have exactly Hankel structure.

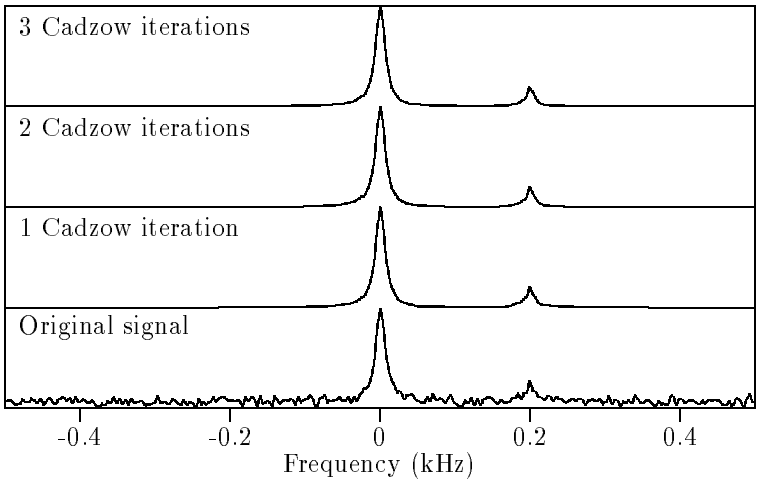

Figure 2.2: *Example of a Cadzow-based signal enhancement. The FT's of the original signal and the enhanced signals after 1, 2 and 3 Cadzow iterations are plotted. The signal was simulated with two exponentially decaying sinusoids and computer-simulated noise. The SNR = 5 (for the smallest peak).*

It now is possible to restore the Hankel structure, while at the same time the rank remains equal to K. To that end the following, *iterative*, procedure should be completed:

- Apply the truncated SVD according to Equation 2.7.
- Restore the Hankel structure by averaging the matrix elements on the anti diagonals.
- Repeate these steps until convergence has been reached.

The fact, that the second step leads to restoring the Hankel structure can be seen as follows. Suppose, starting from the almost Hankel matrix S^T_{LM}, that *in the Least Squares sense* we want to determine a related matrix H with Hankel structure. To that end the sum $\sum |s^T_{lm} - h_{lm}|^2$ needs to be minimized. Differentiating to the matrix elements of H yields

$$\sum 2(s^T_{lm} - n_{l+m} h_{l+m}) = 0 \quad \text{or} \quad h_{l+m} = \sum \frac{s^T_{lm}}{n_{l+m}}, \tag{2.8}$$

where we have used the Hankel property $h_{lm} = h_{l+m}$ and n_{l+m} is the number of matrix elements on the $l+m$ 'th anti diagonal of H.

The signal enhancement technique, just described, was proposed by Cadzow [15]. The method was applied to simulated one-dimensional (1-D) time-domain signals in [16] and to *in vivo* ^{31}P calf muscle signals in [17]. An extension of the Cadzow method was applied

to 2-D simulated NMR FID's in [18]. Another variation on the approach was proposed in [19] [20], where the rank reduction and Hankel restoration is based on the Minimum Variance (MV) estimation method.

In Figure 2.2 an example is presented of a signal enhancement, realized with the Cadzow method. The FT of an enhanced, simulated, time-domain signal is shown, comprising two exponentially decaying sinusoids and computer-simulated noise. After the first iteration step it is visible that the related frequency domain still contains more features than two Lorentz lines. However, after three iteration steps the spectrum shows only the two Lorentz lines. Concerning the parameters of the resulting Lorentz lines (frequency, line width, line intensity and phase) it should be mentioned, that their values still may be influenced by the noise realization, concerned.

Conclusions:

(a) Signal enhancement of *in vivo* NMR FID signals is feasible via truncated SVD and Hankel restoration of the related data matrix.
(b) The procedure leads to a cleaned time domain and corresponding frequency domain, but improvement of the related parameters is not automatically ensured.

2.4.5 Linear Prediction (LP) and SVD

In subsection 2.4.1 it was mentioned that, when applying a noniterative quantification method, the original nonlinear model function needs to be replaced by an alternative model function, then containing exclusively linear parameters. A linear model function, often used in the signal processing world, is the so-called Linear Prediction (LP) model. This model amounts to assuming, that each time-domain data point can be predicted by a linear combination of preceding or future data points. In case of *backwards* prediction one can write

$$\hat{s}_n = q_1 s_{n+1} + q_2 s_{n+2} + \ldots + q_M s_{n+M}. \tag{2.9}$$

where $n = 0, 1, \ldots, N - M - 1$ and usually $M \gg K$ (K is the number of harmonic components). The caret on $\hat{s}_n$ indicates that we are dealing with a model function data point. The coefficients q_m ($m = 1, 2, \ldots, M$) are called the LP coefficients. It is important to mention that they do not depend on n and consequently do not contain information on the amplitudes and phases.

If no noise is present in the time-domain signal and the decay is exponential, it can easily be shown that Equation 2.9 is exactly true. Moreover, in that case the length of the LP equation needs not to be chosen longer than $M = K$. For example, for a noiseless time-domain signal, consisting of two exponentially decaying siusoids, $M = 2$ is enough to decribe the time-domain signal. For the two LP coefficients it can be derived, that

$$q_1 = \frac{\zeta_1 + \zeta_2}{\zeta_1 \zeta_2} \quad \text{and} \quad q_2 = -\frac{1}{\zeta_1 \zeta_2}. \tag{2.10}$$

Furthermore it appears, that the roots of the second-degree polynomial

$$\zeta^2 - q_1 \zeta - q_2 = 0 \tag{2.11}$$

are exactly equal to $\frac{1}{\zeta_1}$ and $\frac{1}{\zeta_2}$, respectively, i.e. to the reciprocals of the signal poles.

In general, when the time-domain signal is disturbed by noise, the LP Equation 2.9 is not exactly true. However, the error that is made, can be kept small if the length of the LP equation $M \gg K$ (see [21]). Loosely speaking one could say, that by choosing $M \gg K$ additional LP coefficients can be used to account for the noise components. As a consequence of this choice not K but M poles need to be determined, of which K are signal related poles and $M - K$ are noise related poles. In matrix notation the LP Equation 2.9 for all n can be written as

$$\begin{pmatrix} \hat{s}_0 \\ \hat{s}_1 \\ \vdots \\ \hat{s}_{N-M-1} \end{pmatrix} = \begin{pmatrix} s_1 & s_2 & s_3 & \cdots & s_M \\ s_2 & s_3 & s_4 & \cdots & s_{M+1} \\ \vdots & \vdots & \vdots & \cdots & \vdots \\ s_{N-M} & s_{N-M+1} & s_{N-M+2} & \cdots & s_{N-1} \end{pmatrix} \begin{pmatrix} q_1 \\ q_2 \\ q_3 \\ \vdots \\ q_M \end{pmatrix}. \tag{2.12}$$

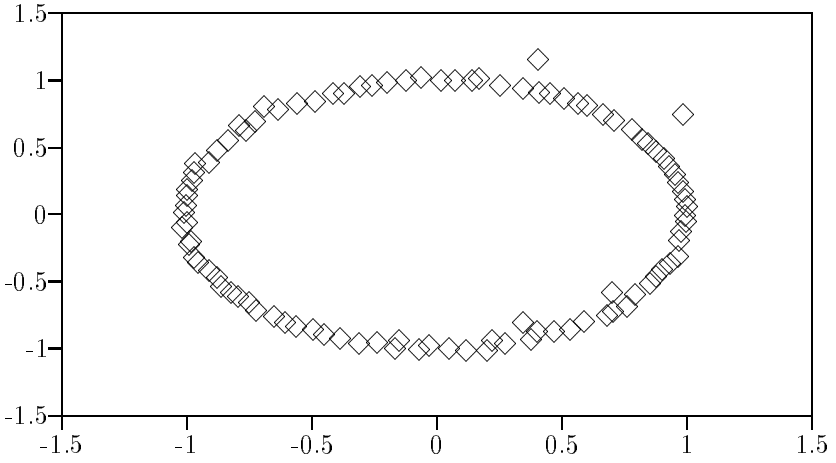

Figure 2.3: *Plot in the complex plane of 2 signal poles and 98 additional poles of a simulated time-domain signal, containing two exponentially decaying sinusoids and computer-simulated noise. Notice that the signal poles are located outside the unit circle and the other poles inside and close to the unit circle.*

Notice that the matrix has the same Hankel structure as the data matrix, introduced in subsection 2.4.2. In order to determine the LP coefficients q_m ($m = 1, 2, \ldots, M$), the sum $\sum |s_n - \hat{s}_n|^2$ for $n = 0, 1, \ldots, N - M - 1$ needs to be minimized. In practice $M \approx \frac{2N}{3}$ is taken (see [21]), i.e. $N - M < M$. This means that we have to deal with an under determined Least-Squares (LS) problem. It has been proven by Lawson and Hanson [14] that the unique, so-called minimum length, solution of this LS problem is equal to

$$\vec{q} = V_{MK} \Lambda_K^{-1} U_{N-M,K}^{\dagger} \vec{s}, \tag{2.13}$$

where the -1 on Λ_K^{-1} indicates the inverse of Λ and it is assumed that the rank of the data matrix $K \leq N - M$. It appears that the truncated SVD helps to solve the LS problem, concerned.

Once the $\vec{q}$ vector has been determined with the procedure, just described, the poles with among them the signal related poles, are to be calculated. It can be shown that for an arbitrary length M of the LP equation the reciprocals of the poles are equal to the roots of the M-degree polynomial (see above for the $M = 2$ example)

$$\zeta^M - q_1\zeta^{M-1} - \ldots - q_M\zeta^0 = 0. \tag{2.14}$$

A problem now is that as many as M poles are determined, whereas only K poles are related to the harmonic components and $M - K$ to the noise. An important point is, however, that in case of *backwards* prediction (see Equation 2.9) the signal poles have a length ≥ 1 and thus are located outside the unit circle, when plotted in the complex plane. It can be shown [21] that the noise related poles are independent of forwards or backwards prediction and that they are always located inside the unit circle. In practice this property can be used to separate the signal and noise related poles (see Figure 2.3).

As a last step in the LPSVD algorithm one has to calculate the complex-valued amplitudes (see Equation 2.2). To that end the found signal poles are substituted into Equation 2.1 and subsequently the remaining *linear* LS problem is solved in one single step. Finally, from the complex-valued amplitudes the real-valued amplitudes (line intensities) and the phases of the sinusoids are calculated.

2.4.6 Example 1: Application of LPSVD to an *in vivo* ^{31}P NMR FID signal

In this example the quantitative data analysis is presented of an *in vivo* ^{31}P NMR FID signal of a tumour, implanted in a mouse [22]. The measurement was performed on the 7T NMR system of the Spin Imaging (SI) group of the Applied Physics Department of the University of Technology in Delft. As quantitative data analysis method the LPSVD approach was applied. Figure 2.4 shows the real part of the complex-valued experimental signal, the fitted model function and the residue. The latter seems to contain only noise.

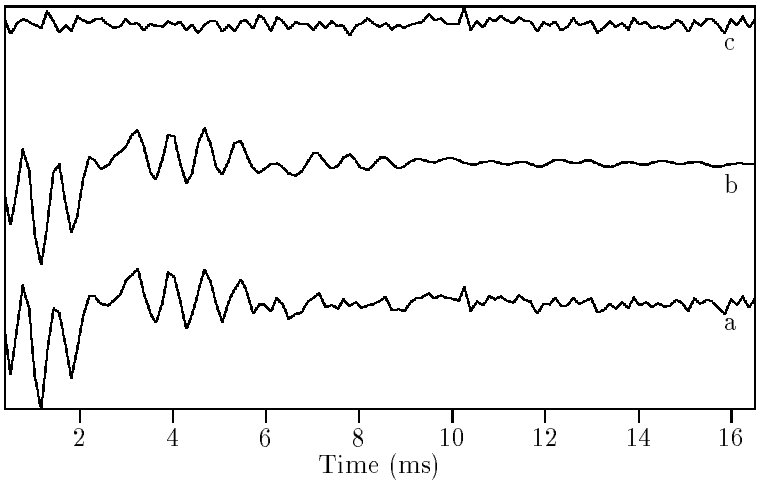

Figure 2.4: *The in vivo ^{31}P NMR FID signal of a tumour, implanted in a mouse. Plot of the real part of (a) the experimental signal, (b) the model function, fitted by LPSVD and (c) the residue.*

In Figure 2.5 a graphical display is presented of the singular values of the data matrix, concerned. It can be seen that a jump exist somewhere in the neighbourhood of singular values #8 or #9. As a result of the low SNR this jump is not clearly visible.

name of signal file:	mouse31p.dat
number of data-points of signal:	125
step-size of signal (ms):	0.130
begin time of signal (ms):	0.390
number of data-points in LPSVD:	125
length of LP equation:	88
number of frequencies:	9
signal noise level:	$0.2097E-01$
RMS error of LPSVD fit:	$0.2188E-01$

Frequency	2CR	Decay	2CR	Amplitude	2CR	Phase	2CR
kHz	kHz	kHz	kHz	a.u.	a.u.	degrees	degrees
-1.2361	0.0094	0.3369	0.0589	0.17	0.02	-79.33	7.32
-0.5237	0.0555	0.0327	0.3486	0.01	0.02	-102.58	206.99
-0.4567	0.0487	0.3177	0.3058	0.06	0.05	-66.37	54.34
-0.1793	0.0122	0.4913	0.0764	0.36	0.05	-92.94	8.86
0.0169	0.0156	0.1123	0.0978	0.03	0.02	-56.36	35.37
0.4300	0.0079	0.2651	0.0494	0.15	0.02	-78.25	8.42
0.7341	0.0198	0.1236	0.1246	0.02	0.01	-74.24	38.18
1.3255	0.0063	0.1950	0.0393	0.12	0.02	-86.68	9.11
1.5711	0.0099	0.4139	0.0621	0.25	0.03	-116.38	6.89

Table 2.1: *Numerical results of the LPSVD quantification of the ^{31}P mouse signal. The amplitudes and phases belong to the time $t = 0$.*

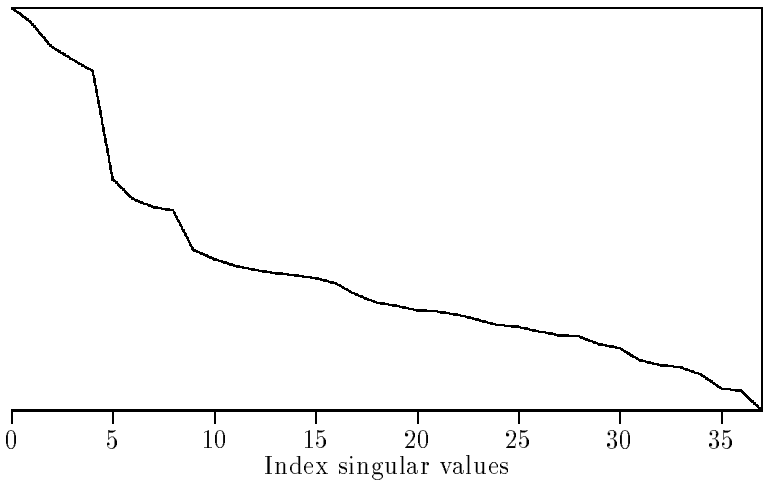

Figure 2.5: *Plot of the singular values of the data matrix, belonging to the ^{31}P mouse signal.*

The results of the quantitative data analysis are presented in Table 2.1. Notice that the root-mean-square (RMS) error of the fitting result is about as large as the standard deviation of the noise (the signal noise level). This numerical result is in agreement with the fact that the graphical presentation of the residue is exclusively noisy (see Figure 2.4). Another point to be mentioned is that the phases of certain harmonic components differ more than tens of degrees from the overall phase factor (the zero-order phase) of the signal (the latter being about -83^0). This variation in individual phases is due to the influence of the noise. Concerning the phase of the second peak in the table it can be added that the related large statistical error indicates that this peak possibly is a noise related component. Other indications for this are the unrealistic small decay constant and the small amplitude (smaller than the standard deviation of the noise).

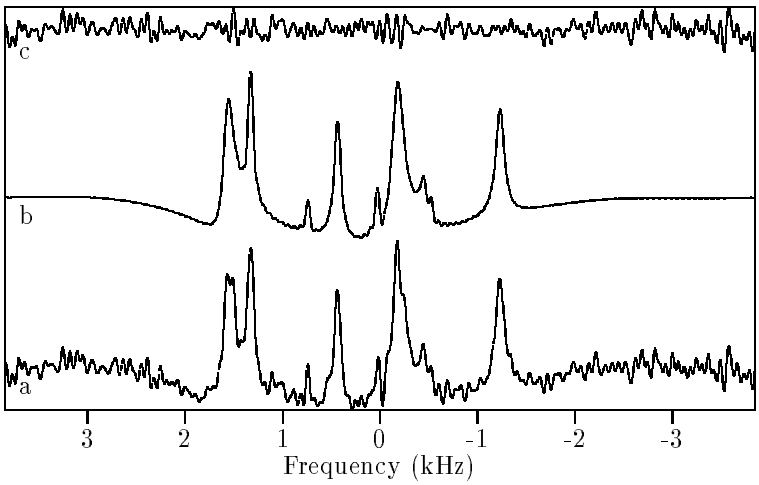

Figure 2.6: *Real part of the FT of (a) the ^{31}P mouse signal (b) the fitted model function and (c) the residue.*

Although the results of the quantification are reflected by the time-domain parameters, presented in Table 2.1, in practice it is often to be recommended to give a graphical presentation of the results in the related frequency domain. In Figure 2.6 the real part of the FT is displayed of the experimental signal, the fitted model function and the residue, respectively. Important to be mentioned is that the FT of the residue shows no features larger than the noise at the position of the peaks.

2.4.7 The SVD-based State Space method

A second noniterative method for quantifying *in vivo* NMR time-domain signals, that will be treated in these lecture notes, is the SVD-based State Space method [23] [24]. Like the LPSVD method, described in the previous subsection, the SVD-based State Space method assumes that the exponential decay model can be applied. The method was first published in [23] and introduced in the NMR world in [24] under the name HSVD. Improvements of the method can be found in [25].

Although described in [23] in a State Space manner, the method will be described in these lecture notes in the context of linear algebra. The basic idea behind HSVD is that a Hankel data matrix of a noiseless exponentially decaying time-domain signal, comprising K sinusoids, can be factorized as follows (see also Equation 2.1).

$$\hat{S} = \begin{pmatrix} 1 & \cdots & 1 \\ \zeta_1^1 & \cdots & \zeta_K^1 \\ \vdots & \cdots & \vdots \\ \zeta_1^{L-1} & \cdots & \zeta_K^{L-1} \end{pmatrix} \begin{pmatrix} c'_1 & \cdots & 0 \\ \vdots & \ddots & \vdots \\ 0 & \cdots & c'_K \end{pmatrix} \begin{pmatrix} 1 & \zeta_1^1 & \cdots & \zeta_1^{M-1} \\ \vdots & \vdots & \cdots & \vdots \\ 1 & \zeta_K^1 & \cdots & \zeta_K^{M-1} \end{pmatrix} = F_{LK} C'_K \tilde{F}_{MK}, \tag{2.15}$$

where $\zeta_k = \exp[(-\alpha_k + i2\pi\nu_k)\Delta t)]$ and $c'_k = c_k \zeta_k^\delta$ for $k = 1, 2, \cdots, K$ and L and M should be chosen greater than K, subject to the constraint $L + M = N + 1$. The matrix F_{LK} is a so-called Vandermonde matrix. The tilde on $\tilde{F}_{MK}$ denotes transposition.

We call Equation 2.15 the Vandermonde decomposition of the model function matrix $\hat{S}$. The essence of the State Space procedure now is that it brings about a Vandermonde decomposition of the data matrix S as closely as possible, i.e. in the LS sense. In order to arrive at this Vandermonde decomposition, the data matrix S is first subjected to truncated SVD according to Equation 2.7. Next we state without proof [23] that the Vandermonde decomposition of Equation 2.15 can always be transformed into a product of matrices that have the same structure and size as the SVD matrices of Equation 2.7, i.e.

$$F_{LK} C'_K \tilde{F}_{MK} \;=\; \hat{U}_{LK} \hat{\Lambda}_K \hat{V}^\dagger_{MK} \tag{2.16}$$

where the caret on the SVD matrices indicates that these matrices are related to the model function matrix rather than to the data matrix. It can be shown that an important property of the Vandermonde matrix F_{LK} also is present in the related left singular vector matrix $\hat{U}_{LK}$, albeit in a slightly different form. In matrix notation this property is

$$F_{LK,t} = F_{LK,b} Z_K \;\text{ and }\; \hat{U}_{LK,t} = \hat{U}_{LK,b} Z'_K, \tag{2.17}$$

where the subscript t or b indicates that either the top or bottom row of the original matrix has been removed, Z_K is a $K \times K$ diagonal matrix with on its diagonal the signal poles ζ_k $(k = 1, 2, \ldots, K)$ and Z'_K is related to Z_K by the diagonalization transformation.

From Equation 2.17 it is straightforward to derive that

$$Z'_K = (\hat{U}^\dagger_{LK,b} \hat{U}_{LK,b})^{-1} \hat{U}^\dagger_{LK,b} \hat{U}_{LK,t}. \tag{2.18}$$

If the NMR FID time-domain signal is noiseless and exponentially decaying, the $\hat{U}_{LK}$ can be replaced by U_{LK} and the solution of Equation 2.18 is exact. However, if the signal is disturbed by noise, or if the decay is nonexponential, or both, then replacing $\hat{U}_{LK}$ by U_{LK} means that Equation 2.18 is solved in the LS sense.

Once the matrix Z'_K has been computed and transformed into Z_K by diagonalization, the decay constants and the frequencies can be determined from the signal poles, present on the diagonal of Z_K. The last step in the State Space procedure then is to calculate the real-valued amplitudes and the phases by fitting Equation 2.1 to the data points with the decay constants and frequencies fixed to the values just found.

2.4.8 Calculation of the SVD via the normal equations approach

Various algorithms are available for calculating the singular values and matrices of general matrices. The computational load of the SVD of a general matrix is proportional to the third power of the size of that matrix [26]. Thus, when the matrix at hand is large, the processing may become prohibitively long. One way of addressing this problem is to calculate the singular values and matrices via the normal equations approach [14]. The essence of this approach is that the SVD is accomplished via diagonalization of the matrix products $SS^\dagger$ or $S^\dagger S$, where S is the Hankel data matrix, introduced in Equation 2.3. The fact that diagonalyzing the above mentioned matrix products leads to the SVD quantities can be seen as follows. If we take the matrix product $SS^\dagger$, we can write

$$SS^\dagger = U\Lambda V^\dagger V\Lambda^\dagger U^\dagger = U\Lambda^2 U^\dagger \quad \text{or} \quad U^\dagger SS^\dagger U = U^\dagger U\Lambda^2 U^\dagger U = \Lambda^2, \tag{2.19}$$

where we have used the property $U^\dagger = U^{-1}$ and $V^\dagger = V^{-1}$ of unitary matrices. Furthermore, Λ^2 represents a square, diagonal, matrix with on its diagonal the squares of the singular values. A similar derivation can be given for the matrix product $S^\dagger S$.

The advantage of the method, just described, is that it is very efficient when considering the computational time. Firstly, the time needed for calculating the matrix products can be minimized, since one can employ the Hankel property $s_{lm} = s_{l+m}$ (see [26]). Secondly, if one chooses the smallest of the two products (in our case the product $SS^\dagger$), then a smaller matrix has to be diagonalized than the original matrix S. A disadvantage of the method could be that some precision might be lost when computing the matrix products. However, in practice this effect is negligible since the calculations can be carried out in double precision and moreover the data values usually have a limited number of significant digits due to the disturbance of the noise.

2.4.9 Rapid SVD of a Hankel data matrix using the Lanczos algorithm

The problem of reducing the long computational time of SVD has been addressed, for instance, in [26], [27], [28] and [29]. An alternative to the normal equations approach, described in the previous subsection, is to compute only those singular values and vectors that represent the signal and ignore all others. Such a strategy can be successfully carried out by invoking the so-called Lanczos algorithm [27]. Theatment of this algorithm is beyond the scope of these lecture notes. Here we restrict ourselves to describing in general terms those points that were given attention in [29].

The main point is that the Lanczos algorithm is capable of *exploiting the Hankel structure* of the data matrix, defined in Equation 2.3. To explain that we first must reformulate the SVD of the $L \times M$ complex-valued data matrix $S = S' + iS''$ as a diagonalization of a real-valued, square, symmetric $2(L + M) \times 2(L + M)$ matrix B, defined as

$$B = \left[\begin{array}{cc|cc} & & S' & S'' \\ & 0 & -S'' & S' \\ \hline \tilde{S}' & -\tilde{S}'' & & \\ \tilde{S}'' & \tilde{S}' & 0 & \end{array}\right]. \tag{2.20}$$

The matrix B is now to be diagonalized according to

$$B = RD\tilde{R}, \tag{2.21}$$

where D is a diagonal matrix and R an orthogonal matrix. The singular values and vectors can be found at specific positions in D and R, respectively. In the following we concentrate on the diagonalization of B by means of the Lanczos algorithm, exploiting the symmetry present in data matrix S. Note that in the actual computer implementation the inflation of the 1-D time-domain data into the matrix S and subsequently from S into B was not carried out literally, so that no computer memory was wasted on this.

The gist of the Lanczos algorithm is that the matrix B is converted into tridiagonal form by means of an iterative process, without generating intermediate and dense submatrices. In this process information about the *larger* eigenvalues can be made available long before total conversion into tridiagonal form has been achieved. Therefore the algorithm lends itself very well to restricting the retrieval of the eigenstructure to *only the signal part* (and not the noise part) of the data matrix.

The most time-consuming part of each Lanczos iteration is the matrix-vector multiplication $B\vec{v}_j$, where $\vec{v}_j$ is a real-valued, so-called Lanczos vector of the j'th iteration and of size $2(L+M)$. For notational convenience the subscript j is dropped from now on. If $\vec{v}$ is partitioned into four vectors $\vec{v_a}$, $\vec{v_b}$, $\vec{v_c}$ and $\vec{v_d}$ of sizes L, L, M and M, respectively, then the calculation of $B\vec{v}$ is seen to amount to calculating $\tilde{S}(\vec{v_a} + i\vec{v_b})$ and $S^*(\vec{v_c} + i\vec{v_d})$, where * denotes complex conjugation. Now, in order to exploit the *symmetry* of the data matrix S, we note that a Hankel matrix is a submatrix of a so-called *circulant* matrix. Every row of a circulant matrix is derived from the previous row by a cyclic permutation. For the problem at hand we require an $N \times N$ circulant matrix Y whose first row equals $(s_0, s_1, \ldots, s_{N-1})$ and the cyclic permutation is to be executed from the left. By embedding S^* into Y^* and zero-padding $\vec{v_c}$ and $\vec{v_d}$ up to size N, we can replace the matrix-vector product $S^*(\vec{v_c} + i\vec{v_d})$ by

$$Y^* \begin{pmatrix} \vec{v_c} + i\vec{v_d} \\ 0 \quad + i0 \end{pmatrix}. \tag{2.22}$$

A similar procedure can be applied to $\tilde{S}(\vec{v_a} + i\vec{v_b})$. It is by writing Equation 2.22 that the opportunity of saving computational time emerges. The underlying idea is that the

product of a circulant matrix and a vector can be carried out very efficiently *with the aid of FFT*. By using this property, the computational burden of SVD of a Hankel matrix can be reduced considerably. Another reduction can yet be achieved by choosing the starting values of $(\vec{v_a} + i\vec{v_b})$ or $(\vec{v_c} + i\vec{v_d})$ equal to zero. By doing so the multiplication $B\vec{v}$ is simplified not only in the first iteration, but also in the subsequent ones.

Concerning the performance of the Lanczos approach, we have reported in [29] a reduction in computational time by a factor of 80, when comparing with the normal equations approach and by a factor of 430, when comparing with the Linpack ZSVDC procedure. The *in vivo* NMR signal, concerned, comprised 15 exponentially decaying sinusoids and the number of the data points (N) was 1024.

When considering the reduction in computational time, just mentioned, a word of caution is in order here. If no clear distinction between signal and noise related singular values is present, a large number of Lanczos iterations are required to obtain the smaller singular values. As a result of that the gain in computational time might be lost. However, a reduction of about a factor of two (relative to the normal equations approach) is still feasible in those cases.

2.4.10 Example 2: Application of HSVD to an *in vivo* ^{31}P NMR FID signal

In this example the HSVD method is applied to the same time-domain signal as of example 1 (see Figure 2.4). The goal is to find out to what extent the quantitative result of HSVD differs from that of LPSVD. Since both methods are based on the same SVD of the data matrix and only differ in the way the signal poles are determined, the quantitative results will not deviate too much.

Table 2.2 shows the HSVD result. The values of the model parameters are to be compared with those of Table 2.1.

The two quantifications particularly differ in the parameters of the components, located in the tails of the largest component. Furthermore it is remarkable that HSVD 'chooses' as smallest component another peak than LPSVD (see Figure 2.7).

name of signal file:	mouse31p.dat
number of data-points of signal:	125
step-size of signal (ms):	0.130
begin time of signal (ms):	0.390
number of data-points in HSVD:	125
size parameter of Hankel matrix:	88
number of frequencies:	9
signal noise level:	$0.2097E-01$
RMS error of HSVD fit:	$0.2206E-01$

Frequency	2CR	Decay	2CR	Amplitude	2CR	Phase	2CR
kHz	kHz	kHz	kHz	a.u.	a.u.	degrees	degrees
-3.5657	0.0201	0.0133	0.1266	0.01	0.01	-128.86	64.06
-1.2390	0.0101	0.3646	0.0632	0.18	0.02	-76.19	7.40
-0.4471	0.0584	0.6272	0.3667	0.13	0.07	-87.90	37.55
-0.1860	0.0199	0.5957	0.1252	0.45	0.09	-81.50	14.35
-0.0268	0.0224	0.1720	0.1410	0.04	0.03	30.35	45.68
0.4300	0.0091	0.2982	0.0573	0.16	0.02	-76.51	9.16
0.7423	0.0296	0.2164	0.1857	0.03	0.02	-80.59	38.40
1.3291	0.0067	0.2074	0.0421	0.13	0.02	-93.16	9.57
1.5662	0.0108	0.4496	0.0676	0.27	0.03	-113.17	7.14

Table 2.2: *Numerical results of the HSVD quantification of the ^{31}P mouse signal. The amplitudes and phases belong to the time $t = 0$.*

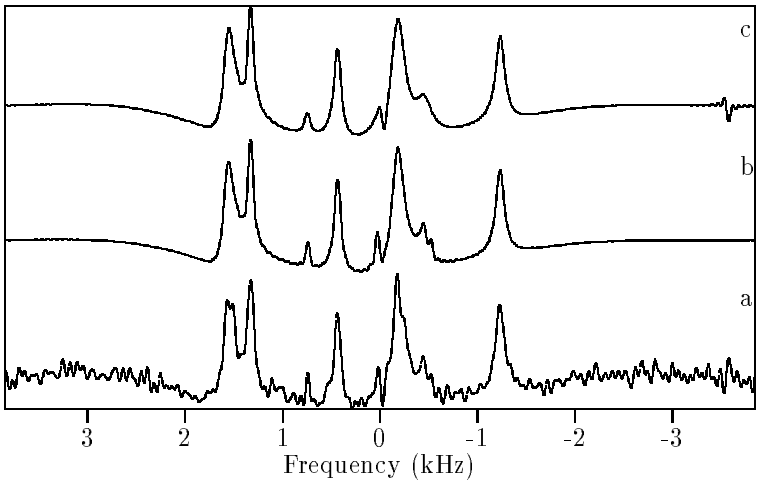

Figure 2.7: *Comparison of LPSVD and HSVD. Real part of the FT of (a) the ^{31}P mouse signal (b) the fitted LPSVD model function and (c) the fitted HSVD model function.*

2.5 Iterative fitting methods

2.5.1 The Maximum Likelihood (ML) method

In section 2.4 we have discussed that model function parameters, entering the model function in a nonlinear manner, can be determined noniteratively if the model function, concerned, can be replaced by an alternative, linear, model function. In this section we omit this step, i.e. we work directly with the original model function. In general this means that one has to deal with nonlinear Least Squares (LS) fitting, which may lead to time-consuming computer algorithms.

At this point it seems in order to ask the question whether there exists a *standard of precision* to which the results of *any* quantification method should be compared. Such a standard is indeed available, in the form of the so-called Cramer-Rao (CR) lower bounds [13]. In order to treat this we must first introduce another concept, namely that of the Maximum Likelihood (ML) method [13].

The starting point of the ML method is that there is a joint probability distribution function for all data points of the time-domain signal, concerned.

More precisely speaking, we assume the following:

- For each data point the probability distribution function of its related noise contribution is known.
- A model function is available that exactly describes the data points if no noise is present.

An important example of a joint probability distribution function is the one, valid for uncorrelated, Gaussian-distributed, noise

$$\rho(\vec{s},\vec{\sigma},\vec{p}) = \prod_{n=0}^{N-1} \left(\frac{1}{2\pi\sigma_n^2}\right)^{\frac{1}{2}} \exp\left[\frac{-1}{2\sigma_n^2}\{s_n - \hat{s}_n(\vec{p})\}^2\right], \tag{2.23}$$

where $\vec{s}$ is the vector of the time-domain data points, $\vec{\sigma}$ is the vector of the noise standard deviations σ_n $(n = 0, 1, \ldots, N-1)$, $\hat{s}_n(\vec{p})$ is the model function value, to be fitted to the n'th data point and $\vec{p}$ is a vector, containing the model function parameters.

Strictly speaking, one should take the product of two distribution functions in case of complex-valued data points, one for the real part and one for the imaginary part (assuming, that there is no correlation between the two parts).

Given the series of data points $\vec{s}$, the ML method now amounts to estimating the model function parameters $\vec{p}$ in such a way that the joint probability distribution function becomes maximal. If we take the Gaussian-noise example of Equation 2.23, it is convenient to maximize the natural logarithm of the distribution function, rather than the distribution function itself. If it is assumed that the standard deviations of all noise contributions are equal to σ, then one obtains to maximize

$$\text{constant} - \frac{1}{2\sigma^2} \sum_{n=0}^{N-1} |s_n - \hat{s}_n|^2. \tag{2.24}$$

Equation 2.24 implies that in case of uncorrelated, Gaussian-distributed, noise the ML method in fact amounts to applying the Least Squares (LS) method.

The question now may be, why should one advocate the usage of the ML method? In this context it should be noted, that the ML method has a number of important statistical properties that justify advertisement:

- For a sufficient number of data points the statistical errors (the standard deviations) of the estimated model function parameters approach certain fundamental lower bounds, the so-called Cramer-Rao lower bounds.
- Assuming that the correct model function is used, the estimated model function parameters have no systematic errors, i.e. they are unbiased.
- If the model function parameters are estimated with the precision of the ML method, then derived functions of these parameters also have the ML property.

The latter point may have important consequences in practical cases. For instance, suppose that the coefficients of the Linear Prediction (LP) model function have been determined by some ML method. This means that the signal poles, obtained via factorization of the LP polynomial, also have the ML precision.

At this point we are ready to turn to the standard of precision, mentioned at the beginning of this subsection. It will be dealed with in the next subsection.

Conclusions:

(a) When quantifying time-domain signals with uncorrelated, Gaussian-distributed, noise, using the Least Squares method means applying the Maximum Likelihood method.
(b) The statistical errors of the ML method approach fundamental lower bounds, the Cramer-Rao lower bounds.
(c) If the model function, used by the ML method, correctly describes the time-domain data points, the estimated parameters have no systematic errors.

2.5.2 The Cramer-Rao (CR) lower bounds

It can be shown that the theory of the Maximum Likelihood estimation leads to lower bounds on the statistical errors (standard deviations) of the estimated model function parameters [13]. The existence of such bounds, called the Cramer-Rao (CR) lower bounds, implies that *irrespective of the method* used to quantify the parameters from the data, there is a lower bound on the precision that *can not be superseded.* For reasons of time and space we present in these lecture notes only a recipe for evaluating the CR lower bounds. For a general description of the CR theory we refer to [13].

We assume the following:

- The data points of the *in vivo* NMR time-domain signal are described by

  $s_n = \hat{s}_n + \epsilon_n$ with $n = 0, 1, \ldots, N-1$,

  where $\hat{s}_n$ is the model function value and ϵ_n the noise contribution of the n'th data point.

- The noise contribution of each data point has a Gaussian distribution function with a mean equal to zero and a standard deviation equal to σ.
- The noise contributions of successive data points are uncorrelated. There is also no correlation between the real and imaginary part of the complex-valued data points.

The essential part of the CR theory now is to construct a so-called Fisher Information matrix I, whose elements in case of Gaussian noise are given by

$$I_{ij} = \frac{1}{\sigma^2} \Re \left[\sum_{n=0}^{N-1} \frac{\partial \hat{s}_n^*}{\partial p_i} \frac{\partial \hat{s}_n}{\partial p_j} \right], \tag{2.25}$$

where $i, j = 1, 2, \ldots, J$, if there are J model function parameters to be estimated.

It can be shown that the CR lower bound on the standard deviation of the i'th parameter is given by

$$\sigma_{p_i} \geq CR_{p_i} = \sqrt{I_{ii}^{-1}}, \tag{2.26}$$

where the -1 on I_{ii}^{-1} indicates, that the inverse of the Fisher Information matrix should be taken.

Equations 2.25 and 2.26 enable one to evaluate the fundamental lower bounds on the precision of the parameter estimates. For certain simple cases one can derive closed-form formulae that can provide useful insight. One result, agreeing with common sense, is that for uncorrelated Gaussian noise the CR lower bounds are proportional to σ (the standard deviation of the noise).

In clinical circumstances, when performing an *in vivo* NMR experiment, there is no time for repeating a measurement. This means that in practice there is no possibility of actually determining the standard deviations of the estimated parameters. Now, if one knows that the quantification method at hand is based upon the Maximum Likelihood principle, one can replace the unknown standard deviations by the related theoretical CR lower bounds [30]. It should be noted, however, that Equation 2.26 contains the model function parameters, of course. This means that calculating the CR lower bounds with the estimated parameters only works if the values of these parameters are not deviating too much from their true values.

The Cramer-Rao inequality, shown in Equation 2.26, works with the diagonal elements of the inverse of the Fisher Information matrix. It should be noted, that the nondiagonal elements of I^{-1} give information about the *correlation* between the model function parameters. For instance, in case of heavily overlapping NMR peaks (when looking in the frequency domain) there will be large correlations between the parameters of the peaks, concerned. Usually this also leads to large statistical errors of the parameters.

2.5.3 The Monte Carlo study

When discussing the concept of the Maximum Likelihood (ML) estimation, the question may arise, how do we know whether our quantification method at hand is a ML method? The answer to that is that it can be tested by means of a Monte Carlo study. According to A. Tarantola in 'Inverse Problem Theory' is [31]

any study that uses at some stage a random generator is called a Monte Carlo study, in homage to the famous casino.

In our case, when using the Monte Carlo study for testing some quantification method of *in vivo* NMR signals, the Monte Carlo study amounts to the following:

- The quantitative data analysis method, concerned, is applied to a series of *simulated* time-domain signals. This means that the quantification can be carried out in a *controlled* way (the true parameter values are known).
- The series of simulated time-domain signals are obtained by adding to a noiseless signal a number of (say of the order of 100) different computer-generated Gaussian noise realizations, each with zero mean and with the same standard deviation.
- All simulated signals are quantified with the method, to be tested, and the mean values and standard deviations of the model function parameters are calculated.
- The theoretical CR lower bounds of the parameters are calculated, using the true parameter values.
- The mean estimated parameter values are compared with the true values.
- The standard deviations are compared with the CR lower bounds.

If the quantification method has the ML property, the mean estimated parameters should be equal to the true parameters and the standard deviations should be slightly larger than the CR lower bounds.

In practice, uncorrelated, Gaussian-distributed, noise can be generated by the computer. A reasonable approximation of a Gaussian distribution is obtained by using the formula

$$\epsilon_n = \sigma(\sum_{k=1}^{12} \eta_{kn} - 6) \quad (n = 0, 1, \ldots, N-1), \tag{2.27}$$

where η_{kn} $(k = 1, 2, \ldots, 12)$ are computer-generated random numbers. The subscript n on η_{kn} indicates that for each data point one should use another series of random values. An eventual deviation from the Gaussian distribution can be tested by calculating the first, second and fourth moment [13]. For example, a test of 10 noise realizations of 1024 data points, generated on a Sun-3/160 workstation, yielded for the first, second and fourth moment 0.00(3), 1.03(6) and 3.1(4), respectively, where the numbers in parentheses are the standard deviations and the standard deviation of the noise was equal to 1.

2.5.4 Quantitative data-analysis methods and the threshold signal-to-noise-ratio

For each quantification method there exists a certain signal-to-noise-ratio (SNR), below which the method can not produce the correct values of the model parameters. This SNR is called the *threshold* SNR. In case of methods, based on the Maximum Likelihood principle, it means that the standard deviations of the parameters are no longer almost

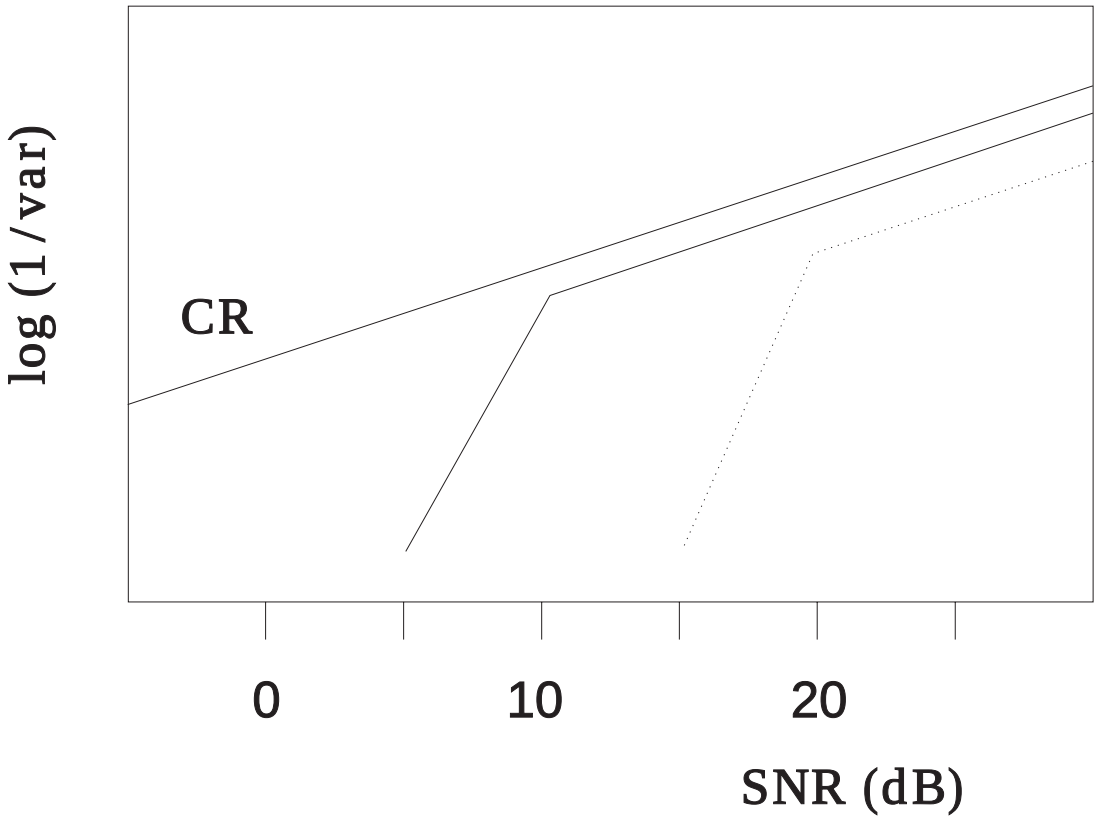

Figure 2.8: *Graphical display of* $\log(\frac{1}{var})$ *as a function of the SNR. The quantity* **var** *is the variance of a certain model parameter. The line represents the dependence of the Cramer-Rao lower bound. The solid curve shows the dependence of a Maximum Likelihood method with a threshold SNR of about 10 dB and the dotted curve the dependence of a method that is not based on the Maximum Likelihood principle.*

equal to the Cramer-Rao lower bounds. Depending on the character of the NMR signals concerning frequency differences and/or magnitudes of the NMR components it may well be that a few NMR components are already 'below threshold' and the others not.

It is difficult to give, in general, a mathematical description of the threshold problem. Nevertheless, for a number of quantification methods an estimation of the magnitude of the threshold SNR is known [21]. These estimated values usually are based on Monte Carlo studies. For instance, for SVD-based methods a threshold SNR of about 10 dB is found, where the SNR is defined as

$$SNR = 10 \log \frac{signal\ power}{noise\ variance} = 10 \log \frac{\sum_{n=0}^{N-1} s_n^* s_n}{2N\sigma_{noise}^2}, \tag{2.28}$$

where the factor 2 is required, if the real- and imaginary part of the complex-valued noise are uncorrelated. In Figure 2.8 a schematic picture is shown of how the result of a Monte-Carlo study would look like, if the study was aiming on determining the threshold SNR.

One of the important aspects of studies for improving quantitative data-analysis methods is to find out, how the threshold SNR of those methods can be lowered. A lower threshold SNR means, for instance, that the measurement time of the NMR experiments can be reduced.

2.5.5 The VARiable PROjection (VARPRO) method

A Maximum Likelihood based method, often applied in nonlinear fitting problems, is the so-called VARiable PROjection (VARPRO) method [5]. The name refers to the fact that the Least Squares (LS) solution of the model function parameters, concerned, projects the vector of the data points on the column space of the related function matrix. This projection of the data vector results from eliminating the linear parameters of the LS problem from the gradient descent process. In case of the *in vivo* NMR time-domain signals this means eliminating the complex-valued amplitudes. The advantage of this approach is that no starting values of the linear parameters are to be supplied.

When looking at Equation 1.6, the model function for an NMR FID time-domain signal can be generalized as

$$\hat{s}_n = \sum_{k=1}^{K} c_k f_k(t_n, \vec{p_k}) \quad \text{with} \quad n = 0, 1, \ldots, N-1, \tag{2.29}$$

where $c_k = a_k \exp(i\phi_k)$ is the complex-valued amplitude, the function $f_k(t_n, \vec{p_k})$ represents the remaining part of the model function and the vector $\vec{p_k}$ denotes the nonlinear parameters of the k'th NMR component (i.e. the decay constant and the frequency in case of the exponential decay model).

At this point it should be noted that the function $f_k(t_n, \vec{p_k})$ in general may be constructed from more than one basis function. Moreover, there may exist linear relations between certain model parameters of these basis functions. For instance, in case of NMR multiplets there are often linear relations between the line intensities, the line widths and the frequencies of the composing multiplet components.

In matrix form Equation 2.29 can be written as

$$\begin{pmatrix} \hat{s}_0 \\ \hat{s}_1 \\ \vdots \\ \hat{s}_{N-1} \end{pmatrix} = \begin{pmatrix} f_1(t_0, \vec{p_1}) & f_2(t_0, \vec{p_2}) & \cdots & f_K(t_0, \vec{p_K}) \\ f_1(t_1, \vec{p_1}) & f_2(t_1, \vec{p_2}) & \cdots & f_K(t_1, \vec{p_K}) \\ \vdots & \vdots & \cdots & \vdots \\ f_1(t_{N-1}, \vec{p_1}) & f_2(t_{N-1}, \vec{p_2}) & \cdots & f_K(t_{N-1}, \vec{p_K}) \end{pmatrix} \begin{pmatrix} c_1 \\ c_2 \\ \vdots \\ c_K \end{pmatrix} = F\vec{c}, \tag{2.30}$$

where we have defined the function matrix F and the linear-parameter vector $\vec{c}$ (constructed from the complex-valued amplitudes). In order to fit the linear parameters $\vec{c}$ and the nonlinear parameters $\vec{p_k}$ $(k = 1, 2, \ldots, K)$, the LS expression

$$| \vec{s} - F\vec{c} |^2 \tag{2.31}$$

needs to be minimized. As said at the beginning of this subsection, the VARPRO approach amounts to eliminating the linear parameters from the gradient descent process, i.e. eliminating the vector $\vec{c}$ from Equation 2.31. The latter can be effectuated by assuming temporary, that the nonlinear parameters of the Function matrix F are known. In that case we can write the following *linear* LS solution for the linear parameters

$$\vec{c} = (F^\dagger F)^{-1} F^\dagger \vec{s}. \tag{2.32}$$

Replacing $\vec{c}$ in Equation 2.31 by Equation 2.32 yields the following expression to be minimized in the iteration process

$$|(I - F(F^{\dagger}F)^{-1}F^{\dagger})\,\vec{s}\,|^2 = |P\vec{s}\,|^2, \tag{2.33}$$

where I is a unit matrix of the proper size and the quantity P can be shown to act as a projection operator.

Although the linear parameters are now eliminated from the gradient descent search, a price that has to be paid, is that the remaining LS expression is more complicated.

After fitting the nonlinear parameters of the function matrix F by minimizing Equation 2.33, the linear parameters $\vec{c}$ are calculated from Equation 2.32.

2.5.6 Example 3: Application of HSVD and VARPRO to ^{23}Na signals of the heart of a rat

In this example HSVD as well as VARPRO are applied to a series of *in vivo* ^{23}Na NMR time-domain signals of the heart of a rat. The NMR experiments were carried out in the University Hospital of the University of Utrecht [32]. One of the goals of the experiments was to investigate whether ischemia of the heart can be studied by ^{23}Na NMR. It is well known that the local concentrations of the Na^+ ions play an important role in the energy household of the living cells. Particularly the intracellular Na is important in that context. It therefore is to be expected that the intensity of the intracellular Na NMR peak changes under the influence of ischemia. This in contrast to the NMR peak of the extracellular Na.

A serious problem in *in vivo* ^{23}Na NMR investigations is that the intra- and extracellular NMR lines overlap completely, i.e. they can not be detected separately. One of the possible solutions to this problem is to employ a so-called shift reagent. The influence of the shift reagent is that the chemical shift of the Na is slightly changed. Since the shift reagent can only affect the extracellular and not the intracellular Na, the two NMR peaks are more or less separated (see Figure 1.3).

In Figure 2.9 the intracellular *in vivo* ^{23}Na peak is shown as function of the time, passed after artificially introducing ischemia in the heart of a rat. Although the extracellular peak has been shifted with respect to the intracellular peak, there is still a strong overlap. An additional complication is that the extracellular peak is not a single line but in fact is composed of several components. These include contributions from vascular and interstitial spaces, as well as from the perfusate surrounding the heart.

name of signal file:	cen11c.dat
number of data-points of signal:	1024
step-size of signal (ms):	0.100
begin time of signal (ms):	0.400
number of data-points in fit:	256
number of frequencies:	5

result of HSVD:
RMS error of fit: $0.1462E+03$

Frequency	2CR	Decay	2CR	Amplitude	2CR	Phase	2CR
kHz	kHz	kHz	kHz	a.u.	a.u.	degrees	degrees
-1.958	0.003	0.374	0.016	5106	156	57	2
0.443	0.007	0.290	0.044	1572	199	-7	7
0.739	0.003	0.348	0.022	28688	2879	16	6
0.765	0.000	0.106	0.002	85052	2242	-2	2
0.817	0.001	0.133	0.005	18282	969	-43	3

result of VARPRO:
RMS error of fit: $0.1482E+03$

Frequency	2CR	Decay	2CR	Amplitude	2CR	Phase	2CR
kHz	kHz	kHz	kHz	a.u.	a.u.	degrees	degrees
-1.958	0.002	0.375	0.014	5109	153	57	2
0.435	0.003	0.256	*****	1448	87	0	*
0.759	0.000	0.066	0.002	36783	2011	25	3
0.761	0.001	0.255	0.007	100501	2415	1	1
0.825	0.001	0.254	0.008	24550	1587	-107	4

Table 2.3: *Quantitative parameters of the last ^{23}Na signal from the ischemia series.*

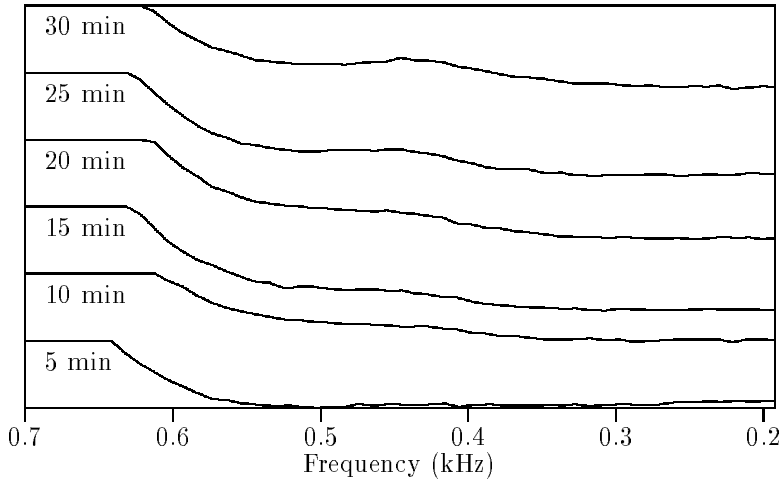

Figure 2.9: *Intracellular in vivo ^{23}Na NMR peak of the hart of a rat as a function of the time, passed after artificially introducing ischemia.*

In Table 2.3 the quantitative result is shown for the last time-domain signal of the series (the one having a waiting time of 30 minutes; see Figure 2.9). First the result of HSVD is presented. Concerning the frequencies it can be noted, that the peak at -1.96 kHz is a reference peak, the peak at 0.44 represents the intracellular Na and the three peaks around 0.8 kHz *together* form the extracellular Na. The second part of Table 2.3 shows the result, obtained by VARPRO. In this case starting values for the nonlinear parameters were required. For this we used the values found by HSVD.

An important aspect of the VARPRO fitting procedure was that the decay constant of the intracellular Na peak was kept fixed at a predetermined value of 0.256 Khz (the mean value of the decay constants, found by a 'free' VARPRO round for the signals with the 20, 25 and 30 minutes waiting time). It can be seen from Figure 2.10 that the process of keeping the decay constant of intracellular Na fixed, clearly improves the quantitative result for this peak. Generally speaking it can be said that exploiting prior knowledge on the model parameters usually yields a significant improvement of the quantitative data analysis.

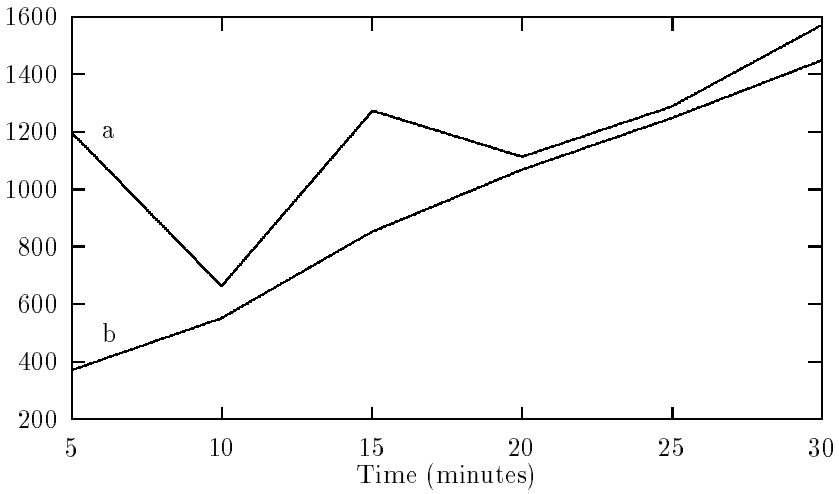

Figure 2.10: *Line intensity of the intracellular ^{23}Na as a function of the waiting time. (a) The HSVD result. (b) The VARPRO result.*

2.5.7 An iterative Least Squares Gauss-Newton implementation for the exponential decay model

The fact that iterative fitting methods, like VARPRO, generally pose no restrictions on the model functions can be very useful. However, if one wishes to entertain the exponential decay model, then the generality of VARPRO entails that the favourable mathematical properties of this particular model function are not exploited, which in turn amounts to wasting computational time. One way of solving this problem would be to convert the existing VARPRO code into a version, dedicated to exponentially decaying sinusoids. Instead, we have chosen to devise a dedicated nonlinear (i.e. iterative) Least Squares (LS) fitting program that uses analytical formulae pertaining exponential damping and that is based upon Gauss-Newton minimization [11]. Another important aspect of the fitting program is, that the updates of the model parameters in each iteration cycle are

judged and steered on spectroscopic rather than on general mathematical principles. For instance, a spectroscopist knows that an update of a frequency should preferably be smaller than the width of the related spectral component (supposing that the widths are known approximately, of course).

The starting point of the dedicated Gauss-Newton program is that we write the general basis function $f_k(t_n, \vec{p_k})$ of Equation 2.29 as

$$\begin{aligned} f_k(t_n, \vec{p_k}) \quad &= \quad \exp[(-\alpha_k + i2\pi\nu_k)(n+\delta)\Delta t] \\ &\text{with} \quad k = 1, 2, \ldots, K \\ &\text{and} \quad n = 0, 1, \ldots, N-1, \end{aligned} \tag{2.34}$$

where the sampling time of the first data point is $t_{beg} = \delta\Delta t$. An important aspect of NMR FID time-domain signals now is that the phases of the individual sinusoids usually are *equal* at the time $t = 0$. We therefore assume that the complex-valued amplitudes (see Equation 2.29) can be written as $c_k = a_k \exp(\phi_0)$, where ϕ_0 is the overall zero-order phase.

In the Gauss-Newton approach one expands the model function in a Tayler series about the current values of the nonlinear model parameters, and retains only the first-order terms. In this way the nonlinear dependence on the parameters is approximated by a linear dependence on the small updates of these parameters. In our case of the exponential decay model, assuming that we have *reasonable starting values* for the nonlinear parameters, we can write in first-order approximation for the basis function 2.34

$$\begin{aligned} &\exp[i(\phi_0 + \Delta\phi_0)] \;\; \exp\{[-(\alpha_k + \Delta\alpha_k) + i2\pi(\nu_k + \Delta\nu_k)][n\Delta t + (t_{beg} + \Delta t_{beg})]\} \approx \\ &\exp(i\phi_0) \;\; [\, 1 + i\Delta\phi_0 + (-\alpha_k + i2\pi\nu_k)\Delta t_{beg} + (-\Delta\alpha_k + i2\pi\Delta\nu_k)(n\Delta t + t_{beg})\,] \;\; f_k(t_n, \vec{p_k}) \end{aligned}, \tag{2.35}$$

where we have included the zero-order phase and $\Delta\phi_0$, Δt_{beg}, $\Delta\alpha_k$ and $\Delta\nu_k$ are the updates of the various nonlinear model parameters.

Using expansion 2.35 converts the general matrix equation 2.30 into

$$\begin{pmatrix} \hat{s}_0 \\ \hat{s}_1 \\ \vdots \\ \hat{s}_{N-1} \end{pmatrix} = \begin{pmatrix} F' & TF' & iTF' & iF'\vec{a} & F'P\vec{a} \end{pmatrix} \begin{pmatrix} \vec{a} \\ \vec{a}' \\ \vec{a}'' \\ \Delta\phi_0 \\ \Delta t_{beg} \end{pmatrix} = G\vec{v}, \tag{2.36}$$

where

$$\begin{aligned} F' &= \exp(i\phi_0)F, \\ T &= \text{diag}\ (t_0, t_1, \ldots, t_{N-1}), \\ P &= \text{diag}\ (p_1, p_2, \ldots, p_K) \ \text{with} \ p_k = -\alpha_k + i2\pi\nu_k, \\ \vec{a} &= \text{the vector of the amplitudes} \ a_k \ \ (k = 1, 2, \ldots, K), \\ a'_k &= -a_k\Delta\alpha_k \ \text{and} \\ a''_k &= a_k 2\pi\Delta\nu_k. \end{aligned} \tag{2.37}$$

For the sake of simplicity we embed $\exp(i\phi_0)$ into the function matrix and replace F' by F for the remaining of this subsection. Analogous to Equation 2.32 we may write as linear LS solution for the vector $\vec{v}$

$$\vec{v} = [\ \Re\,(G^\dagger G)\ ]^{-1}\ \ \Re\,(G^\dagger \vec{s}\ ), \tag{2.38}$$

where the real parts of $G^\dagger G$ and $G^\dagger \vec{s}$ are to be taken since the vector $\vec{v}$ is real (see Equation 2.36).

It appears that the matrix product $G^\dagger G$ can be written in a highly structured way, which is an advantage for the related computer implementation

$$G^\dagger G = \begin{pmatrix} M_0 & M_1 & iM_1 & iM_0\vec{a} & M_0P\vec{a} \\ & M_2 & iM_2 & iM_1\vec{a} & M_1P\vec{a} \\ & & M_2 & M_1\vec{a} & -iM_1P\vec{a} \\ & & & \tilde{\vec{a}}M_0\vec{a} & -i\tilde{\vec{a}}M_0P\vec{a} \\ & & & & \tilde{\vec{a}}P^\dagger M_0P\vec{a} \end{pmatrix}, \tag{2.39}$$

where $M_0 = F^\dagger F$, $M_1 = F^\dagger T F$ and $M_2 = F^\dagger T^2 F$. Furthermore, the tilde on $\tilde{\vec{a}}$ denotes transposition. The left lower-triangle of $G^\dagger G$ needs not to be given explicitly since the product yields an hermitian matrix.

An important aspect of the current method is the presence of the exponential functions in the matrix elements of $G^\dagger G$. It can be shown that the calculations of these matrix elements merely involves the evaluation of sums of the simple form

$$Sum_i = \sum_{n=0}^{N-1} n^i z^n \ \ (i = 0, 1, 2), \tag{2.40}$$

where z are complex numbers, constructed from the products $\zeta_k^* \zeta_{k'}$, with ζ_k and $\zeta_{k'}$ denoting the signal poles introduced in Equation 2.2.

For $i = 0$ Equation 2.40 reduces to the simple closed-form analytical expression

$$Sum_0 = \frac{1 - z^N}{1 - z}. \tag{2.41}$$

For $i \geq 1$ a somewhat more complicated analytical expression is obtained

$$Sum_i = \frac{z \sum_{j=0}^{i-1} [\ \binom{i}{j} Sum_j\ ] - N^i z^N}{1 - z}. \tag{2.42}$$

Other closed-form expressions are given in [33] for the special case $z \to 1$.

As a result of the analytical expressions for the matrix elements, the calculation of $G^\dagger G$ requires little time. Should the decay of the NMR FID signal, concerned, be non-exponential or should the sampling times be nonuniform, then the computation of $G^\dagger G$ becomes a burden.

Another acceleration of the computational speed can be obtained by using the relation $f_k(t_{n+1}, \vec{p_k}) = \zeta_k f_k(t_n, \vec{p_k})$ in calculating the product $G^\dagger \vec{s}$ in Equation 2.38. Again

this acceleration is exclusively possible for the exponential decay model and for uniform sampling.

2.5.8 Imposing linear relations on model parameters (Prior Knowledge) in the Gauss-Newton program

Another important property of the dedicated Gauss-Newton based program, described in the previous subsection, is that linear relations between model parameters of the same type can be imposed rather easily. These linear relations between parameters often occur in NMR spectroscopy and can be considered as important spectral prior knowledge. For instance, in case of NMR *multiplets* there may be relations between the amplitudes, the decay constants or the frequences of the multiplet components. Also the fact that at $t = 0$ the phases of the NMR harmonic components may be equal to an overall zero-order phase can be considered as prior knowledge.

Introducing linear relations between model parameters in the Gauss-Newton fitting program is based upon the special structure of the matrix-vector multiplication of equation 2.36. Working out this multiplication shows that the linear relations simply can be imposed by introducing corresponding linear relations in the related columns of the function matrix F. This introduction results in a reduction of the size of the matrix-vector multiplication (see Figure 2.11).

In the software of the computer implementation the above mentioned spectral prior knowledge is introduced by using two special 1-D-arrays, an integer-array KPRIOR(I) and a real-array APRIOR(I) (I $= 1, 2, \ldots, 3K$, with K being the number of NMR components).

The integer-array KPRIOR contains integer numbers, denoting the *type* of spectral prior knowledge. We distinguish:

- 0 : The parameter of the harmonic component, concerned, is fitted *without knowing a linear relation* with a parameter of the same kind of any other component.
- -1 : The parameter of the harmonic component, concerned, acts as *reference parameter* for the corresponding parameter of one or more related harmonic components.
- n : The parameter of the harmonic component, concerned, has a linear relation with the corresponding parameter of the n'th harmonic component.
- -2 : The parameter of the harmonic component, concerned, *is kept constant* during the fitting process at a predetermined value.

The real-array APRIOR contains real numbers, indicating the *values* of the linear relations, concerned. We thereby distinguish fixed *ratios* of amplitudes or decay constants and fixed *differences* between frequencies.

An example of the contents of the arrays KPRIOR and APRIOR, used for real-world *in vivo* NMR FID signals, is presented in Table 2.4. The linear relations, concerned, are often used for the multiplet components of the ATP molecule in the *in vivo* NMR FID signals of the ^{31}P nucleus (see also the example in the next subsection).

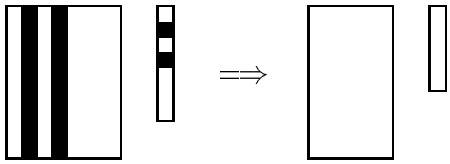

Figure 2.11: *Reduction of the size of the matrix-vector multiplication $G\vec{v}$ due to a linear relation between two model parameters.*

Nr.	KPRIOR (1 - K)	APRIOR (1 - K)	KPRIOR (K+1 - 2K)	APRIOR (K+1 - 2K)	KPRIOR (2K+1 - 3K)	APRIOR (2K+1 - 3K)
1	-1	1.00	-1	1.00	-1	0.000
2	1	2.22	1	1.00	1	0.016
3	1	1.27	1	1.00	1	0.032
4	1	2.40	-1	1.00	-1	0.000
5	1	2.07	4	1.00	4	0.016
6	1	2.33	-1	1.00	-1	0.000
7	1	2.13	6	1.00	6	0.016
8	0	0.00	0	0.00	0	0.000
9	0	0.00	0	0.00	0	0.000
10	0	0.00	0	0.00	0	0.000

Table 2.4: *Example of the contents of the arrays KPRIOR and APRIOR. The prior knowledge, concerned, is often used for the multiplet components of the ATP molecule in the in vivo NMR FID signals of the ^{31}P nucleus. From the table it can be seen, that the amplitudes of components 1,2,3,4,5,6 and 7 are in the proportion of 1 : 2.22 : 1.27 : 2.40 : 2.07 : 2.33 : 2.13. Furthermore it appears, that the decay constants of the harmonic components 1,2 and 3, of 4 and 5 and of 6 and 7 are equal. Finally it can be seen, that the frequency differences of components 1, 2 and 3, of 4 and 5 and of 6 and 7 are equal to 0.016 kHz. It should be noted that the above mentioned prior knowledge is valid for a constant magnetic field of 1.5 T.*

2.5.9 Example 4: Application of the Gauss-Newton program to an *in vivo* ^{31}P NMR FID of calf muscle

In this example the Gauss-Newton based fitting program is applied to an *in vivo* ^{31}P NMR FID signal of calf muscle. The experiment was carried out on a whole-body 1.5 T MRI/MRS system of Philips Medical Systems in Best.

Typical of *in vivo* ^{31}P NMR calf muscle spectra is that the NMR lines are rather narrow, as can be inspected in Figure 2.12. In this figure the quantification results are presented for fitting without and with prior knowledge on the ATP multiplets. The prior knowledge, used for ATP, is the same as given in Table 2.4.

In Table 2.5 the numerical results for the ^{31}P calf muscle signal are listed. It can be noticed, that the errors of the ATP parameters (two times the Cramer-Rao lower bounds) are much smaller as a result of applying the spectral prior knowledge. Particularly, the results for the β-ATP triplet are improved. It should also be noticed, that in this example the zero-order phase as well as the begin time were fitted.

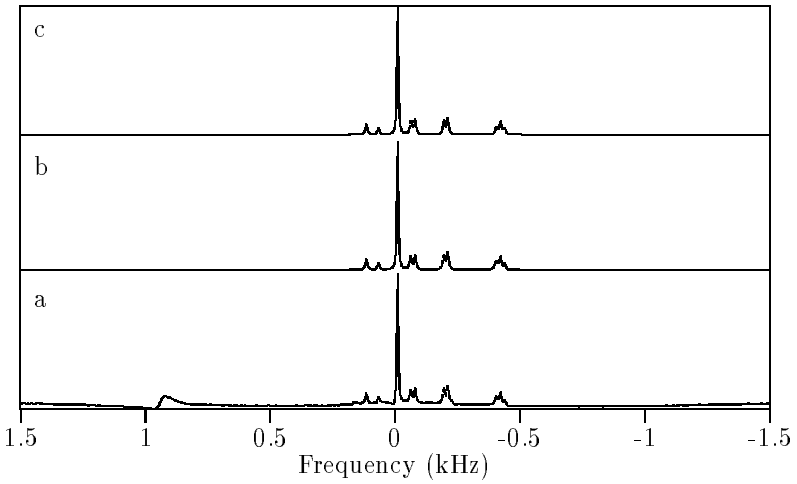

Figure 2.12: *In vivo ^{31}P NMR of calf muscle. (a) Spectrum of the experimental signal. (b) Spectrum of the fitted model function without using prior knowledge on ATP. (c) Spectrum of the fitted model function with using prior knowledge on ATP. The quantification was carried out with the Gauss-Newton based fitting program.*

name of signal file:	testcalf.dat
number of data-points of signal:	1024
time step of signal (ms):	0.333
starting value of phzero (degrees):	200
starting value of begin time (ms):	0.133
number of data-points of fit:	512
index of first data-point:	5
number of peaks of fit:	10
number of iterations of fit:	35

(a)

Frequency	2CR	Decay	2CR	Amplitude	2CR	Phase
kHz	kHz	kHz	kHz	a.u.	a.u.	degrees
-0.4402	0.0014	0.0178	0.0135	3.27	1.83	0.00
-0.4234	0.0008	0.0270	0.0085	11.29	2.99	0.00
-0.4059	0.0016	0.0410	0.0166	10.30	3.46	0.00
-0.2118	0.0005	0.0256	0.0052	14.87	2.32	0.00
-0.1954	0.0006	0.0250	0.0060	12.25	2.29	0.00
-0.0815	0.0005	0.0227	0.0054	11.51	2.06	0.00
-0.0634	0.0007	0.0260	0.0068	11.19	2.21	0.00
-0.0112	0.0000	0.0142	0.0004	79.72	1.49	0.00
0.0659	0.0010	0.0204	0.0097	5.12	1.77	0.00
0.1145	0.0008	0.0265	0.0077	9.54	2.03	0.00

phzero	2CR	tbegin	2CR
degrees	degrees	ms	ms
205.75	0.73	0.267	0.029

(b)

Frequency	2CR	Decay	2CR	Amplitude	2CR	Phase
kHz	kHz	kHz	kHz	a.u.	a.u.	degrees
-0.4395	0.0006	0.0285	0.0044	5.43	0.34	0.00
-0.4235	0.0006	0.0285	0.0044	12.06	0.76	0.00
-0.4065	0.0006	0.0285	0.0044	6.90	0.43	0.00
-0.2118	0.0004	0.0228	0.0028	13.04	0.82	0.00
-0.1958	0.0004	0.0228	0.0028	11.24	0.71	0.00
-0.0807	0.0005	0.0271	0.0036	12.66	0.80	0.00
-0.0647	0.0005	0.0271	0.0036	11.57	0.73	0.00
-0.0112	0.0000	0.0142	0.0004	79.59	1.51	0.00
0.0659	0.0011	0.0202	0.0097	5.09	1.77	0.00
0.1146	0.0008	0.0270	0.0078	9.66	2.06	0.00

phzero	2CR	tbegin	2CR
degrees	degrees	ms	ms
205.74	0.74	0.229	0.030

Table 2.5: *Numerical results of the Gauss-Newton quantification of the ^{31}P calf muscle signal. (a) Without using prior knowledge on ATP. (b) With using prior knowledge on ATP.*

2.6 Quantification of two-dimensional (2-D) *in vivo* NMR time-domain signals

2.6.1 Introduction

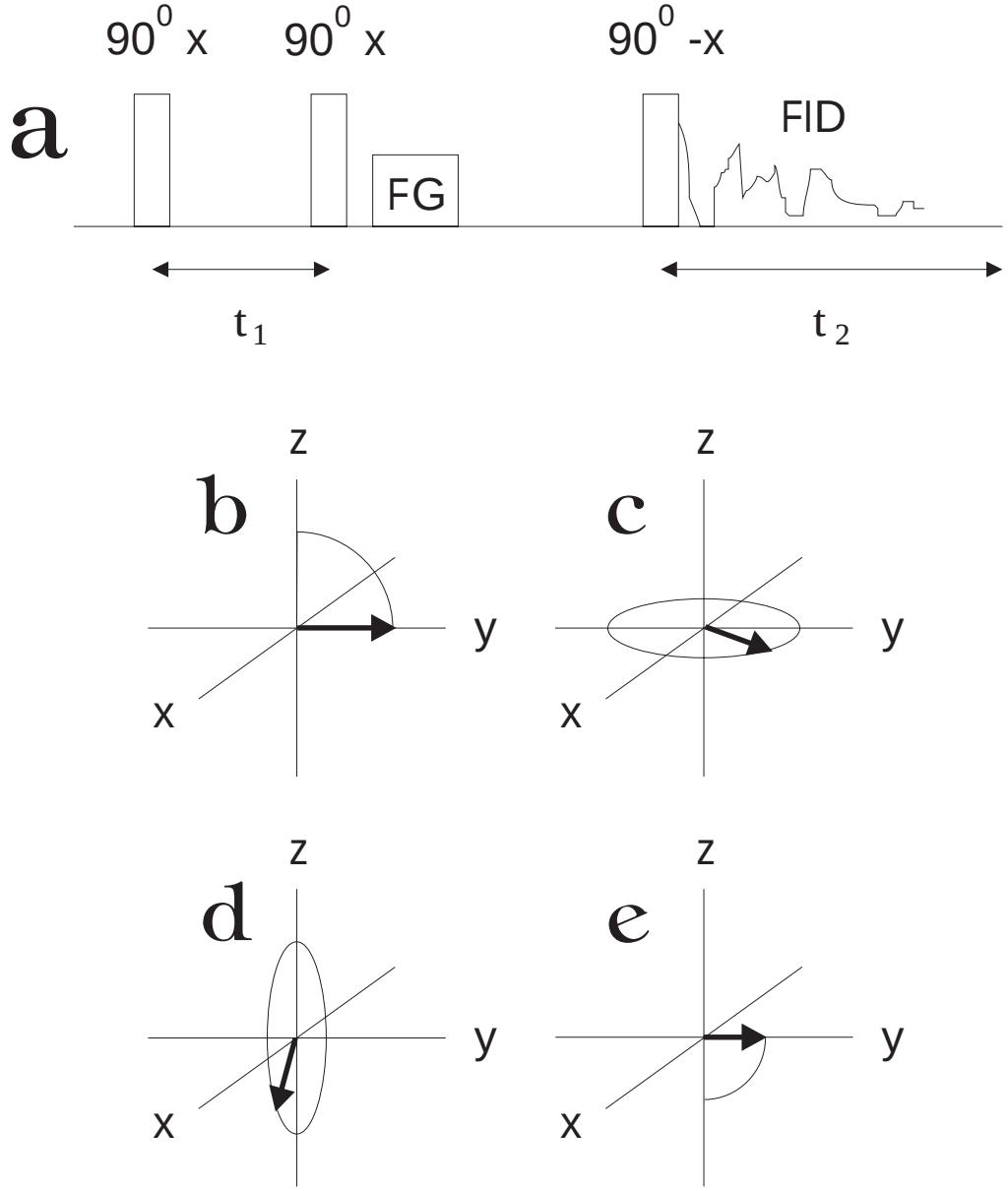

Figure 2.13: *(a) Example of a 2-D NMR experiment (see text). The other figures show the magnetization (b) just after the first pulse, (c) just before the second pulse, (d) just after the second pulse and (e) just after the third pulse.*

When describing the NMR FID and spin-echo experiments, we implicitly have used that the related time-domain signals are a function of *only one* discretely changing time variable. One speaks of a one-dimensional (1-D) measurement. In general, NMR experiments can be carried out in more than one dimension. Especially the two-dimensional (2-D) experiments, in which two time variables are changed, are often applied in NMR spectroscopy [34]. At present, many variations on the 2-D NMR experiment are known. Most

of them have in common, that they are based on transfer of magnetization from one nucleus to another.

In order to get an idea of the principle of 2-D NMR spectroscopy we consider the following example. In the sample, to be investigated by NMR, there are supposed to exist two non-equivalent nuclei A and B in each others neighbourhood. Suppose, that the two nuclei can exchange chemically, i.e. nuclues A can take the place of nucleus B and vice versa. We follow the behaviour of the magnetization of nucleus A in the rotating frame, when three 90^0 r.f. pulses are given, the first and second pulse along the x-axis and the third one along the -x-axis. Just after the first 90^0 pulse the magnetization vector is aligned along the y-axis (see Figure 2.13). In the time t_1 between the first and second pulse the magnetization makes a precession over an angle $(2\pi\nu_A t_1)$, where ν_A is the precession frequency of nucleus A. Just after the second pulse the magnetization is located in the xz-plane (see Figure 2.13), with its x- and z-component being proportional to $\sin(2\pi\nu_A t_1)$ and $-\cos(2\pi\nu_A t_1)$, respectively. Now, as a consequence of applying a magnetic field gradient in the time between the second and third pulse, the x-component of the magnetization is destroyed. i.e. only the z-component remains. After the third pulse, now being applied along the -x-axis, an FID is detected as a function of a second time t_2, and being proportional to $\cos(2\pi\nu_A t_1)$.

Essential in this simple description with magnetization vectors now is the assumption, that due to chemical exchange a number of nuclei of type A and B have changed their mutual positions. As a result a fraction of the FID signal, coming from nucleus A, will be modulated by $\cos(2\pi\nu_B t_1)$, and vice versa. This means that a 2-D signal $s(t_1, t_2)$ is obtained if the measurement is repeated as a function of the first time t_1. A two-dimensional DFT of the signal $s(t_1, t_2)$ yields a 2-D spectrum, with 2-D peaks located at positions (ν_A, ν_A), (ν_B, ν_B), (ν_A, ν_B) and (ν_B, ν_A). The two latter peaks are called the cross peaks. The presence of these cross peaks is a direct prove that the chemical exchange has taken place (see Figure 2.14).

In the simple example, just described, the transfer of magnetization from one nucleus to the other was based upon chemical exchange. However, transfer of magnetization is also possible via other processes, such as via scalar magnetic interaction (J-coupling) or via magnetic dipole-dipole interaction. The presence of the cross peaks then proves the occurrence of the corresponding interaction. In case of the magnetic dipole-dipole interaction the intensity of a cross peak is proportional to $\frac{1}{r^6}$, where r is the distance between the interacting nuclei. Quantification of the 2-D cross peaks then yields information about the value of r.

The following applications of 2-D NMR spectroscopy can be mentioned:

- Separation of overlapping peaks (when compared to the corresponding 1-D spectrum).
- Supply of information about the type and magnitude of the magnetic interactions between the nuclei, present in the sample.

In practice, the 2-D NMR is particularly employed for giving help in the structure determination of large molecules (e.g. proteins). In the *in vivo* NMR world the 2-D spectroscopy is only applied on a limited scale, probably due to the length of the measurement time.

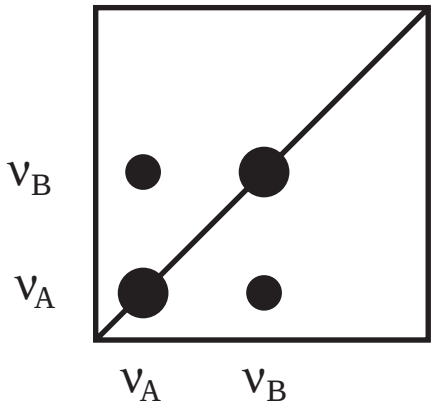

Figure 2.14: *Contour plot of a 2-D NMR spectrum.*

2.6.2 Examples of 2-D NMR time-domain model functions

Depending on the nature of the 2-D NMR experiment, concerned, various 2-D time-domain model functions may be required for describing the 2-D data sets.

As a first example, we consider the 2-D analogue of the 1-D NMR FID model function (see Equation 2.1; We assume for the sake of simplicity, that the begin time in both dimensions is equal to zero.)

$$\hat{s}_{nm} = \sum_{k=1}^{K} \sum_{k'=1}^{K'} \zeta_k^n c_{kk'} {\zeta'_{k'}}^m, \tag{2.43}$$

where
$n = 0, 1, \cdots, N-1$,
$m = 0, 1, \cdots, M-1$,
$c_{kk'} = a_{kk'} \exp(i\phi_{kk'})$,
$\zeta_k = \exp[(-\alpha_k + i2\pi\nu_k)\Delta t)]$ and
$\zeta'_{k'} = \exp[(-\alpha'_{k'} + i2\pi\nu'_{k'})\Delta t')]$.

In matrix notation, Equation 2.43 may be written as

$$\hat{S} = \begin{pmatrix} 1 & \cdots & 1 \\ \zeta_1^1 & \cdots & \zeta_K^1 \\ \vdots & \cdots & \vdots \\ \zeta_1^{N-1} & \cdots & \zeta_K^{N-1} \end{pmatrix} \begin{pmatrix} c_{11} & \cdots & c_{1K'} \\ \vdots & \cdots & \vdots \\ c_{K1} & \cdots & c_{KK'} \end{pmatrix} \begin{pmatrix} 1 & {\zeta'_1}^1 & \cdots & {\zeta'_1}^{M-1} \\ \vdots & \vdots & \cdots & \vdots \\ 1 & {\zeta'_{K'}}^1 & \cdots & {\zeta'_{K'}}^{M-1} \end{pmatrix}, \tag{2.44}$$

or

$$\hat{S} = F_{NK} C_{KK'} \tilde{F}'_{MK'} \ . \tag{2.45}$$

It is of importance to note that the rank of the matrix $\hat{S}$ is equal to $\min(K, K')$. This implies, that in case of $K \neq K'$ the SVD of the related experimental 2-D data matrix

can not yield the correct number of singular values for the dimension with the highest number of spectral components and that consequently the correct signal poles can not be determined for that dimension. In subsection 2.6.3 we will present a workaround for this 2-D rank problem.

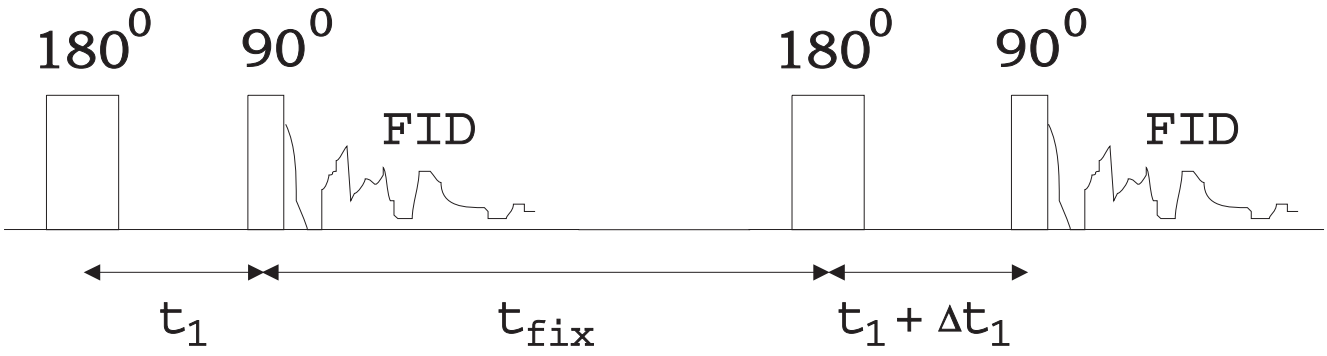

Figure 2.15: *Pulse sequence of a 2-D NMR experiment for measuring the longitudinal relaxation times of individual metabolites (see text).*

A second example of a 2-D model function concerns the measurement of the longitudinal relaxation time T_1 (see Equation 1.1). In Figure 2.15 the pulse sequence for such an experiment is shown. The experiment can be described as follows: Starting from the Boltzmann equilibrium (magnetization along the z-axis), the magnetization is inverted by means of a 180^0 r.f. pulse. Subsequently a time t_1 is waited, so that the magnetization can return towards equilibrium via the mechanism of the longitudinal relaxation. After the time t_1 a second r.f. pulse is given, now with a rotation angle of 90^0. This results in an FID with its magnitude being proportional to

$$[1 - 2\exp(\tfrac{-t_1}{T_1})].$$

If the measurement is carried out as a function of the delay time t_1, a 2-D time-domain signal is obtained that can be described by the following 2-D model function

$$\hat{s}_{nm} = \sum_{k=1}^{K} c_k[1 - 2\exp(\frac{-n\Delta t'}{T_{1k}})]\zeta_k^{m+\delta}, \tag{2.46}$$

where $n = 0, 1, \ldots, N-1$, $m = 0, 1, \ldots, M-1$, $\zeta_k = \exp[(-\alpha_k + i2\pi\nu_k)\Delta t]$ and $\delta\Delta t$ is the begin time of the FID.

Equation 2.46 is exactly true if the fixed time t_{fix} between succeeding $180^0 - 90^0$ pulse sequences is taken long compared to the longitudinal relaxation times T_{1k}. In practise this means, that the measurement time becomes too long. Therefore the time t_{fix} is taken too short, which introduces the need for a correction term in the 2-D model function. The new, corrected, 2-D model function is

$$\hat{s}_{nm} = \sum_{k=1}^{K} c_k\{1 - [2 - \exp(-\frac{t_{fix}}{T_{1k}})]\exp(\frac{-n\Delta t'}{T_{1k}})\}\zeta_k^{m+\delta}. \tag{2.47}$$

Notice, that Equation 2.47 changes into Equation 2.46 for $t_{fix} \longrightarrow \infty$.

2.6.3 The 2-D version of the SVD-based State Space method

In the previous subsection it was reported, that a rank problem exists for the SVD of the 2-D data matrix, related to the 2-D FID experiment (see below Equation 2.45).

Recently we have found a way of working around this problem [35]. The essence of the solution is that a *block* matrix of the form

$$H = (H_0 H_1 \dots H_{N-1}) \tag{2.48}$$

is used, with $H_n (n = 0, 1, \dots, N-1)$ being matrices with Hankel structure, constructed from each row of the experimental 2-D data matrix. Notice, that all data points are contained in H. It can be shown that the number of singular values of H corresponds to K', i.e. the number of harmonic components in the primed dimension. This implies that the primed signal poles are obtained from the left singular vector matrix of matrix H. Subsequently, transposition of the data matrix and repetition of the procedure yields the signal poles for the unprimed dimension. Finally, the real-valued amplitudes and phases follow from a same linear Least Squares fitting procedure as applied in the 1-D FID case.

2.6.4 Example 5: Application of 2-D HSVD to a 2-D *in vivo* ^{1}H FID of the brain of a rat

In ^{1}H NMR spectra of compounds, dissolved in protonated solvents such as water, often serious problems are encountered due to the high concentration of the solvent protons [36]. If solvent signals are to be suppressed one can choose between applying experimental methods that operate prior to data acquisition or off-line methods that are based upon using software techniques [37].

In multidimensional NMR the solvent signal may not be so large a problem as in 1-D NMR since the cross peaks of interest may be located well away from the solvent region. Nevertheless, there may be a need for solvent signal suppression. This is especially true for *in vivo* ^{1}H spectroscopy on selected regions of humans or animals where the solvent, i.e. the water, is to be suppressed AND localized at the same time. Another complicating aspect of *in vivo* localized spectroscopy is that there are various mechanisms leading to additional line broadening.

In this example we present the results of addressing the 2-D HSVD approach, described in the previous subsection, to a 2-D *in vivo* ^{1}H FID of the brain of a rat. The experiment was carried out in the 'Groupe d'Application de la RMN a la Neurobiologie' of M. Decorps at the University Joseph Fourier in Grenoble. The data matrix, concerned, comprised 256×128 data points. In order to fit the proton signals, coming from the water as well as from the other molecules, the number of model function components was chosen to be 100 in the unprimed and 30 in the primed dimension. After the fitting process the 2-D model function components, whose frequencies were located in the water region, were subtracted from the time-domain data matrix. The result of the water suppression can be inspected by looking at the contour plots, displayed in Figure 2.16. The contours, shown, represent the level at 0.17% of the maximum of the uncleaned 2-D spectrum. The frequencies in both dimensions were normalized, i.e. assuming that the sample steps are equal to one.

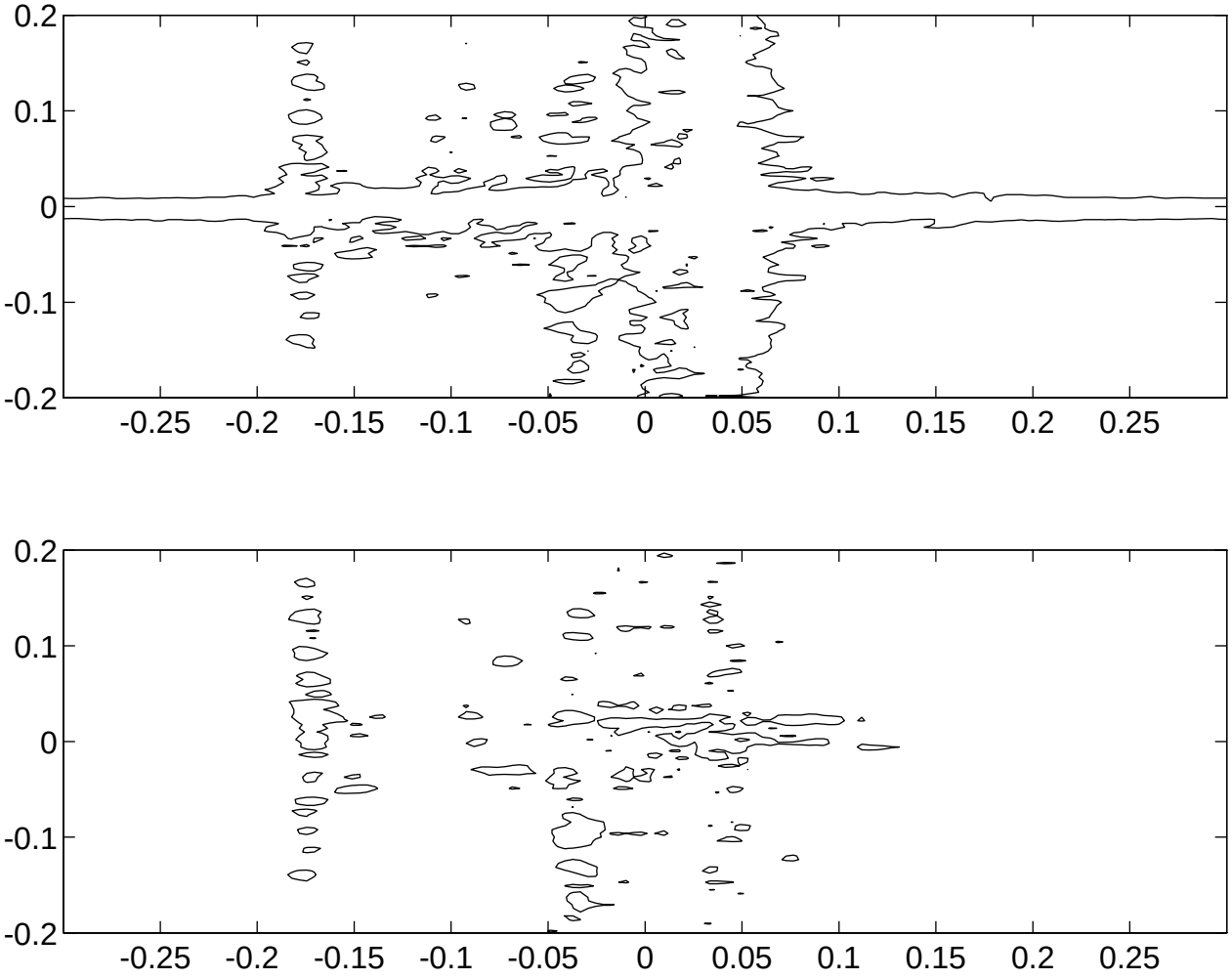

Figure 2.16: *Contour plots of a 2-D in vivo* ^1H *spectrum of the brain of a rat. The upper picture shows a dominant water peak in the (0,0) region and the bottom picture a reduced peak in that region. The latter is the result of applying the 2-D HSVD procedure.*

2.6.5 Example 6: Application of a 2-D version of the Gauss-Newton program to an *in vivo* ^{31}P longitudinal relaxation experiment of a human brain

In this example a 2-D version of the Gauss-Newton program is applied to an *in vivo* ^{31}P longitudinal relaxation experiment of a human brain. The experiment was carried out on a 1.5 T whole-body MRI/MRS system of Philips Medical Systems in Best.

In Figure 2.17 the cosine DFT of the FID is displayed as a function of the delay time t_1 between the 180^0 and 90^0 pulse. In addition, in Figure 2.18 the amplitude of an individual NMR component is shown as a function of t_1, namely that of the PCr metabolite. The curvature of the latter indicates that the relaxation behaviour can be described by a single exponential function, i.e. by one T_1 value.

In order to determine the parameters of the FID's as well as the T_1 values of the individual metabolites, the 2-D model function of Equation 2.47 was fitted to the data points of all FID's. For the fixed time t_{fix} a value of 3 s was taken in the fitting process. Furthermore, prior knowledge on the spectral parameters of the ATP multiplets was exploited.

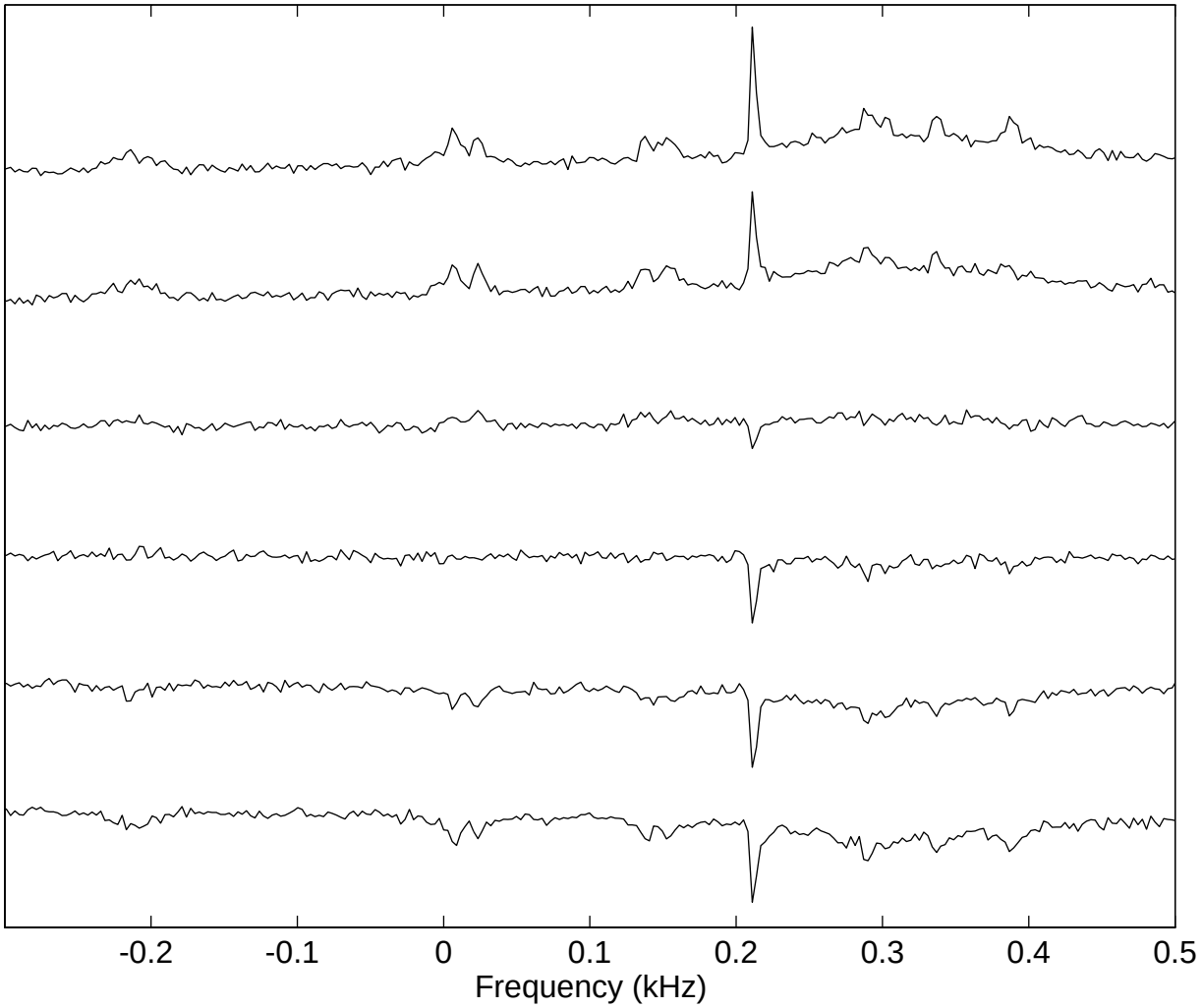

Figure 2.17: *Spectrum of a proton-decoupled in vivo ^{31}P FID of a human brain as a function of the delay time t_1 between the 180^0 and 90^0 pulse of a T_1 experiment.*

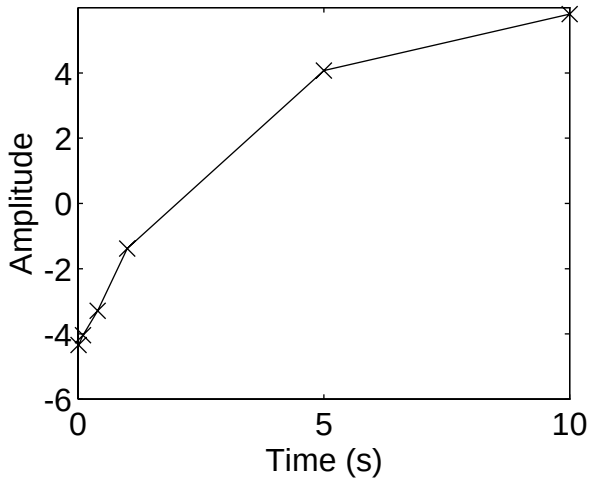

Figure 2.18: *Amplitude of the PCr-component as a function of the delay time t_1.*

Component	Amplitude	CR	T_1 (s)	CR
β-ATP	4.56	0.11	0.64	0.05
DPDE	2.82	0.58	3.9	1.3
α-ATP	4.55	0.11	0.61	0.03
γ-ATP	4.54	0.11	0.67	0.04
PCr	6.55	0.17	3.17	0.14
PDE	29.2	2.1	1.06	0.06
GPC	2.00	0.32	4.7	1.1
GPE	1.71	1.4	12.	12.
Pi	2.42	0.21	2.16	0.32
PME	5.36	0.43	3.13	0.43

Table 2.6: *The 'overall' amplitudes and the longitudinal relaxation times of the various components of the in vivo* ^{31}P *FID.*

The results of the 2-D quantification are listed in Table 2.6. It is interesting to see, that the T_1's of the three ATP multiplets are equal to each other (within the standard deviations). Moreover it is remarkable, that the shortest and longest relaxation time differ by an order of magnitude.

Chapter 3

Magnetic Resonance Imaging (MRI) and Spectroscopic Imaging (MRSI)

3.1 Introduction

So far, in these lecture notes the issue of *quantification* was reserved to quantitative data analysis of Magnetic Resonance Spectroscopy (MRS) signals. That is to say, signals containing information about the *spectral* properties of the molecules (metabolites), contributing to the NMR signal. This in contrast to Magnetic Resonance Imaging (MRI) signals, which contain information about the *spatial* properties of the metabolites (e.g. about their concentrations as a function of the positions in a selected slice of a human body).

Since a number of years a method exists that combines the properties of spectroscopy AND imaging. The method is called Magnetic Resonance Spectroscopic Imaging (MRSI). During the MRSI experiment spectral coding as well as spatial coding is applied. As a result, after carrying out the proper signal processing and quantification steps, one can reconstruct images of individual metabolites. An application for metabolite images, for instance, is the image of the NAA molecule in the human brain. This metabolite can be considered as a marker for the brain cells. A low intensity in the NAA image may indicate a certain brain damage.

On the hand of the NAA example it may be clear that metabolite imaging via the MRSI method may become an important diagnostic tool in clinical situations. In order to understand the MRSI method, in the next section first the basic principle of the traditional MRI method will be addressed. Then, in the next section the essence of MRSI will be discussed. Further, in the succeeding section some signal processing aspects of real-world MRSI signals will be described. Finally, in the last section of this chapter an alternative way of writing the MRSI equation will be treated.

3.2 Basic principle of MRI

The basic principle of the MRI method will be addressed on the hand of Figure 3.1. In this figure the pulse sequence of a simplified MRI experiment is shown.

The spatial coding, needed for MRI, is obtained via the use of magnetic field gradients. First, a slice at height z and thickness dz of the *in vivo* object is selected. This is done by means of a selective 90^0 r.f. pulse, combined with a z-gradient. Next, the spatial coding for the x-direction is obtained by means of an x-gradient. The latter is changed with discrete steps during a fixed time t_x. Finally, the spatial coding for the second direction, i.e. the y-direction, is obtained by means of an y-gradient. This gradient is not stepped, but has a fixed value during the acquisition of the FID data (in the time t_x to $t_x + t_y$).

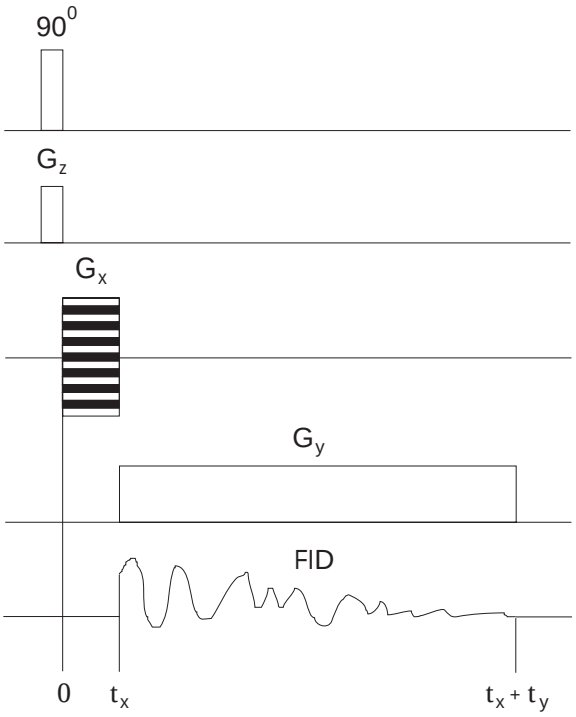

Figure 3.1: *Pulse sequence of a simplified MRI experiment.*

After this qualitative explanation we now will give a quantitative description. We suppose, that at position (x, y, z) and time t a resulting magnetic field is present, that in the rotating frame is given by

$$\vec{B}(x, y, z, t) = [B_0 + \frac{\omega}{\gamma} + G_x(t)x + G_y(t)y + G_z(t)z]\ \vec{u}_z + B_1(t)\ \vec{u}_x. \tag{3.1}$$

During the time 0 to t_x only the x-gradient is switched on. If the rotating frame precesses with an angular velocity $-\gamma B_0$, the angular velocity of the k-th NMR component in that rotating frame is equal to

$$\Delta\omega_k = \omega - \omega_{0k} = \gamma G_x x(1 - \sigma_k) - \gamma B_0 \sigma_k. \tag{3.2}$$

We now suppose that the effect of the chemical shift can be neglected with respect to that of the x-gradient. In that case the equation for the angular velocity reduces to

$$\Delta\omega_k = \gamma G_x x. \tag{3.3}$$

During the acquisition of the FID in the time t_x to $t_x + t_y$ only the y-gradient is swiched on, which in the same way leads to an angular velocity $\gamma G_y y$. The final consequence of

the pulse sequence is, that at time $t_x + t_y$ the FID signal of the k'th NMR component, coming from a volume element $dxdydz$ of the selected slice, can be written as

$$s_k(t_x + t_y) = \rho_k(x, y, z)\ dxdydz\ \exp[-\alpha_k(t_x + t_y) + i\gamma(G_x x t_x + G_y y t_y)], \tag{3.4}$$

where $\rho_k(x, y, z)$ is the density and α_k the decay constant of the k'th component. The total signal, coming from the selected slice, follows after summation over all components and integration over the slice

$$s(t_x + t_y) = \sum_{k=1}^{K} \int_x \int_y \rho_k(x, y, z)dz\ \exp[-\alpha_k(t_x + t_y) + i\gamma(G_x x t_x + G_y y t_y)]\ dxdy. \tag{3.5}$$

Equation 3.5 can be written in a slightly different way by introducing the so-called k-domain parameters

$$k_x = \gamma G_x t_x \text{ and } k_y = \gamma G_y t_y. \tag{3.6}$$

If only one NMR component is taken into account (e.g. the water component), the effect of the decay is neglected and the index k, the slice height z and slice thickness dz are dropped from the formula, Equation 3.5 reduces to

$$s(k_x, k_y) \propto \int_x \int_y \rho(x, y)\ \exp[i(k_x x + k_y y)]\ dxdy. \tag{3.7}$$

The last step in obtaining an MRI of the water protons in the selected slice is to perform a 2-D Fourier transformation from the 2-D k-domain to the spatial domain

$$\begin{aligned} S(x', y') &\propto \textstyle\int_{k_x} \int_{k_y} \int_x \int_y \rho(x, y)\ \exp[i(k_x x + k_y y)]\ \exp[-i(k_x x' + k_y y')]\ dxdy\ dk_x dk_y \\ &\propto \rho(x', y'). \end{aligned} \tag{3.8}$$

Notice, that the field of view (the maximum length of x and y in the selected slice) is determined by the Nyquist theorem. This yields the requirement $\gamma G_y y_{max} \Delta t_y \leq \pi$ for the sampling step Δt_y during the acquisition of the FID data.

3.3 Basic principle of MRSI

In this section the basic principle of the MRSI method will be described. Again this will be done on the hand of a simplified NMR pulse sequence, as can be seen in Figure 3.2.

During an MRSI experiment there are two aspects that clearly differ from the MRI experiment:

- Since the issue is to make an image of *other* molecules (not water but the metabolites), the signal coming from the water protons should be suppressed. Today, several experimental methods are available to achieve this.

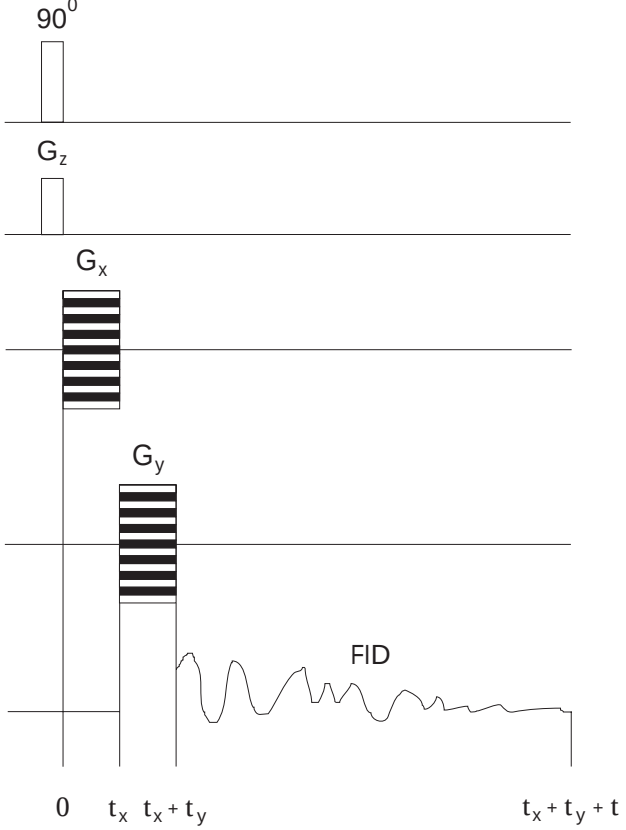

Figure 3.2: *Pulse sequence of a simplified MRSI experiment.*

- Spectral coding should be added to the pulse sequence of the traditional MRI experiment. This is done by performing the acquisition of the FID data in a period, during which *no magnetic field gradients are switched on.*

When comparing Figures 3.1 and 3.2, it can be concluded, that in case of the MRSI experiment Equation 3.7 changes into

$$s(k_x, k_y, t) \propto \sum_{k=1}^{K} \int_x \int_y \rho_k(x, y)\ \exp[i(k_x x + k_y y)]\ \exp[(-\alpha_k + i\Delta\omega_k)t]\ dxdy, \tag{3.9}$$

where $\Delta\omega_k = -\gamma B_0 \sigma_k$ (see Equation 3.2).

That is to say, there is now a summation over the metabolite components AND the FID term, obtained by the data-acquisition in the period $t_x + t_y$ to $t_x + t_y + t$, has been added.

After 2-D Fourier transformation from the k-domain to the spatial domain, the final result is

$$S(x, y, t) \propto \sum_{k=1}^{K} \rho_k(x, y)\ \exp[(-\alpha_k + i\omega_k)t], \tag{3.10}$$

where, for the sake of simplicity, we have dropped the Δ of the angular frequency. The important result of this signal is that the amplitudes of the individual metabolite components depend on (x, y). Furthermore it should be noted, that Equation 3.10 is derived, as if phases play no role. In real-world signals they generally do play a role.

If one succeeds in quantifying $\rho_k(x, y)$ as a function of (x, y), the image of the metabolite, concerned, has been determined. A way of doing that is to perform a 1-D Fourier transformation from the time domain to the frequency domain and to integrate the area of the related NMR peak. In these lecture notes, however, we choose to quantify the densities by means of fitting of the time-domain signals. This is demonstrated in the next section.

3.4 Example 7: Application of time-domain fitting techniques to *in vivo* ^{1}H MRSI signals

In this section the Gauss-Newton and the HSVD program are applied to ^{1}H MRSI data sets, measured on human brains. The experiments were performed on a whole-body 1.5T MRI/MRS system of Philips Medical Systems in Best.

A typical MRSI data matrix has a size of $32 \times 32 \times 1024$ data points, i.e. 32×32 k-domain steps and 1024 time-domain steps. The 2-D k-domain is sampled symmetrically around zero in the following way: $k_i = n_i \Delta k_i \;\; (n_i = -16, \ldots, 0, \ldots, 15) \;\; (i = x, y)$. The time domains of the ^{1}H signals usually are echoes and not FID's. The acquisition of the 1024 time-domain echo points often is such that the top of the echo is near point 234.

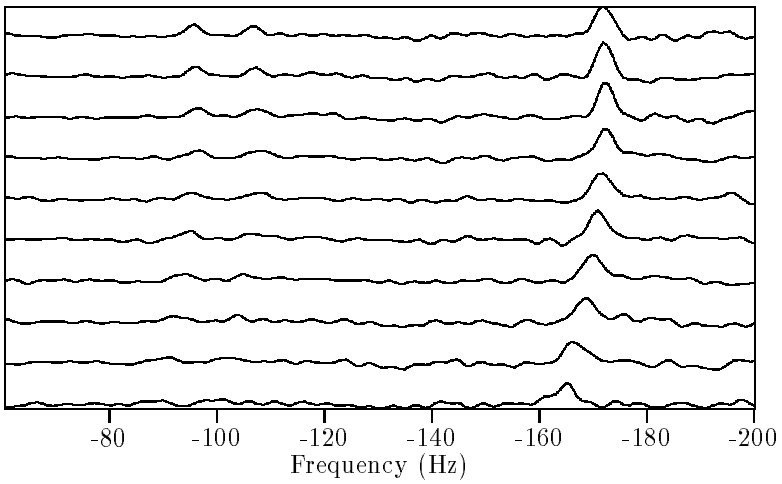

Figure 3.3: *Absolute-value ^{1}H spectra, coming from a series of voxels in a selected slice of a human head. The three peaks are due to Choline, Creatine and NAA (going from left to right).*

In Figure 3.3 a number of absolute-value spectra are displayed, coming from a series of voxels in a selected slice of a human head. It can be seen that the offset frequency of the spectra changes as a function of the voxels. At this point it is not clear, whether these changes are due to the inhomogeneity of the main magnetic field or due to susceptibility effects of the living object (or both).

As a consequence of the offset variations it is difficult to determine the peak areas of neighbouring peaks by means of frequency-domain integration with *only one* integration region. One way of solving this problem is to carry out the quantification in the time domain and to fit the frequency changes [37]. Another way is to perform a separate reference measurement on the *unsuppressed* water signal with the same pulse sequence

as is used for the MRSI measurement and to use the unsuppressed water proton echoes for correcting for the magnetic field strength fluctuations [38]. The latter approach is based on a paper by Ordidge and Cresshull [39]. An additional advantage of applying the Ordidge & Cresshull correction is that also voxel-dependent phase variations are taken into account.

Another aspect of working with real-world *in vivo* ^{1}H MRSI data sets is the presence of unwanted, overlapping, broad background features. These features may arise from various sources, such as from water or lipid signals. Before quantifying the ^{1}H echoes by means of a nonlinear Least Squares fitting procedure it may be worthwhile to remove the overlapping features with an SVD-based method. In Figure 3.4 an example is given of such a procedure. The second half of the echoes, concerned, were fitted with the HSVD method. After the fitting, the exponential decaying sinusoids with frequencies in the lipid region were subtracted from the time-domain echo signals. It can be seen from Figure 3.4 that the neighbouring NAA peak is separated from the lipid signal by this procedure [38]. A same approach can be applied to dominating signals in the water region [37].

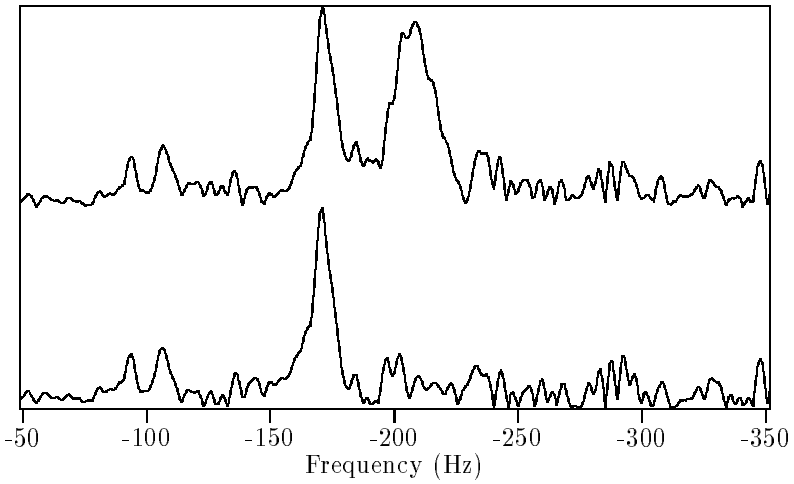

Figure 3.4: *Removal of overlapping lipid signal by means of the HSVD method. The upper picture shows the original spectrum and the lower picture the cleaned spectrum. The remaining peaks are due to the protons in Choline, Creatine and NAA, respectively.*

In order to reconstruct the metabolite maps from the $32 \times 32 \times 1024$ MRSI data sets, the following signal processing and quantitative data-analysis protocol may be convenient:

- Transformation from the k-domain to the spatial domain by 2-D FFT.
- Correction for the voxel-dependent frequency- and phase variations by the Ordidge & Cresshull approach [38] [39].
- Reduction of the number of data points to the second half of the echoes, in order to obtain FID-like time-domain signals.
- Removal of unwanted, overlapping, background features by means of the HSVD method [37] [38].
- Quantification of the resulting, cleaned, echoes with the Gauss-Newton fitting program [11] [33] [40].

- Calculation of the metabolite maps from the time-domain amplitudes, obtained in the previous step.
- Increasing the final size of the metabolite maps from 32×32 to 128×128 by means of cubic-spline interpolation in the spatial domain [37].

In Figures 3.5 and 3.6 examples of the images of NAA and Choline are shown, as obtained from frequency-domain integration and time-domain fitting (with the Gauss-Newton program). They belong to a selected slice in the head of a healthy volunteer. Concerning the time-domain fitting aproach it is important to mention, that in this case the *whole echoes* were fitted [40] (i.e. not only the second half of the echoes [37]). Using the whole echoes may be important for MRSI data sets having a poor SNR of the metabolite maps.

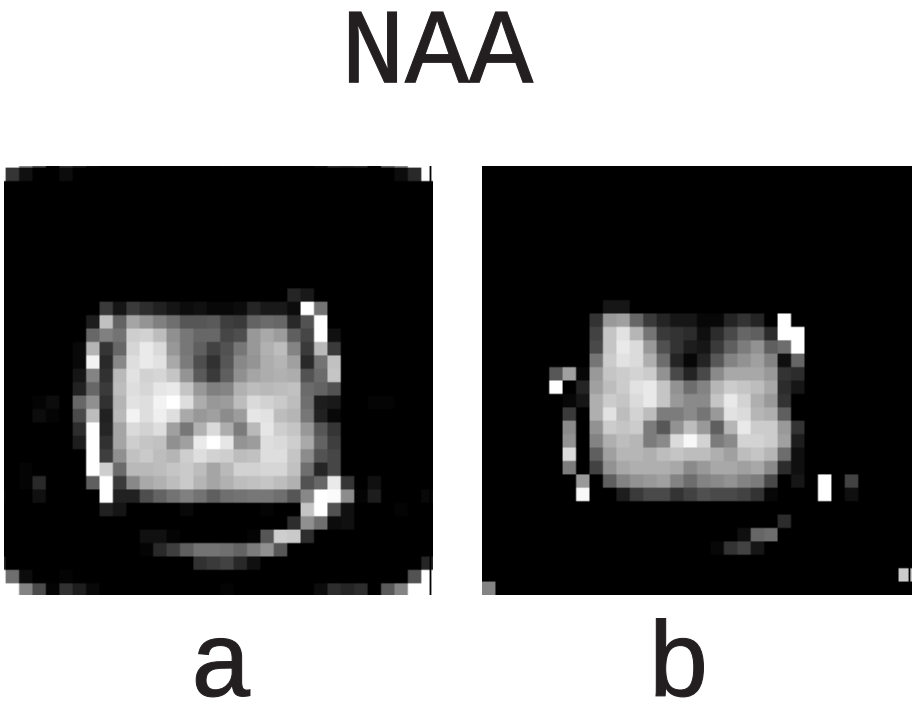

Figure 3.5: *Metabolite image of NAA, as obtained from (a) frequency-domain integration and (b) time-domain fitting.*

3.5 An alternative way of writing the MRSI equation

Transforming Equation 3.9 into Equation 3.10, in order to arrive at the final MRSI equation, was based upon integrating over the *whole* slice and 2-D Fourier transformation from the k-domain to the spatial domain.

Alternatively, we may consider the selected slice as being partitioned into a finite, discrete set of adjoining rectangular parallelepipeds, with edges Δx and Δy in the slice directions, placed on a rectangular grid at positions (x, y) (again we do not take into account the z-direction aspects). Within each parallelepiped the density of any substance

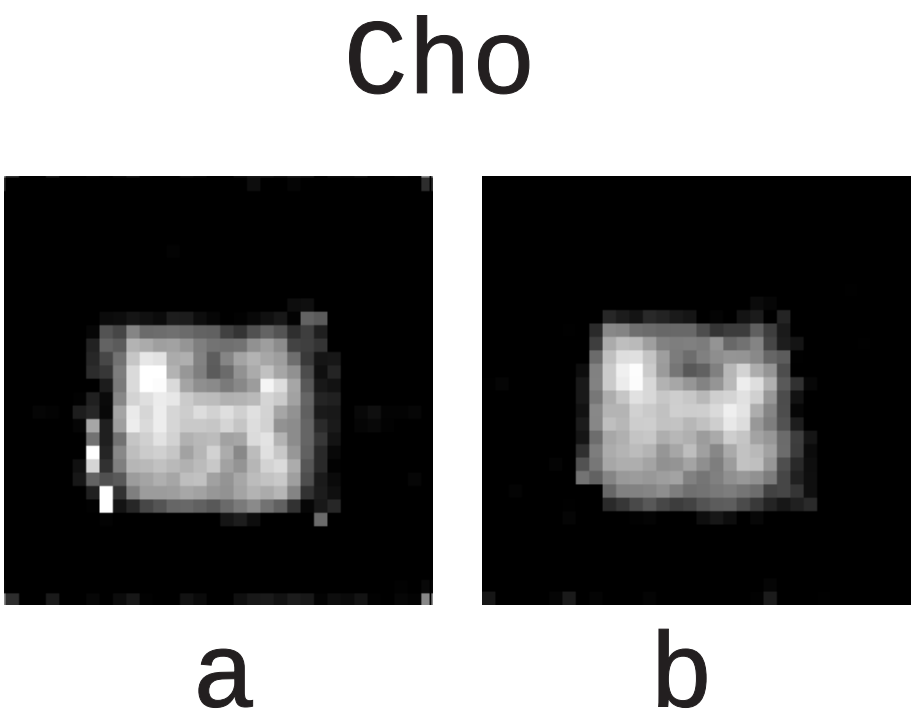

Figure 3.6: *Metabolite image of Choline, as obtained from (a) frequency-domain integration and (b) time-domain fitting.*

(metabolite) $\rho_k(x,y)$ is assummed to be *constant*. Then, integrating Equation 3.9 over one parallelepiped yields

$$s(k_x,k_y,t) \propto \sum_{k=1}^{K} \rho_k(x,y)\ \exp[i(k_x x + k_y y)]\ \mathrm{sinc}(\frac{1}{2}k_x\Delta x)\mathrm{sinc}(\frac{1}{2}k_y\Delta y)\ \exp[(-\alpha_k + i\Delta\omega_k)t]. \tag{3.11}$$

We now suppose, that there is a certain sampling strategy with $L = N_{k_x} \times N_{k_y}$ k-domain steps and N time-domain steps.

If there are M parallelepipeds located *within* the *in vivo* object, the total signal coming from the selected slice can be now expressed as a product of three matrices, i.e.

$$s(t,l) \propto \sum_{k=1}^{K}\sum_{m=1}^{M} Z(t,k)P(k,m)\Psi(m,l), \tag{3.12}$$

where $Z(t,k)$ is an $N \times K$ Vandermonde matrix, representing the time evolution of the NMR signal of each metabolite

$$Z(t,k) = \begin{pmatrix} \zeta_1^{t_0} & \zeta_2^{t_0} & \cdots & \zeta_K^{t_0} \\ \zeta_1^{t_1} & \zeta_2^{t_1} & \cdots & \zeta_K^{t_1} \\ \vdots & \vdots & \cdots & \vdots \\ \zeta_1^{t_{N-1}} & \zeta_2^{t_{N-1}} & \cdots & \zeta_K^{t_{N-1}} \end{pmatrix}, \tag{3.13}$$

in which the ζ_k are the signal poles, containing the spectral information and $t_0, t_1, \ldots, t_{N-1}$ denote the sampling times.

The matrix $P(k,m)$ is a $K \times M$ matrix, comprising the densities $\rho_k(\vec{r}_m)$ of the metabolites in the parallelepiped, positioned at $\vec{r}_m = (x_m, y_m)$ with $m = 1, 2, \ldots, M$

$$P(k,m) = \begin{pmatrix} \rho_1(\vec{r}_1) & \rho_1(\vec{r}_2) & \cdots & \rho_1(\vec{r}_M) \\ \rho_2(\vec{r}_1) & \rho_2(\vec{r}_2) & \cdots & \rho_2(\vec{r}_M) \\ \vdots & \vdots & \cdots & \vdots \\ \rho_K(\vec{r}_1) & \rho_K(\vec{r}_2) & \cdots & \rho_K(\vec{r}_M) \end{pmatrix}. \tag{3.14}$$

The third matrix $\Psi(m,l)$ is an $M \times L$ matrix comprising the functions

$$\psi(\vec{r}_m, \vec{w}_l) = \exp[i(k_{xl}x_m + k_{yl}y_m)] \ \operatorname{sinc}(\frac{1}{2}k_{xl}\Delta x) \operatorname{sinc}(\frac{1}{2}k_{yl}\Delta y), \tag{3.15}$$

where $\vec{w}_l = (k_{xl}, k_{yl})$ with $l = 1, 2, \ldots, L$ are the sample positions in the k-domain. We have

$$\Psi(m,l) = \begin{pmatrix} \psi(\vec{r}_1, \vec{w}_1) & \psi(\vec{r}_1, \vec{w}_2) & \cdots & \psi(\vec{r}_1, \vec{w}_L) \\ \psi(\vec{r}_2, \vec{w}_1) & \psi(\vec{r}_2, \vec{w}_2) & \cdots & \psi(\vec{r}_2, \vec{w}_L) \\ \vdots & \vdots & \cdots & \vdots \\ \psi(\vec{r}_M, \vec{w}_1) & \psi(\vec{r}_M, \vec{w}_2) & \cdots & \psi(\vec{r}_M, \vec{w}_L) \end{pmatrix}. \tag{3.16}$$

An image of each metabolite can be obtained by fitting the model function, described by Equation 3.12, to the data. In this equation the elements of the matrix $\Psi(m,l)$ are all known: The coordinates $\vec{r}_m$ are chosen by the person who process the data, whereas the sample positions $\vec{w}_l$ in the k-domain are set by the person who operates the NMR scanner. The optimal choice of the $\vec{r}_m$ and $\vec{w}_l$ is a subject of research. The traditional method is, as can be seen in the previous section, to distribute the $\vec{w}_l$ uniformly, and to then invoke the 2-D Fourier transformation.

Chapter 4

Miscellaneous

4.1 DFT as linear Least Squares fit in the time domain

In subsection 1.2.4 we have described the discrete Fourier Transform (DFT) of an exponentially decaying NMR FID signal. For a general model function $\hat{s}_n$ ($n = 0, 1, \ldots, N-1$) the DFT can be written, in matrix form, as

$$\vec{\hat{S}} = F\vec{\hat{s}}, \tag{4.1}$$

where the vector $\vec{\hat{S}}$ stands for the frequency-domain model points, also called the Fourier coefficients. In Equation 4.1 we have introduced the Fourier matrix, defined as [41]

$$F = \frac{1}{\sqrt{N}} \begin{pmatrix} 1 & 1 & 1 & \cdots & 1 \\ 1 & w^1 & w^2 & \cdots & w^{(N-1)} \\ \vdots & \vdots & \vdots & \cdots & \vdots \\ 1 & w^{(N-1)} & w^{2(N-1)} & \cdots & w^{(N-1)^2} \end{pmatrix}, \tag{4.2}$$

with w being the exponential $e^{\frac{-i2\pi}{N}}$. We should note, that we have set the time-domain sampling at $\Delta t = 1$, i.e. we work with the normalized frequency region of -0.5 to 0.5. Defining the Fourier matrix F, as done in Equation 4.2, has the important consequence that F is a unitary matrix, i.e. $F^{-1} = F^{\dagger}$.

If we assume, that the vector $\vec{s}$ of the data points of an NMR time-domain signal can be written as the sum of a vector $\vec{\hat{s}}$ of model function points and a vector $\vec{\epsilon}$ of noise contributions

$$\vec{s} = \vec{\hat{s}} + \vec{\epsilon}, \tag{4.3}$$

then applying the inverse procedure of Equation 4.1 yields

$$\vec{s} = F^{-1}\vec{\hat{S}} + \vec{\epsilon}. \tag{4.4}$$

Equation 4.4 implies, that the Fourier coefficients can be obtained from a standard linear Least Squares (LS) fit to the data vector $\vec{s}$, having as solution (see Equation 2.32)

$$\hat{\vec{S}} = (FF^{\dagger})^{-1}F\vec{s}, \tag{4.5}$$

where we have used the property $F^{-1} = F^{\dagger}$. Notice, that $FF^{\dagger}$ equals the identity matrix.

Conclusion:

Calulating the DFT of discretely sampled time-domain signals in fact is the same as performing a linear LS fit to the time-domain data, with the Fourier coefficients being the unknown linear parameters and the model function being a sum of undamped sinusoids with frequencies located on a uniformly distributed grid (see also [42]).

At the end of this section we like to repeat the words of G. Strang in 'Linear Algebra and its Applications' [41]

the exponentials e^{ikx} are special, and we can pinpoint one central cause: If you differentiate e^{ikx} , or integrate it, or translate x to $x + h$, the result is still a multiple of e^{ikx}.

4.2 Zero-residue modelling by the SVD-based State Space method

Often the signal processing and successive quantitative data analysis of *in vivo* NMR signals is hampered by interference from the signals of water or other substances resident in the human body. Removal of such signals prior to quantification is desired. In Example 7, Figure 3.4, we already have seen that removal of *non*descript unwanted components, such as lipid signals, by means of SVD-based State Space modelling [23] is feasible. Other successful examples are shown in [11], [37] and [38]. Several important aspects of modelling *non*descript signals are yet to be resolved. First, criteria guaranteeing success of the modelling seem lacking. This is crucial in the context of automated processing of large numbers of signals. Second, little is known about the extent to which successful State Space modelling yields the true model function parameters. This is important for establishing whether removal of unwanted components affects the remaining wanted components. In this section both aspects are addressed.

In subsection 2.4.2 we have seen that the rank of a Hankel data matrix of a noiseless time-domain signal, comprising K exponentially decaying, complex-valued, sinusoids is equal to K. Furthermore, if noise is present, in general the rank becomes full. However, if the SNR is not too low, the rank still can be approximated by K.

The question now is whether the rank statement is reversible, i.e. does the rank being equal to K always implies that the signal comprises K sinusoids? The answer is negative. In view of this we propose a simple *regularization* of the SVD-based State Space method, that should render *all conceivable signals* tractable, albeit at a cost.

Our approach is inspired by **Theorem 7.9** of M. Fiedler in 'Special Matrices and their Applications in Numerical Mathematics', stating that [43]:

any complex-valued, square $M \times M$ **Hankel** *matrix with full rank can be decomposed according to the* **Vandermonde** *decomposition* (see Equation 2.15) *, the number of realizations being* **infinite**.

The $2M-1$ entries of the $M \times M$ Hankel matrix can be looked upon as a signal comprising $2M-1$ data points. According to Fiedler there is a realization among the infinite number of Vandermonde decompositions such that any subsequent data point, i.e. point number $2M$, is fitted exactly. This result can applied to *zero-residue* modelling [44] of signals, comprising an even number of $N = 2M$ data points. First, we consider the square $M \times M$ Hankel data matrix formed from the first $2M-1$ data points. Second, this matrix is given *full rank* by adding a square $M \times M$ Hankel matrix with entries ϵ on its longest cross-diagonal and zeroes elsewhere. Alternatively, one can say that an outlier ϵ is added to data point number $M-1$, where the counting starts at zero. As a result of this regularization, an infinite number of Vandermonde decompositions is now possible, irrespective of the form of the original signal. The third step is that we include the last data point, resulting in an $(M+1) \times M$ Hankel data matrix, and add a row of zeroes to the regularizing matrix. This yields a regularized matrix

$$S_r = \begin{pmatrix} s_0 & s_1 & s_2 & \cdots & s_{M-2} & s_{M-1} \\ s_1 & s_2 & s_3 & \cdots & s_{M-1} & s_M \\ \vdots & \vdots & \vdots & \cdots & \vdots & \vdots \\ s_{M-2} & s_{M-1} & s_M & \cdots & s_{2M-4} & s_{2M-3} \\ s_{M-1} & s_M & s_{M+1} & \cdots & s_{2M-3} & s_{2M-2} \\ s_M & s_{M+1} & s_{M+2} & \cdots & s_{2M-2} & s_{2M-1} \end{pmatrix} + \begin{pmatrix} 0 & 0 & 0 & \cdots & 0 & \epsilon \\ 0 & 0 & 0 & \cdots & \epsilon & 0 \\ \vdots & \vdots & \vdots & \cdots & \vdots & \vdots \\ 0 & \epsilon & 0 & \cdots & 0 & 0 \\ \epsilon & 0 & 0 & \cdots & 0 & 0 \\ 0 & 0 & 0 & \cdots & 0 & 0 \end{pmatrix}. \quad (4.6)$$

The reason for choosing an $(M+1) \times M$ Hankel data matrix is, that in the SVD-based State Space method the top or bottom of the left singular vector matrix U is to be removed (see Equation 2.17), which for a square Hankel data matrix leads to a disallowed reduction of the rank.

The SVD-based State Space method can now be applied, using the M leading singular vectors of U. Fitting the ensuing M exponentially decaying sinusoids to the signal, including the regularizing outlier ϵ, yields a residue equal to zero. The task is then to identify those sinusoids that represent the original wanted signal, and to evaluate the extent to which unwanted components and the regularizing outlier have affected the parameters of the wanted components.

4.3 Example 8: Zero-residue modelling of a noiseless simulated signal

In this section the zero-residue modelling approach of the previous section is applied to a noiseless simulated signal of $N = 2M = 32$ data points, comprising a single exponentially decaying sinusoid perturbed by an outlier δ on the last data point. Note that the spectrum, corresponding to the outlier, is maximally wide and that modelling by the original State Space algorithm fails.

The results of the regularized State Space modelling are presented in Table 4.1. For both the regularizing outlier ϵ and the unwanted outlier δ a value of 1 was taken. It appeared, that the singular values of the 17×16 regularized Hankel data matrix were ranging from 7.332 to 0.736, indicating that the matrix was well-conditioned.

k	a_k	ϕ_k	α_k	ν_k
1	0.0451	213.4	-0.0107	0.4977
2	0.0451	190.2	-0.0108	0.4357
3	0.0449	166.7	-0.0109	0.3730
4	0.0448	142.8	-0.0110	0.3108
5	0.0448	117.7	-0.0107	0.2487
6	0.0458	88.0	-0.0079	0.1874
7	**0.9943**	**0.8**	**0.0633**	**0.1244**
8	0.0501	68.6	-0.0026	0.0581
9	0.0472	40.7	-0.0074	-0.0036
10	0.0463	16.0	-0.0088	-0.0657
11	0.0460	-7.8	-0.0095	-0.1280
12	0.0457	-31.2	-0.0098	-0.1904
13	0.0456	-54.4	-0.0101	-0.2527
14	0.0454	-77.4	-0.0103	-0.3151
15	0.0453	-100.5	-0.0105	-0.3775
16	0.0452	-123.5	-0.0106	-0.4399
True	**1.0000**	**0.0**	**0.0670**	**0.1230**

Table 4.1: *Results of regularized State Space modelling of a noiseless simulated exponentially decaying sinusoid with an outlier on the last data point. The model function is described by* $\hat{s}_n = \sum_{k=1}^{16} a_k \exp(i\phi_k) \exp[(-\alpha_k + i2\pi\nu_k)n]$ *with* $n = 0, 1, \ldots, 31$.

With the 16×4 estimated parameters, listed in Table 4.1, the sum of squared residues was as small as 5.9×10^{-15}, hence we can speak of *zero-residue modelling*. In this case the identification of the original signal is easy, considering the combinations of amplitudes, phases, decay constants and frequencies. As might be expected, the corrupting outlier δ and regularizing outlier ϵ give rise to a wide, constant, background signal that consequently overlaps with the wanted component. As a result of the overlap, the estimate of the wanted amplitude (a_7) is off by about 0.6%.

4.4 Frequency-selective quantitative data analysis in the time domain

Sometimes it is of importance to quantify a sub-set of the total set of components, being present in an NMR signal. If we ignore the components, located outside the frequency regions of interest, we speak of *frequency-selective* quantification. In the frequency domain this comes in a very natural fashion, since we just fit or integrate the peaks that we are interested in. Recently we have established [9], that frequency-selective quantification is

equally well feasible, when performing nonlinear Least Squares (NLLS) fitting in the time domain.

The vehicle chosen for carrying out the NLLS fit is the VARPRO method. If we take Equation 2.29 to describe a complex-valued NMR time-domain signal, the task at hand is to minimize the sum of squared residues

$$R = \sum_{n=0}^{N-1} |s_n - \sum_{k=1}^{K} c_k f_k(t_n, \vec{p_k})|^2 \tag{4.7}$$

as a function of the model parameters $\vec{p_k}$. Now, in order to make the equation for R tractable, we assume that we are dealing with a simulated noiseless signal, comprising only *two* damped sinusoids. Furthermore, we only want to fit the component with frequency ν_1 and *ignore* the other component with frequency ν_2. In the actual fitting process this means that a starting value of the frequency is to be chosen close to frequency ν_1.

The essence of the VARPRO method is that it eliminates the linear parameters c_k in the sum of squared residues. This fact, together with the setup, just described, results into a new expression

$$R' = \sum_{n=0}^{N-1} s_n^* s_n - \frac{\{\Re\,[\sum_{n=0}^{N-1} f_1(t_n, \vec{p_1})^*\, s_n]\,\}^2}{\sum_{n=0}^{N-1} f_1(t_n, \vec{p_1})^*\, f_1(t_n, \vec{p_1})}. \tag{4.8}$$

Notice, that the *model* amplitude a_1 is not present in Equation 4.8. However, the *signal* amplitudes are still present in R' (via the data points s_n). Furthermore, it can be seen that $R' = 0$ when the signal and model function are identical, as it should. If the signal contains two sinusoids, only one of which is fitted, then $R' > 0$.

The task is now to minimize R' by putting the derivatives of R' with respect to the nonlinear parameters to zero. In this process the contribution of the *second* sinusoid is seen to arise through the term

$$\sum_{n=0}^{N-1} f_1(t_n, \vec{p_1})^*\, s_n = \sum_{n=0}^{N-1} decay_1\, s_n \exp(-i2\pi\nu_1 n), \tag{4.9}$$

where $decay_1$ describes the decay part of the model function. Apparently, this contribution equals the DFT of the signal at the frequency ν_1 (apart from the decay term). This leads to the following important conclusion:

The contribution of the ignored second component with frequency ν_2 to the time-domain residue R' relates to the height of the corresponding frequency-domain peak at the position of ν_1.

For $|\nu_2 - \nu_1|$ being much greater than the decay constant of the second component, this height becomes small but does not tend to zero. In fact, it contributes to lifting the baseline (baseline tilt).

A consequence of the latter is that frequency-domain tactics, aiming at reducing the baseline tilt, are also effective for the present objective. One of these tactics is to multiply the time-domain data with a suited weighting function. In this context it is important to note here, that weighting the data to reduce the baseline tilt, does not corrupt the time-domain quantification provided that *the model function is subjected to the same treatment.*

For the sake of analytical presentation we now assume that the decay of the signal is described by the exponential function. In that case the noiseless signal is

$$s_n = c_1 e^{(-\alpha_1 + i2\pi\nu_1)n} + c_2 e^{(-\alpha_2 + i2\pi\nu_2)n} \tag{4.10}$$

and the model is

$$\hat{s}_n = c e^{(-\alpha + i2\pi\nu)n}. \tag{4.11}$$

Using these expressions, *in absence of weighting* the following trends can be derived:

- The systematic error in the frequency is proportional to $-(\frac{c_2}{c_1}) \times \alpha_1^3(\alpha_1 + \alpha_2)$.
- The systematic error in the decay constant is proportional to $-(\frac{c_2}{c_1})\alpha_1^2$.
- The systematic error in the amplitude is proportional to $c_2\alpha_1$.

Since α_1 is usually much smaller than 1, it follows that the frequency is the least and the amplitude is the most affected by excluding component 2 from the fit. Furthermore, in the limit of very small damping all errors become insignificant.

If both s_0 and $\hat{s}_0$ now are weighted by $\frac{1}{\sqrt{2}}$, as inspired by [45], then the powers of α_1 in the errors for the decay constant and the amplitude are raised by 1. In view of the smallness of α_1 this result constitutes a significant improvement.

The weighting function, just described, involves only the first data point and therefore hinges on the condition that the latter be intact. Should several initial data points have been lost due to a dead-time problem, more elaborate weighting is called for. We suggest that in general a smooth weighting function, reaching from zero to one in about 10 to 20 sample intervals, is needed to bring about the necessary reduction of ignored spectral components in the residue R'. So far, *quarter-sine-wave* weighting at the beginning of both the data and the model function yielded satisfactory results.

At the end of this section we present the results of quantifying a subset of the 17 components, comprising an *in vivo* ^{13}C NMR signal investigated earlier [33]. The NMR parameters were determined with the VARPRO method, first by fitting all components and then by fitting only two components. In the latter case the quantification was done without and with applying the weighting function. In Table 4.2 the values for the frequencies, damping constants and amplitudes of the two components are listed. It can be concluded that the weighting function clearly improves the result of the frequency-selective fitting.

parameter	no weighting	weighting	all
ν_1	-3.1722	-3.1769	-3.1769
ν_2	-3.1101	-3.1104	-3.1104
dam_1	0.150	0.118	0.119
dam_2	0.071	0.064	0.064
amp_1	725	583	585
amp_2	462	429	430

Table 4.2: *Model parameters of two NMR components, found by fitting with the VARPRO method. The total number of NMR components was 17. The columns "no weighting" and "weighting" refer to fitting only the two components without and with applying the weighting function (see text). The column "all" refers to fitting all 17 NMR components.*

Chapter 5

Examples

5.1 Example 9: An EU multicentre quantification trial of *in vivo* NMR test signals

One of the objectives of the EU Concerted Action "Cancer and brain disease characterization and therapy assessment by quantitative magnetic resonance spectroscopy" (Biomed 1-PL 920432) is to define and adopt *standard procedures* for the quantitative data analysis of *in vivo* NMR signals.

In the context of that objective a multicentre quantification trial was carried out in a number of participating biochemical research groups. The goal was to find out, whether protocols can be established for quantifying *in vivo* NMR signals, having the additional problem of containing unwanted broad background features, overlapping with NMR peaks of interest.

To be able to compare the performance of the various data-analysis methods, used in the multicentre trial, it was important to carry out the quantifications in a *controlled way*, i.e. to work with *simulated* signals of which the true values of the model parameters are known (not to the participants of the trial, of course). To that end two series of test signals were generated, each one containing 10 FID-like NMR time-domain signals.

The two series were derived from two specific real-world *in vivo* NMR signals. The first one was an *in vivo* ^{1}H NMR echo signal, taken from the right parietal lobe of a human brain by using a 20 ms STEAM sequence (supplied by P. Gilligan, J. MacEnri and J.T. Ennis, The Institute of Radiological Sciences, Dublin). The second signal was a water suppressed 600 MHz single pulse signal of human blood plasma (supplied by J.C. Lindon, The Wellcome Research Laboratories, Beckenham).

Both types of test signals had in common that they contained a noiseless part, comprising a number of exponentially decaying sinusoids, superimposed on a broad background signal. Furthermore, in order to obtain the two series of test signals, to each of the two noiseless parts 10 computer generated noise realizations were added, all being different but having the same standard deviation.

The following protocol was applied for generating the brain test series:

- *Mathematical* fit of the experimental brain signal by means of time-domain fitting with the HSVD method [24], using 20 exponentially decaying sinusoids as base functions.

- Separation in the time domain of the background-related signal and the NMR components by subtracting 8 HSVD-found exponentials from the experimental signal.
- Removal of the noise from the background-related time-domain signal by means of the Cadzow enhancement method [17].
- Simulation of a noiseless FID time-domain signal, using the noiseless background-related signal and the 8 exponentials, described previously. The 8 exponentials were given the same phase. The time of the first datapoint of the FID was taken equal to zero.
- Addition to the noiseless signal of the previous step of 10 different, computer generated, Gaussian-distributed noise realizations, each with the same standard deviation.

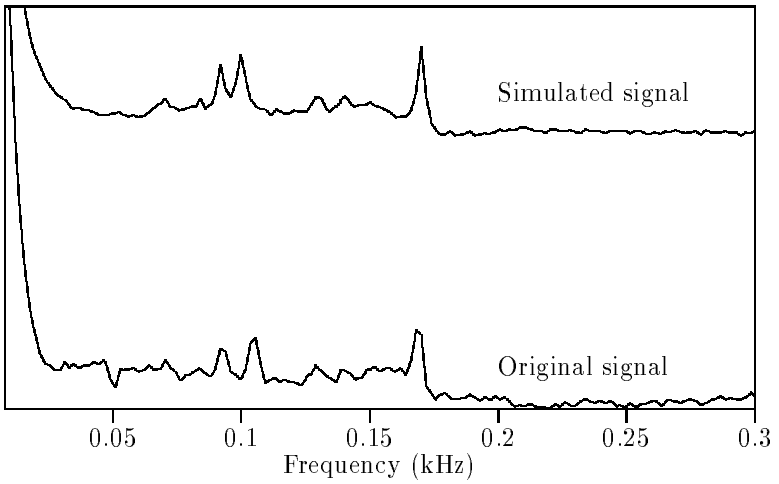

Figure 5.1: *Spectrum of the original brain signal and of one of the simulated brain test signals.*

In Figure 5.1 a comparison is made between the spectrum of the original brain signal and of one of the simulated brain test signals. Notice, that at the left side a part of the residual water peak can be seen. The parameters of the 8 NMR components, used for the simulation, are listed in Table 5.1. Another impression of the simulation of the brain test signals can be obtained from Figure 5.2.

name of signal file:	brain
number of data-points of signal:	512
step-size of signal (ms):	1.000
begin time of signal (ms):	0.000
number of frequencies:	8

Freq.	Damp.	Ampl.	Phase
kHz	ms	a.u.	degr.
0.070	73	2	-10
0.084	130	0.5	-10
0.092	110	3	-10
0.100	89	5	-10
0.130	75	2	-10
0.140	110	1	-10
0.150	17	10	-10
0.170	91	7	-10

Table 5.1: *Spectral parameters, used for simulating the brain test signals.*

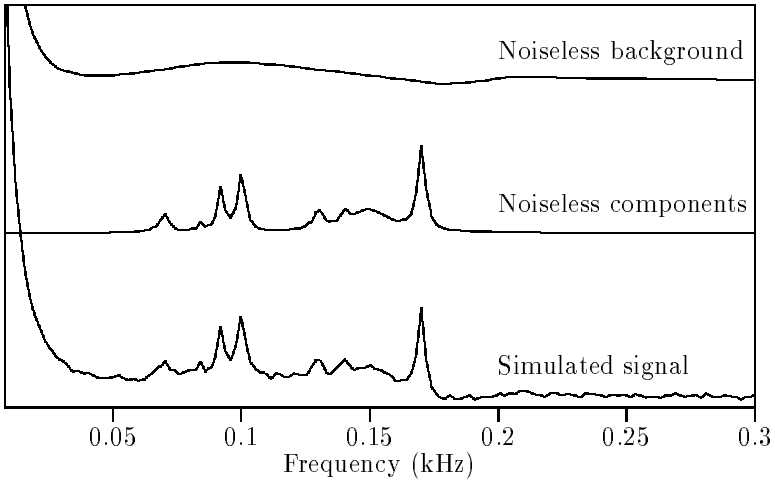

Figure 5.2: *Spectrum of a simulated brain signal, of the noiseless components and of the noiseless background.*

To generate the blood plasma test series, a slightly different protocol was applied:

- Reduction of the number of complex-valued datapoints of the experimental blood plasma signal from 32768 to 2048 by truncation at the end of the data record.
- *Mathematical* fit of the truncated signal by means of time-domain fitting with the HSVD method, using 70 exponentially decaying sinusoids as base functions.

- *Frequency-selective* quantification [9] of 9 NMR components in the so-called Fossel region by means of time-domain fitting with the VARPRO method [5].
- Simulation of a noiseless FID time-domain signal, using the HSVD-found exponentials outside the Fossel region and the 9 VARPRO-found exponentials inside the Fossel region. The latter components were all given the same phase. The time of the first datapoint of the FID was taken equal to zero.
- Addition to the noiseless signal of the previous step of 10 different, computer generated, Gaussian-distributed noise realizations, each with the same standard deviation.

name of signal file:	blood plasma
number of data-points of signal:	2048
step-size of signal (ms):	0.054
begin time of signal (ms):	0.000
number of frequencies:	9

Freq.	Damp.	Ampl.	Phase
kHz	ms	a.u.	degr.
-4.779	3.2	37000	-170
-4.691	5.6	7500	-170
-4.655	7.5	5500	-170
-4.585	8.8	3000	-170
-4.298	2.9	40000	-170
-4.231	53.0	9000	-170
-4.217	51.0	10000	-170
-4.075	66.0	1700	-170
-4.061	53.0	2000	-170

Table 5.2: *Spectral parameters, used for simulating the blood plasma test signals.*

The parameters of the 9 NMR components, used for the simulation, are listed in Table 5.2. In Figure 5.3 a plot is shown of the spectrum of a simulated blood plasma signal, of the noiseless components and of the noiseless background.

In order to quantify the two series of test signals, various methods were applied in the participating research groups, such as nonlinear Least Squares (NLLS) model function fitting (in either domain), the Maximum Entropy (MaxEnt) method [46] and the Wavelet transformation [47]. It is beyond the scope of these lecture notes to give a discussion of the latter two methods. However, it is within the scope to give the quantification results, as obtained by the VARPRO approach. They are presented in Table 5.3.

Brain test series				
Nr.	Mean	St.dev.	True	CR
1	1.81	0.13	2.0	0.15
2	0.51	0.08	0.5	0.14
3	3.10	0.14	3.0	0.17
4	5.32	0.20	5.0	0.17
5	1.92	0.18	2.0	0.22
6	1.06	0.20	1.0	0.22
7	9.87	0.71	10.0	0.61
8	6.98	0.20	7.0	0.15
Plasma test series				
Nr.	Mean	St.dev.	True	CR
1	37242	591	37000	612
2	7601	1129	7500	1501
3	5718	754	5500	1125
4	3228	171	3000	230
5	38579	303	40000	253
6	8881	67	9000	67
7	10182	68	10000	66
8	1589	40	1700	49
9	1920	45	2000	52

Table 5.3: *Mean amplitudes and standard deviations of the two series of test signals, as obtained by the VARPRO method. Also listed are the true values of the amplitudes and the related Cramer-Rao lower bounds.*

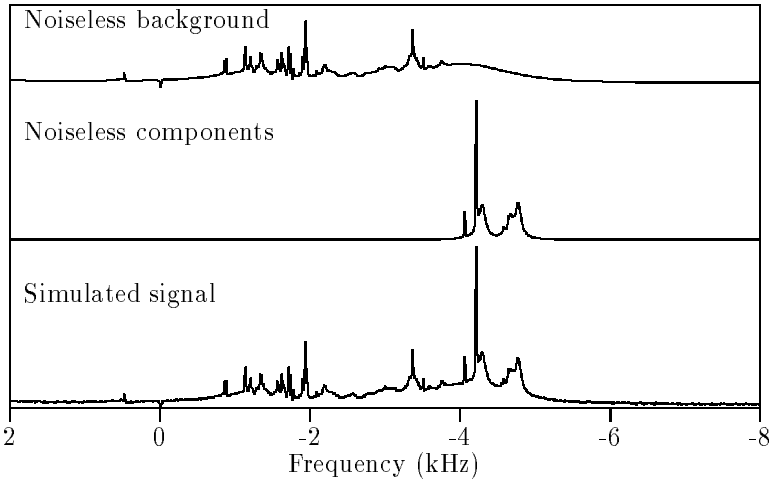

Figure 5.3: *Spectrum of a simulated blood plasma signal, of the noiseless components and of the noiseless background.*

Before applying the VARPRO method to the brain test signals, the signals were first cleaned from the dominating water signal by applying the Lanczos version of the HSVD method. To that end the 10 brain signals were fitted with 20 exponentials, using a 212×300 Hankel data matrix. The exponentials with their frequency in the water region were subtracted from the time-domain signals.

For both the brain and the blood plasma signals the broad backgrounds were handled by truncating a number of data points at the beginning of the data records (5 points for the brain signals and 20 points for the blood plasma signals). Furtheremore, in both cases the frequency-selective option was chosen, using a weighting function for the first (new) 20 datapoints.

When inspecting Table 5.3, it can be concluded, that the standard deviations more or less follow the pattern of the Cramer-Rao lower bounds. This confirms VARPRO being a Maximum Likelihood method.

5.2 Example 10: Quantification of a water suppressed 600 MHz single pulse signal of human blood plasma

In this example the quantification is described of a water suppressed 600 MHz single pulse signal of human blood plasma. It is, in fact, the same signal, as already used in the previous section for obtaining a series of blood plasma-related test signals. In this section, however, the quantification of the real-world signal itself is discussed.

An aspect, to be mentioned, when quantifying high-resolution *in vitro* NMR signals, is the working memory, required for running a computer program based on some form of model function fitting. If the computer program at hand requires a working matrix, containing the derivatives of the model function to the parameters for all sampling times, then a working memory of at least $N \times L \times 16$ is needed, where N is the number of data points and L the number of parameters. The number 16 indicates that we are dealing with double precision complex-valued numbers.

A typical example tells that for $N = 8192$ and $L = 200$ a working memory of at least 26 MBytes is required.

In Figure 5.4 the frequency region of about -4 to -5 KHz of the blood plasma signal is depicted. It can be seen that narrow NMR components as well as broad ones are present. The narrow components appear to be doublets.

Since the broad components most probably are due to unresolved overlapping NMR components, one has to decide to eiher avoid the fitting of the broad components or to fit them with one or more exponentials (see also [48]).

The following protocol was applied for the two cases:

- The model function, fitted to the data, was a sum of exponentially decaying sinusoids.
- The quantification was carried out with NLLS fitting, using the VARPRO approach.

- Only a selected part of the frequency region was quantified, using the frequency-selective fitting option of the VARPRO implementation [9].
- The data record was truncated at the end, reducing the number of data points from 32768 to 4096.
- The narrow NMR components were fitted with one exponential.
- The broad NMR components were fitted with one or more exponentials, or were not included in the fitting process by truncating the data record at the beginning with 600 data points.
- The following prior knowledge was used: One overall (zero-order) phase; Constraints for the doublet structure; Fixed, predetermined, values of the decay constants of one of the doublets.

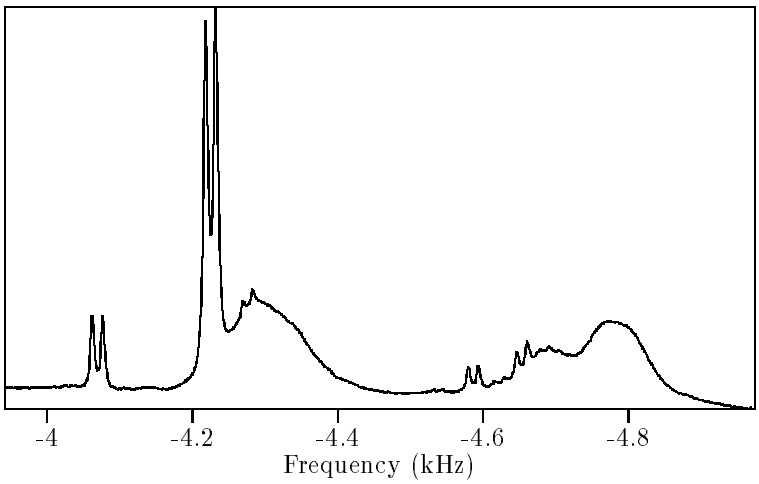

Figure 5.4: *Part of the spectrum of the 600 MHz single pulse signal of human blood plasma.*

When reducing the number of data points from 32768 to 4096, it was first verified that this truncation does not seriously affect the quantification results. The latter can be inspected in Figure 5.5. Another remark to be made is, that the choice of omitting 600 data points at the beginning was also verified before (see also Figure 5.5).

One of the results of the quantifications is illustrated in Table 5.4. It concerns the approach with fitting all components, including the broad ones. The related graphical presentation of the results is given in Figure 5.6. It can be seen that the residual signal (see Figure 5.6c) clearly shows features, larger than the noise. This may indicate a deviation from the exponential decay model.

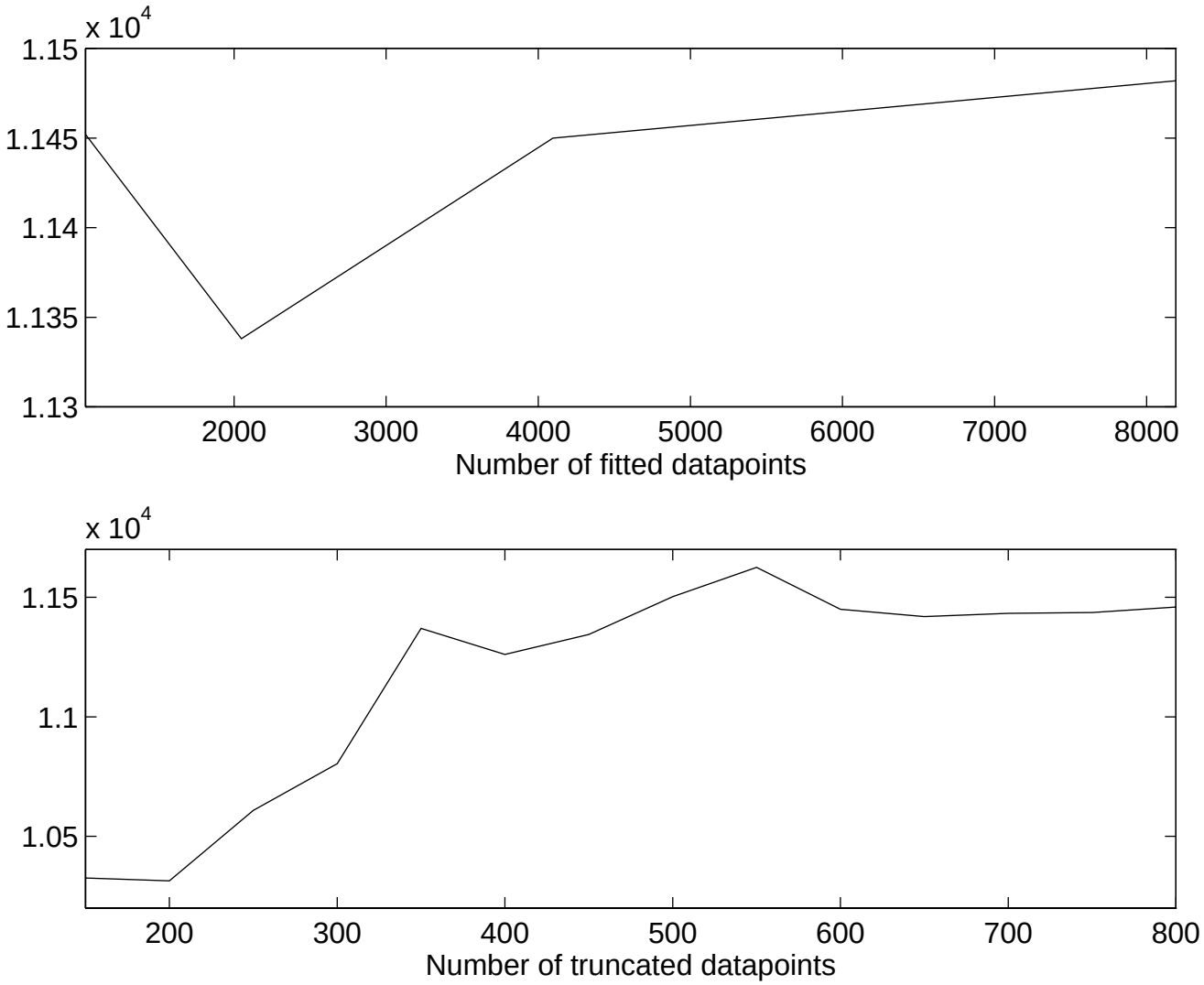

Figure 5.5: *Estimated amplitude of the largest doublet of the blood plasma signal as a function of (top) the number of fitted datapoints and (bottom) the number of truncated initial datapoints. The effects on the other doublets were similar.*

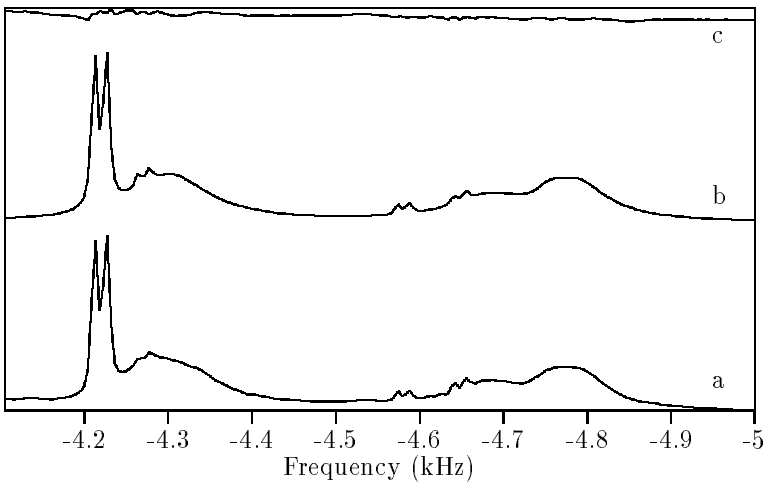

Figure 5.6: *VARPRO results for the blood plasma signal. Spectrum of (a) the experimental signal, (b) the fitted signal and (c) the residual signal.*

name of signal file:	p19tot.dat
number of data-points of signal:	32768
step-size of signal (ms):	0.054
fitted zero-order phase (degrees):	196.7(0.1)
constrained value of begin time (ms):	0.000
number of data-points in VARPRO fit:	4096
index of first data-point:	1
number of frequencies:	14
number of iterations:	21
root mean square of VARPRO fit:	$0.1653E+03$

Frequency	2CR	Decay	2CR	Amplitude	2CR
kHz	kHz	kHz	kHz	a.u.	a.u.
-4.0610	0.0000	0.0193	0.0002	1996	13
-4.0755	0.0000	0.0193	0.0002	1996	13
-4.2172	0.0000	0.0200	0.0000	9716	17
-4.2310	0.0000	0.0200	0.0000	9716	17
-4.2688	0.0001	0.0193	0.0002	811	15
-4.2819	0.0001	0.0193	0.0002	811	15
-4.3057	0.0002	0.3656	0.0014	46427	172
-4.5788	0.0001	0.0193	0.0002	663	12
-4.5927	0.0001	0.0193	0.0002	663	12
-4.6457	0.0001	0.0193	0.0002	480	14
-4.6600	0.0001	0.0193	0.0002	480	14
-4.6855	0.0005	0.3424	0.0040	21087	290
-4.7600	0.0004	0.1090	0.0071	3366	395
-4.7931	0.0007	0.2751	0.0028	26997	602

Table 5.4: *Numerical results of the VARPRO quantification of the blood plasma signal.*

Bibliography

[1] P.G. Morris: Nuclear Magnetic Resonance Imaging in Medicine and Biology, Clarendon Press, Oxford, 1986.

[2] P. Diehl, E. Fluck, H. Gunther, R. Kosfeld and J. Seelig (editors): In-Vivo Magnetic Resonance Spectroscopy I, II and III, *NMR Basic Principles and Progress 26, 27 and 28*, Springer-Verlag, Berlin, 1992.

[3] R.A. Meyer, M.J. Fisher, S.J. Nelson and T.R. Brown: Evaluation of Manual Methods for Integration of *in vivo* Phosphorous NMR Spectra, *NMR IN BIOMEDICINE*, **1** (1988) pp. 131-135.

[4] R. de Beer, J.A. den Hollander, A.J.H. Marien, D. van Ormondt and C.M. Segebarth: Evaluation of the Reproducibility of Spectral Parameters obtained by Quantitative Analysis of In Vivo ^{31}P NMR Spectra, *Proceedings of the Seventh Annual Meeting of the SMRM*, San Francisco, August 22-26, 1988, p. 303.

[5] J.W.C. van der Veen, R. de Beer, P.R. Luyten and D. van Ormondt: Accurate Quantification of In Vivo ^{31}P NMR Signals using the Variable Projection Method and Prior Knowledge, *Magn. Reson. in Medicine*, **6** (1988) pp. 92-98.

[6] J.C. Haselgrove, V.H. Subramanian, R. Christen and J.S. Leigh: Analysis of In-Vivo NMR Spectra, *Rev. Magn. Reson. in Medicine*, **2** (1987) pp. 167-222.

[7] A.F. Mehlkopf and W.M.M.J. Bovee: Spinafbeelding: theorie, methoden en instrumentatie, *Lecture Notes c58*, University of Technology Delft, 1992.

[8] E.O. Brigham: The Fast Fourier Transform, Prentice-Hall, Englewood Cliffs, 1974

[9] A. Knijn, R. de Beer and D. van Ormondt: Frequency-Selective Quantification in the Time Domain, *J. Magn. Reson.*, **97** (1992) pp. 444-450.

[10] G.C. McKinnon, C. Burger and P. Boesiger: Spectral Baseline Correction using CLEAN, *Magn. Reson. in Medicine*, **13** (1990) pp. 145-149.

[11] R. de Beer and D. van Ormondt: Analysis of NMR Data using Time Domain Fitting Procedures, Chapter in *NMR Basic Principles and Progress 26*, Springer-Verlag, Berlin, 1992, pp. 202-248

[12] H. Flores-Llamas, A. Cabral-Prieto, H. Jimenez-Dominguez and M. Torres-Valderrama: An expression for an approximation of the Voigt profile I, *Nuclear Instruments and Methods in Physics Research*, **A300** (1991) pp. 159-163.

[13] M.B. Priestley: Spectral Analysis and Time Series, Academic Press, London, 1981.

[14] C.L. Lawson and R.J. Hanson: Solving Least Squares Problems, Prentice Hall, Englewood Cliffs, 1974.

[15] J. Cadzow: Signal Enhancement. A Composite Property Mapping Algorithm, *IEEE Trans. on Acoustics, Speech, and Signal Processing*, **ASSP-36** (1988) pp. 49-62.

[16] H.F.M. Lohman: Enige Aspecten van Signaalverwerking met Singuliere Waarden Decompositie, *Doctoral thesis*, University of Technology Delft, 1989.

[17] A. Diop, A. Briguet and D. Graveron-Demilly: Automatic *In Vivo* NMR Data Processing Based on an Enhancement Procedure and Linear Prediction Method, *Magn. Reson. in Medicine*, **27** (1992) pp. 318-328.

[18] Yung-Ya Lin and Lian-Pin Hwang: NMR Signal Enhancement Based on Matrix Property Mappings, *J. Magn. Reson.*, Series A **103** (1993) pp. 109-114.

[19] S. van Huffel: Enhanced Resolution Based on Minimum Variance Estimation and Exponential Modeling, *Signal Processing*, **33** (1993) 333.

[20] H. Chen, S. van Huffel, C. Decanniere and P. van Hecke: A Signal-Enhancement Algorithm for the Quantification of NMR Data in the Time Domain, *J. Magn. Reson.*, **A 109** (1994) pp. 46-55.

[21] R. Kumaresan and D.W. Tufts: Estimating the Parameters of Exponentially Damped Sinusoids and Pole-zero Modeling in Noise, *IEEE Trans. Acoust., Speech, Signal Process.*, **ASSP-30** (1982) pp. 833-840.

[22] H. Barkhuijsen, R. de Beer, W.M.M.J. Bovee and D. van Ormondt: Retrieval of Frequencies, Amplitudes, Damping Factors and Phases from Time-Domain Signals, using a Linear Least-Squares Procedure, *J. Magn. Reson.*, **61** (1985) pp. 465-481.

[23] S.Y. Kung, K.S. Arun and D.V. Bhaskar Rao: State Space Singular Value Decomposition based Methods for the Harmonic Retrieval Problem, *J. Opt. Soc. Am.*, **73** (1983) pp. 1799-1811.

[24] H. Barkhuijsen, R. de Beer and D. van Ormondt: Improved Algorithm for Noniterative Time-Domain Model Fitting to Exponentially Damped Magnetic Resonance Signals, *J. Magn. Reson.*, **73** (1987) pp. 553-557.

[25] L. Aerts and J. Bervoets: Nauwkeurige bepaling van fysisch signifikante parameters, uitgaande van nucleaire magnetische resonantie-signalen, *Doctoral thesis*, Katholieke Universiteit Leuven, 1991.

[26] H. Barhuijsen, R. de Beer abd D. van Ormondt: Aspects of the Computational Efficiency of LPSVD, *J. Magn. Reson.*, **64** (1985) pp. 343-346.

[27] G.L. Millhauser, A.A. Carter, D.J. Schneider, J.H. Freed and R.E. Oswald: Rapid Singular Value Decomposition for Time-Domain Analysis of Magnetic Resonance Signals by Use of the Lanczos Algorithm, *J. Magn. Reson.*, **82** (1989) pp. 150-155.

[28] S. van Huffel: Partial Singular Value Decomposition algorithm (Algorithm 32), *J. Comput. Appl. Math.*, **33** (1990) pp. 105-112.

[29] W.W.F. Pijnappel, A. van den Boogaart, R. de Beer and D. van Ormondt: SVD-based Quantification of Magnetic resonance Signals, *J. Magn. Reson.*, **97** (1992) pp. 122-134.

[30] H. Barhuijsen, R. de Beer abd D. van Ormondt: Error Theory for Time-Domain Signal Analysis with Linear Prediction and Singular Value Decomposition, *J. Magn. Reson.*, **67** (1986) pp. 371-375.

[31] A. Tarantola: Inverse Problem Theory, Elsevier, Amsterdam, 1987.

[32] J.H. Schreur: Influence of Reperfusion and Extracellular milieu on Myocardial Energy and Ions, PhD Thesis, University Hospital Utrecht, 1993.

[33] R. de Beer, D. van Ormondt and W.W.F. Pijnappel: Improved Harmonic Retrieval from Noisy Signals by Invoking Prior Knowledge, SIGNAL PROCESSING IV: Theories and Applications, J.L. Lacoume, A. Chehikian, N. Martin and J. Malbos (Editors) Elsevier, Amsterdam, 1988.

[34] A. Bax: Two-Dimensional Nuclear Magnetic Resonance in Liquids, PhD Thesis, University of Technology Delft, 1981.

[35] R. de Beer, D. van Ormondt and W.W.F. Pijnappel: Quantification of 1-D and 2-D Magnetic Resonance Time Domain Signals, *Pure and Appl. Chem.*, **64** (1992) pp. 815-823.

[36] M. Gueron, P. Plateau and M. Decorps: Solvent Signal Suppression in NMR, *Progress in NMR Spectroscopy*, **23** (1992) pp. 135-209.

[37] R. de Beer, A. van den Boogaart, D. van Ormondt and W.W.F. Pijnappel: Application of Time-domain Fitting in the Quantification of In Vivo ^{1}H Spectroscopic Imaging Data Sets, *NMR IN BIOMEDICINE*, **5** (1992) pp. 171-178.

[38] R. de Beer, F. Michels, D. van Ormondt, B.P.O. van Tongeren, P.R. Luyten and H. van Vroonhoven: Reduced Lipid Contamination in In Vivo ^{1}H MRSI using Time-domain Fitting and Neural Network Classification, *Magnetic Resonance Imaging*, **11** (1993) pp. 1019-1026.

[39] R.J. Ordidge and I.D. Cresshull: The Correction of Transient B_0 Field Shifts following the Application of Pulsed Gradients by Phase Correction in the Time Domain, *J. Magn. Reson.*, **69** (1986) pp. 151-151.

[40] J.E. van Dijk, A.F. Mehlkopf, D. van Ormondt and W.M.M.J. Bovee: Determination of Concentrations by Time Domain Fitting of Proton NMR Echo Signals using Prior Knowledge, *Magn. Reson. in Medicine*, **27** (1992) pp. 76-96.

[41] G. Strang: Linear Algebra and its Applications, Harcourt Brace Jovanovich Publishers, San Diego, 1988.

[42] A. van den Bos: Estimation of Fourier Coefficients, *IEEE Transactions on Instruments and Measurement*, **38** (1989) pp. 1005-1007.

[43] M. Fiedler: Special Matrices and their Applications in Numerical Mathematics, Martinus Nijhoff Publishers, Dordrecht, 1986.

[44] I. Dologlou and G. Garayannis: LPC/SVD Analysis of Signals with Zero Modelling Error, *Signal Processing*, **23** (1991) pp. 293-299.

[45] G. Otting, H. Widmer, G. Wagner and K. Wuthrich: Origin of t_1 and t_2 Ridges in 2D NMR Spectra and Procedures for Suppression, *J. Magn. Reson.*, **66** (1986) pp. 187-193.

[46] S.F. Gull and J. Skilling: Quantified Maximum Entropy User's Manual (MemSys5), *Maximum Entropy Data Consultants Ltd.*, Royston, 1991.

[47] N. Delprat, B. Escudie, P. Guillemin, R. Kronland-Martinet T. Tchamitchian and B. Torresani: Asymptotic Wavelet and Gabor Analysis. Extraction of Instantaneous Frequencies, *IEEE TRans. Information Theory*, **38** (1991) pp. 644-664.

[48] A. van den Boogaart, M. Ala-Korpela, J. Jokisaari and J.R. Griffiths: Time and Frequency Domain Analysis of NMR Data Compared. An application to 1D ^{1}H Spectra of Lipoproteins, *Magn. Reson. in Medicine*, **31** (1994) pp. 347-358.